APPLICATION OF AN
INTEGRATING TYPE IONIZATION CHAMBER
TO MEASUREMENTS OF RADIATION IN SPACE

by

Sharad R. Kane

September 1967

Technical Report No. CR-106

Contract NAS5-2071

COSMIC RAY GROUP

School of Physics and Astronomy

UNIVERSITY OF MINNESOTA

APPLICATION OF AN INTEGRATING TYPE IONIZATION CHAMBER

TO MEASUREMENTS OF RADIATION IN SPACE

A THESIS

SUBMITTED TO THE FACULTY OF THE GRADUATE SCHOOL

OF THE UNIVERSITY OF MINNESOTA

by

Sharad Ramchandra Kane

IN PARTIAL FULFILLMENT OF THE REQUIREMENTS

FOR THE DEGREE OF

DOCTOR OF PHILOSOPHY

December, 1967

TABLE OF CONTENTS

iii

LIST OF TABLES

LIST OF FIGURES

ABSTRACT

An integrating type ion chamber experiment, using a resetting drift-type electrometer and designed to fly on the OGO-I and III satellites is described. The chamber is demonstrated to have an accuracy and stability of ~1% during its operation in space over a period of nearly three years.

The minimum energy for penetration by protons and electrons is 12 and 0.6 MeV respectively. The response to 40 KeV electrons (through bremsstrahlung) is about 10^{-7} x (response at energies >600 KeV). The response to x-rays in 10-150 KeV range is peaked at ~20 KeV; below 10 KeV the response is $\approx 10^{-2}$ x (response at 20 KeV). For 1 particle cm^{-2} sec^{-1} of 20 KeV photons, electrons with energy $\gtrsim 1$ MeV, and minimum ionizing nuclei with charge Ze the pulsing rate of the chamber is respectively 0.2, 7,0, and 5.5 Z^2 NPPS (Normalized Pulses Per Second) x 10^3.

The OGO-I and III ion chamber measurements reported here cover the period 10 September, 1964 - 2 July, 1966, a period following the minimum in solar activity. The cosmic ray maximum, as determined from these measurements, occurred during 11-15 May, 1965 when the ion chamber rate in free space was 65.5 NPPS x 10^3. For this time the total chamber rate computed from the "known" cosmic ray spectrum is 74 NPPS x 10^3, the contributions from protons, He-nuclei, S-nuclei, electrons and nuclear interactions being about 31, 18, 33, 5 and 13 percent respectively. The difference of 12% between the total computed and observed rates could be due to a number of known factors.

The relationship between the free space ion chamber and Deep

River neutron monitor during March 1960 - May 1965 is found to be
linear: fractional change in free space chamber $\approx$ k x (fractional
change in Deep River monitor), where K $\approx$ 4.5. After May, 1965
K is <4.5 which implies a hysteresis effect.

The differential response curve of the OGO chamber for the
primary cosmic rays is peaked at about 1 and 2 BV at solar minimum
and solar maximum respectively. Most of the response of an ion
chamber is found to be concentrated in a rather narrow rigidity
interval of the primary spectrum, the precise interval depending
on the location of the chamber:

Free space	1.5 - 2.5 BV
High latitude (10 mb)	2.5 - 3.5 BV
Minneapolis (10 mb)	3.0 - 4.0 BV

These results give the rigidity dependence of the modulation
consistent with $P^{-0.9}$. (period 1960-1965, $1.5 \leq P \leq 4.0$ BV).

At high latitudes variation of the chamber rate with altitude
was computed taking into account the earth's shadow effect and the
observed chamber rate in free space. At balloon altitudes the
computed rate is found to be lower than the observed rate; the
difference is maximum (~100%) at solar maximum and is presumably
due to the secondaries produced in the atmosphere.

Fluctuations of ~5% magnitude, observed in the free space chamber
rate averaged over about 90 seconds, can be explained in terms of the
statistical fluctuations in (a) number of primaries passing through
the chamber, (b) number of nuclear interactions in the chamber,
(c) energy deposited in individual interactions and (d) heavy nuclei
stopping inside the chamber gas. No single process was found to be
the dominating factor.

I. INTRODUCTION

(A) STATEMENT OF THE PROBLEM

Integrating type ionization chambers have long been in use
for measurements of various kinds of radiations. Such a chamber
measures the total amount of ionization produced in a given
time by the incident radiation, the amount of ionization being
proportional to the energy deposited inside the chamber. Because
of its relatively high stability against drifts, it is
particularly well suited for continuous monitoring of radiation
intensity.

Most of the early investigations of cosmic rays were carried
out with the help of an integrating type ionization chamber.
For example, using the ion chamber measurements at sea level,
Forbush (1938, 1954) discovered the well known Forbush decreases
and the 11 year variation in cosmic ray intensity. During the
past three decades Millikan (1936), Neher (1962, 1964) and their
co-workers have made extensive measurements of the variation of
cosmic ray ionization with atmospheric depth by flying the ion
chambers on balloons.

Since 1959 ionization measurements have also been made in
space. Arnoldy et al. (1960, 1962a, 1962b) and Hoffman et al.
(1962a, 1962b) have made such measurements in the Van Allen
radiation belts with an ion chamber aboard the Explorer VI satellite.
Measurements in free space (outside the earth's magnetic field)
have been made with ion chambers aboard the Pioneer V space
probe (Arnoldy et al. 1964), Mariners II and IV (Neher and

Anderson, 1964, 1965) and the OGO-I and III satellites (present study).

An ion chamber responds to all particles and photons energetic enough to penetrate the chamber wall although the chamber cannot, by itself, determine either the nature or the energy of the incident radiation. Therefore an ion chamber can be used effectively for the detection and exploration of new phenomena which may subsequently be studied in detail by the more sophisticated detectors. The first attempt on these lines was made by Winckler (1960) who used constant level balloons to detect solar cosmic rays, solar x-rays and auroral x-rays.

The above discussion shows the wide range of phenomena which can be explored and studied with an integrating type ion chamber. When properly designed, it should be possible for such a chamber to measure, for example, the relatively low ionization due to primary cosmic rays and also the intense radiation in the Van Allen radiation belts. In fact the OGO-I and III ion chambers did record many different phenomena of which the following are being studied:

1. Solar x-ray bursts in the 10-50 KeV energy range and their correlation with the solar radio and energetic particle emission.

2. Observed time-structure of solar particle events and its relation to the propagation characteristics of solar particles inside the magnetosphere and the transition region.

3. Recurrence tendencies (period 27 days) in the solar particle and x-ray emission.

4. Ionization due to galactic cosmic rays in free space, its variation during the solar cycle, and its relation to the changes in the primary cosmic ray spectrum.

5. "Ionization bursts" in an ion chamber in free space and the heavy nuclei in the primary cosmic rays.

6. Changes in the location and depth of the "slot" region (between the inner and outer radiation zones) with the variation in solar activity and the mechanism responsible for the existence of the slot.

7. Spatial and temporal characteristics of the semi-trapped radiation in the region between the outer radiation zone and the magnetopause. (the "skirt" region).

8. Spatial distribution of the transient electron fluxes in the magnetosphere and the transition region.

9. Radiation dosage environment in the vicinity of the earth and in free space.

Some of these studies such as solar x-ray bursts (Arnoldy et al, 1967) and the interpretation of the cosmic ray measurements (Kane et al, 1965, 1966) have already been published and others are in progress.

Although numerous ion chamber measurements have been made in space and on balloons, their significance is not well understood. For example, in case of cosmic ray measurements it is not known to what part of the primary spectrum a given ion chamber measurement is related. In order to solve this problem of 'interpretation of ion chamber measurements', it is necessary to understand thoroughly the basic response characteristics of the chamber. This fundamental work

is undertaken in this thesis. To be explicit, the objects of the
present study are the following:

(1) To construct a highly reliable ionization chamber experiment
(to be flown on OGO-I and III satellites) with a dynamic
range of over six orders of magnitude and an accuracy of
about one percent especially for low rates of ionization.
The chamber should retain its calibration for long periods
in space.

(2) To determine the response of the ion chamber to electrons,
protons, heavier nuclei and x-rays.

(3) To compute the differential rigidity response of the chamber
to the "known" differential rigidity spectrum of the galactic
cosmic rays.

As an application of the response characteristics obtained
above, the following problems are studied in this thesis.

(4) Comparison of the observed OGO ion chamber rate in free
space with the total rate computed from the response
characteristics of the chamber and the known galactic
cosmic ray spectrum.

In free space the only quiescent radiation to which the ion
chamber is sensitive is assumed to be the galactic cosmic rays. An
agreement between the observed and computed chamber rates may
therefore be taken as an evidence in support of the above assumption.
On the other hand, if there exists an unexplained discrepancy between
the observed and the computed rates an unknown radiation somehow

not detected by the conventional particle detectors may be present.

(5) The long-term variation of the observed ion chamber rate in free space and its relation to the long-term changes in the primary cosmic ray spectrum.

With the help of the differential response curve computed earlier, the response of the chamber to the primary cosmic rays and their variations can be understood. It is then possible to relate the observed changes in the chamber rate to the corresponding changes in that part of the primary spectrum to which the chamber is most sensitive.

(6) The relation between the observed long-term variations of the ion chamber rates in free space and on high altitude balloons.

Ion chamber measurements with high altitude balloons at medium latitudes (Minneapolis, Bismarck) and high latitudes (Churchill, Thule) are now available over more than a solar cycle in the form of rate vs. time plots. The problem of interpreting these measurements is similar to that for the neutron monitors. With the help of latitude surveys made with balloon ion chambers a differential rigidity response curve is obtained. It is then possible to understand how a balloon ion chamber responds to primary cosmic rays without a detailed knowledge of the complex atmospheric processes. Thus the measurements made with the various ion chambers can be ordered in terms of the regions of the primary rigidity spectrum which these chambers represent. These regions of rigidities are expected to lie between those represented by the neutron monitors and those covered by the particle detectors.

(7) The rigidity dependence of the long-term variation

during the period 1960-1965.

During the period 1960-1965 ion chamber measurements are available in free space, on high latitude balloon and on Minneapolis balloon. If the rigidity intervals of the primary spectrum which these ion chambers represent are known (above discussion), fractional changes in these ion chamber rates can be plotted against the rigidity intervals they represent. Using similar procedure for the measured intensities of He nuclei in different rigidity intervals, the form of the modulation spectrum can be deduced.

(8) Variation of the ion chamber rate with altitude above

the earth's surface.

Simultaneous measurements with an ion chamber in free space and on a balloon are now available so that such a study can be made. The factors to be considered are (a) the absorption of the particles within the solid angle subtended by the solid earth at the location of the chamber, (b) geomagnetic cut-off rigidity at the location of the chamber (c) secondary particles produced in the atmosphere.

(9) Fluctuations in the ion chamber rate in free space.

Large fluctuations are expected to be caused by nuclear inter-actions or very heavy nuclei stopping inside the chamber. Since OGO-I and III ion chamber data in free space is now available for about 12000 hours, it may be possible to detect rare heavily ionizing cosmic ray nuclei even if their intensity is extremely low.

(B) THE OGO SPACECRAFT

The Orbiting Geophysical Observatory (OGO) spacecraft is
shown in Figure 1 in its flight configuration. The spacecraft
has been described in detail by Ludwig (1963). It was built
by Space Technology Laboratories, Inc. of Redondo Beach,
California for the National Aeronautics and Space Administration
(NASA). The spacecraft carried 20 experiments mounted either in
its main body or on its appendages. The locations of the
University of Minnesota experiments are indicated in Figure 1.
The ionization chamber experiment, with which this thesis is
concerned, is located on a boom which extends about four feet
from the main body of the spacecraft. The solid angle subtended
by the spacecraft at the position of the ionization chamber
is less than that subtended by the base of the experimental
package. The latter subtends a solid angle of 2.25 steradians
which is only 18 percent of the total solid angle 4π steradians.
The chamber can therefore be considered essentially in free space.

The experimental package is enclosed in a thin box-like
enclosure of total thickness equal to about 0.003 inches of
aluminum mylar. With the help of a heater located at the bottom
of the experimental package, the temperature inside the enclosure
could be maintained between 0° - 40° C.

ELECTRON
SPECTROMETER

ION CHAMBER
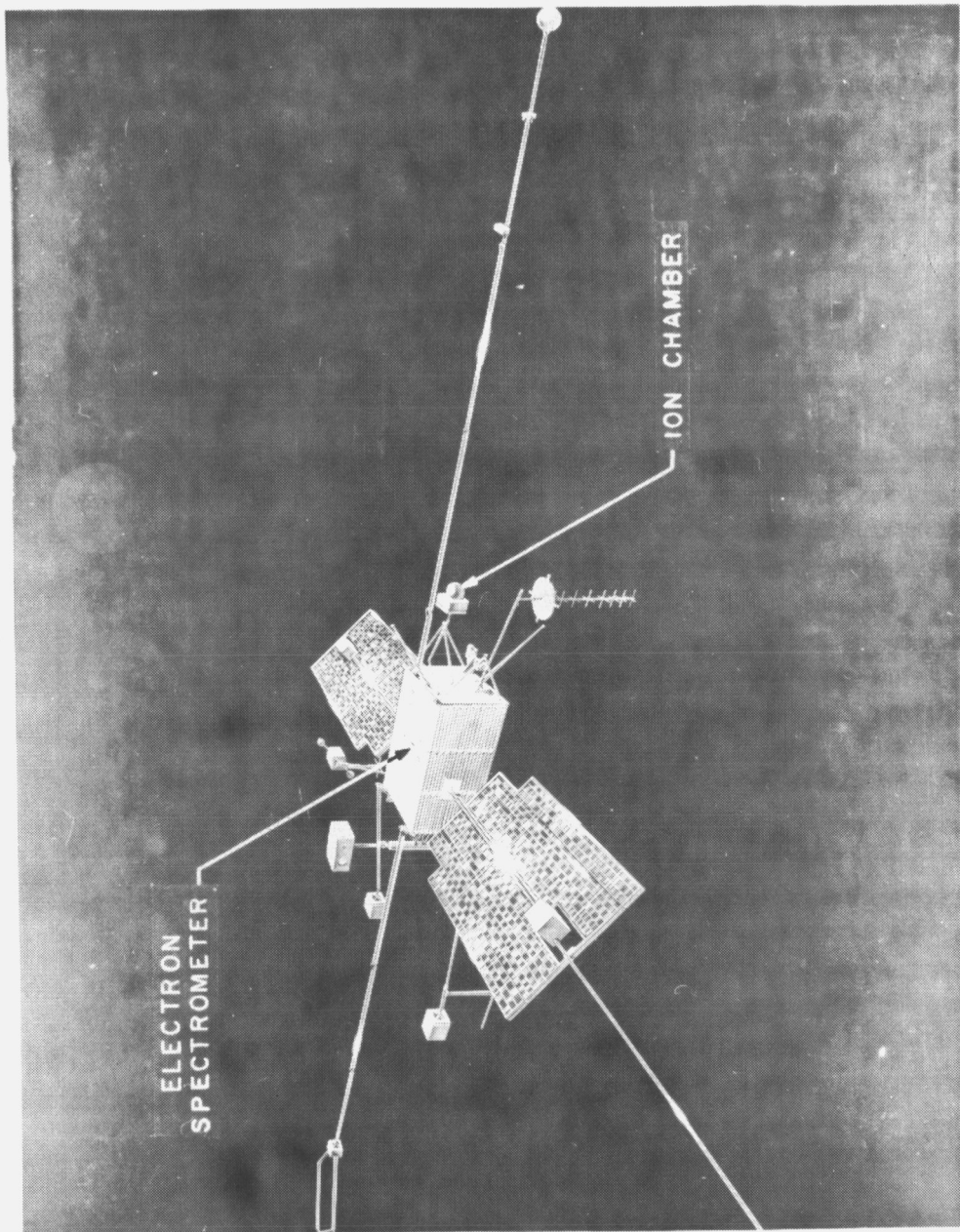
Figure 1

TABLE I

	OGO-I	OGO-III
Launch date	5 Sept. 1964	7 June 1966
Height of perigee	280.5 km	295.3 km
Height of apogee	149,408.5 km	122,219.7 km
Inclination to equator	31.11 degrees	30.97 degrees
Local time at apogee	≈2100 hrs.	≈2300 hrs.
Orbital period	63.98 hrs.	48.63 hrs.
Spin period	11.85 sec.	≈96 sec (variable)

The OGO-I satellite was launched on September 5, 1964 into a highly eccentric orbit. A brief summary of the orbital elements is presented in Table 1. The geocentric distances of perigee and apogee are about 1.04 and 24.4 earth radii. The orbital period is about 64 hours while the spin period is about 12 seconds.

In order to be able to view the orbit in relation to the geomagnetic field, the radius vector from the earth's center to a point in the orbit may be rotated about the sun-earth line until it lies in the geomagnetic equatorial plane. Such a procedure assumes that the geomagnetic field is symmetrical about the extended sun-earth line. This assumption is adequately justified for the present purpose by the actual field measurements. The image of the initial orbit obtained in this manner in the geomagnetic equatorial plane is shown schematically in Figure 2. In such a diagram the position of the satellite with respect to the sun-earth line can be conveniently specified in terms of the "local time" of the satellite. It is defined in such a way that the local time of 1200 hours corresponds to the location of the satellite on the sun-earth line in the solar direction. The local time of 0000 hours corresponds to
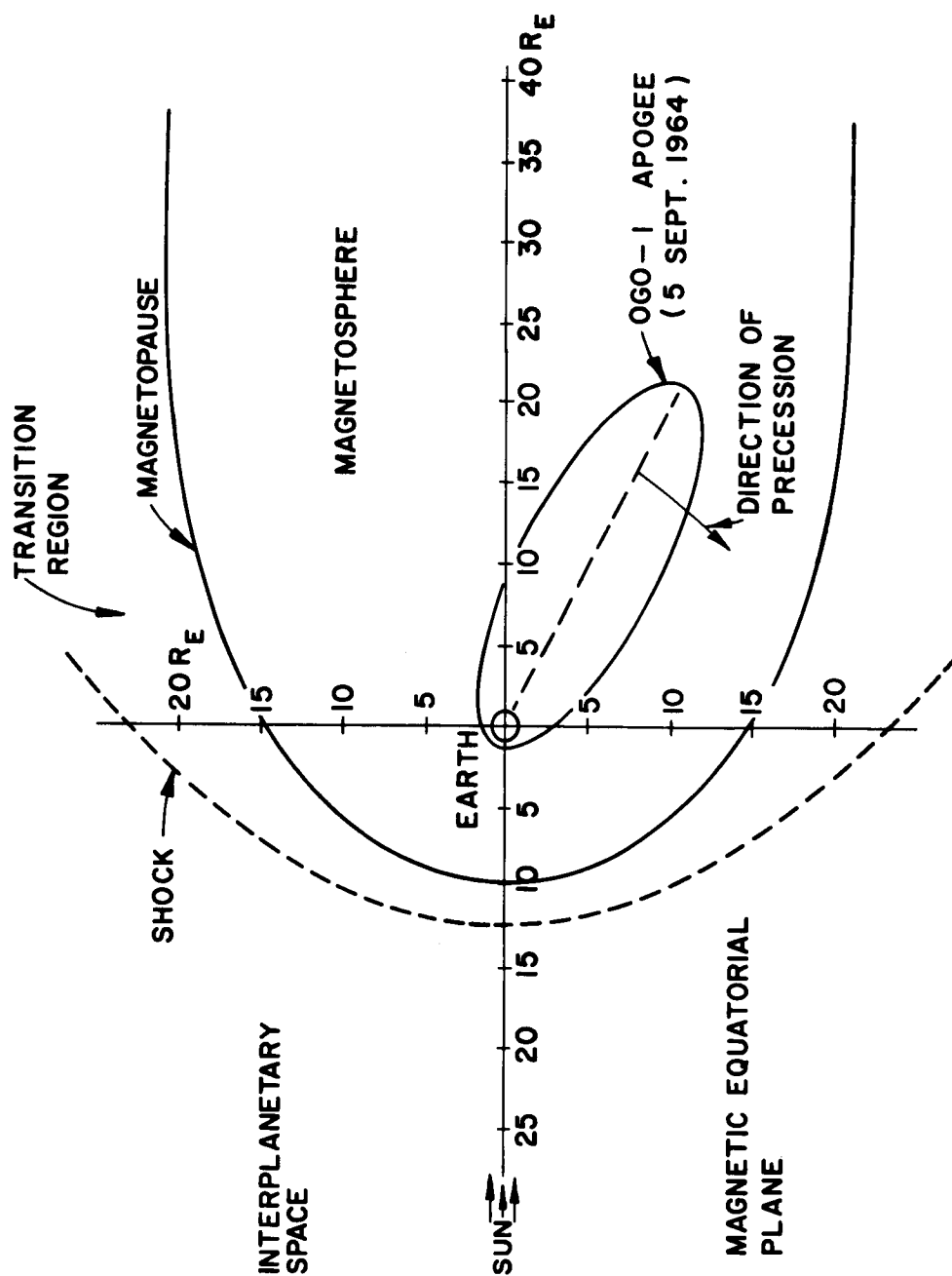
Figure 2.

the location of the satellite on the sun-earth line in the anti-solar direction.

From Figure 2 it can be seen that the initial position of the apogee corresponded to about 2200 hours local time. Since then the apogee has precessed about 4 minutes per day in the direction of decreasing local time. Thus the local time at apogee has a period of one year. Since its launch, the OGO-I satellite has completed about two and a half revolutions in local time and hence measurements are available at a variety of locations in the magnetosphere and outside it.

The OGO-III satellite was launched on June 7, 1966 in an orbit similar to that of the OGO-I satellite but with an apogee about 4 earth radii closer to the earth than that for the OGO-I satellite. Also, the orbital period for the OGO-III satellite is shorter (48.63 hours) compared to that (63.98 hours) for the OGO-I satellite. At launch the local time of the OGO-III satellite at the apogee was 2300 hours. Thus, at apogee, the OGO-I satellite is ahead of the OGO-III satellite in local time by about 4 hours.

(C) OBJECTIVES OF THE OGO IONIZATION CHAMBER EXPERIMENT

The principal objective of the ionization chamber experiment aboard the OGO-I and OGO-III satellites is to measure the

ionization due to primary cosmic rays in free space with an
accuracy and stability of about one percent. Such a measurement
when added to the previous measurements by other workers was
expected to give the variation of ionization in free space during
the solar cycle.

The other objective was to make measurements in the earth's
radiation belts and the transition region. Since the pulsing
rate of the ionization chamber in the heart of the belts was
expected to be as high as a million times the rate due to cosmic
rays in free space, it was necessary that the chamber had a
dynamic range over six orders of magnitude without sacrificing
the basic accuracy and stability of one percent for the cosmic
ray measurements. This requirement was satisfied, as described
in the next chapter, by using a vacuum tube electrometer
amplifier instead of the conventional Neher type quartz fiber
electrometer for measuring the rate of ionization in the chamber.
However, since the rate of ionization depends on the nature
as well as the energy of the particles, the interpretation
of the pulsing rate of the chamber in terms of particle fluxes
is not unambiguous unless measurements with other detectors, like
the electron spectrometer (K. A. Pfitzer, University of Minnesota)
aboard the OGO satellites, are available.

In addition to the above objectives it was hoped that the
chamber would detect x-ray bursts and solar particles associated
with solar flares. Measurements during the past two years have
revealed that the chamber did indeed detect many such events.
An extensive study of these events is being done separately.

II. DESCRIPTION OF THE OGO EXPERIMENT

(A) REQUIREMENTS AND DESIGN CONSIDERATIONS

As stated earlier the primary objective of the University
of Minnesota ion chamber experiment aboard the OGO satellite was
to measure the ionization due to primary cosmic rays in free
space and to study its variation with time. A secondary
objective was to measure the ionization in the radiation belts
and its time variation. The cosmic ray studies required an
accuracy and stability of the order of one percent. Since the
ionization due to cosmic rays is small, a large chamber with
high gas pressure was desirable. On the other hand, due to
intense radiation in the radiation belts, a small chamber with
low gas pressure was to be preferred so that the chamber-
electrometer system would not be saturated. Thus, the problem
was to design a chamber-electrometer system which could measure
cosmic ray ionization with an accuracy and stability of about
one percent and yet would not be over-loaded in the radiation
belts where the rate of ionization was expected to be over a
million times that due to primary cosmic rays in free space.

In an ionization chamber, the rate of ionization is
proportional to the rate at which the collector electrode
collects the charge. In the case of an integrating type
ionization chamber this rate of charge collection is averaged
over a time long enough so that many particles pass through
the chamber during that time. Since it is difficult to measure
the collected charge accurately, the basic measurement is

usually reduced to the measurement of the time required to collect
a fixed amount of charge. As soon as this amount of charge is
collected, the collector is somehow discharged and the process
of charge collection is repeated. Such a chamber is called a
"pulsing" type integrating chamber. The time between successive
pulses is inversely proportional to the rate of ionization
inside the chamber.

An accurate automatic electrometer system using the above
principle has been designed by Neher (1953). Several variations
of this system are now in use. Basically it consists of a
collecting rod and a gold-coated fiber fixed at one end to the
collecting rod but electrically insulated from it. This entire
assembly is located inside the chamber. Initially both the
fiber and the collector are at the same positive potential and
so the free end of the fiber stays away from the collector.
As the collector collects the electrons in the ionized gas
inside the chamber, the positive charge on the collector is
gradually neutralized causing the fiber to be attracted towards
the collector. At some stage the fiber flies towards the collector,
charges it, and consequently the fiber is repelled back to its
initial position. The whole process is then repeated.

When such a chamber-electrometer system is exposed to more
and more intense radiation, the fiber moves back and forth
more and more frequently. When the frequency of this movement
approaches the natural frequency of oscillation of the fiber,
a resonance may occur resulting in a complete or partial mechanical
breakdown of the fiber electrometer system. This effect was,

in fact, observed during the construction of the ion chambers flown on Pioneer V space probe and the Explorer VI satellite (Arnoldy, R. L., University of Minnesota Ph. D. Thesis, 1962).

The obvious way out of this problem with the chambers fitted with Neher type electrometers is to use a small chamber filled with argon at a relatively low pressure. Thus, the ionization in the chamber is small and so the chamber pulses at a rate low compared to the critical frequency. This procedure, however, seriously limits the time resolution of the chamber for cosmic ray measurements. It was therefore found desirable to reject the Neher type electrometer in favor of an electrometer system consisting of a simple collector rod and an external vacuum tube (electrometer) amplifier with its input connected electrically to the collector. In this system, as the collector inside the chamber collects charge, the output voltage of the amplifier increases proportionately. When the voltage reaches a fixed value, the input and the output of the amplifier are momentarily (3 milliseconds) shorted through a mechanical switch. This resets the output to zero volts and the process is then repeated. Thus, in this electrometer system the "pulsing" is done by a mechanical switch which is conveniently located outside the chamber. This enables one to choose a switch with high electrical resistance, high rate of operation, and long life. The inherent accuracy of a "pulsing" type electrometer is retained by measuring the time between resets. Stability of the electrometer is assured by the large feed-back loop gain. Such an electrometer system is described in detail

TABLE 2

ION CHAMBER PULSING RATE INTEGRATED OVER ONE OGO-I ORBIT

REGION OF SPACE	TIME SPENT (HOURS)	SENSITIVITY	INTEGRATED RATE* (N.Pulses x 10^3)	TOTAL NO. OF RESETS
Inner zone	1.0	Low	9×10^{10}	6×10^4
Outer zone	4.3	High	8×10^9	1×10^6
	2.7	Low	5×10^{10}	3×10^4
Space	56.0	High	1×10^7	2×10^3
Total	64.0		$\approx 10^{11}$	$\approx 10^6$

Total radiation dose ≈3500 Roentgens

*Pulsing rate not corrected for "droop" (Figure 7)

(Total corrected rate is 6.5×10^{11} N. Pulses x 10^3)

later. Its accuracy is comparable to that of the Neher type
electrometers, and it has the advantage of having a dynamic range
over six orders of magnitude.

The OGO ionization chamber experiment had to withstand
the launch environments and also to operate continuously in
space for over a year. The vacuum tube electrometer system was
found to satisfy these requirements quite well and was therefore
chosen for this experiment. An idea of the reliability of the
electrometer and the reed-relay switch which resets the ramp
can be obtained from the following estimate of the total number
of ramp resets that occurred in the OGO-I ion chamber experiment
during the period of 30 months following the launching of the
satellite. During this period the satellite completed about
338 orbits, and the ion chamber experiment was operating on about
135 of these orbits. The integrated pulsing rate during a single
orbit is shown in Table 2. Here the average time spent by the
satellite in the inner radiation zone, outer radiation zone,
and in space outside these two regions is given for one orbit
of the OGO-I satellite. Also given are the integrated pulsing
rate and the total number of ramp resets in each of the above
regions. From this table it can be seen that during an orbit
of the satellite most of the ramp resets occur in the outer
radiation zone. The total for one orbit is $\approx 10^6$ resets and,
since the experiment was operated over 135 orbits, the reed-relay
has switched $\approx 10^8$ times causing the same number of resets.
In spite of such a long operation of the reed-relay switch
and the electrometer, there is no apparent change in the calibration

of the experiment. In fact, the comparison of the OGO-I and OGO-III ion chambers during flight (given in Section D, Chapter IV) shows that the drift in the OGO-I ion chamber is ≤ 0.1 percent.

(B) CONSTRUCTION OF THE CHAMBER

The chamber consists of a spherical aluminum shell and a brass (collector) rod which protrudes inside the shell but is electrically insulated from it with the help of a glass feed-through. The spherical shell is 7 inches in diameter and was constructed from two hemispherical shells obtained by spinning a 0.035 inch thick sheet of aluminum (Aluminum Association type 3003). The thickness of the two shells varied between 0.032 and 0.035 inches. The two hemispherical shells were heli-arc welded together. A plane annular flange used for mounting the chamber on the experimental package, a cylindrical socket to hold a radioactive source, and a filling tube were then welded to the chamber.

The glass feed-through, shown in Figure 3, is a very crucial part of the chamber because the ionization current to be measured is $\simeq 10^{-14}$ amperes. In the normal operation the chamber shell is connected to -380 volts, and the collector rod is connected to the ground through a capacitor (see Figure 4). Therefore, to insure that the leakage current across the feed-through is $\leq 10^{-15}$ amperes, a feed-through with a guard-ring was used, and the latter was electrically connected to the circuit ground so that the potential of the guard-ring was always close to that of the collector rod. The glass feed-through

CHARGE COLLECTING ROD

SPHERICAL ALUMINUM SHELL

MOUNTING FLANGE

GUARD RING

GLASS
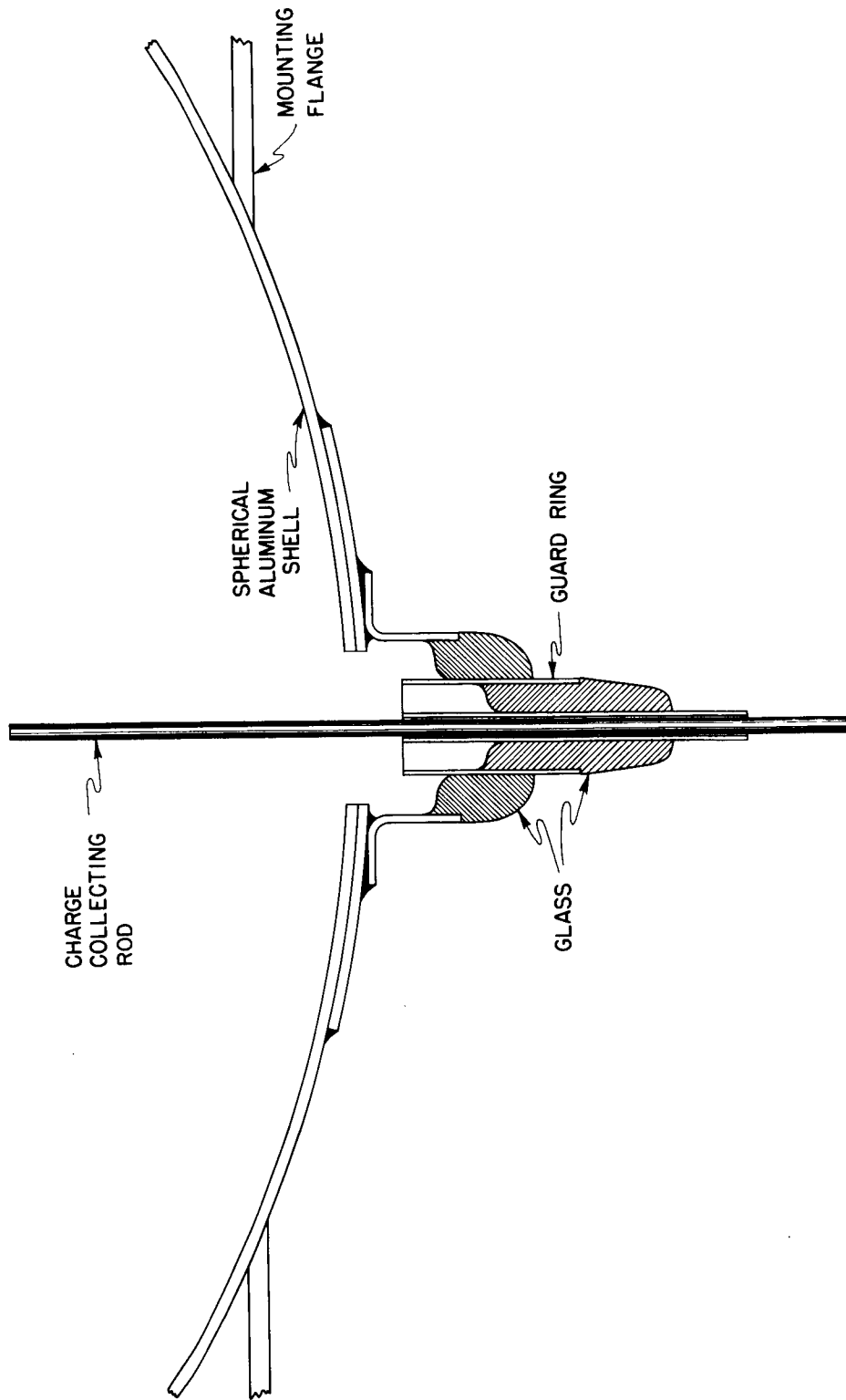
Figure 3

used on the OGO-I and OGO-III chambers were manufactured by the Carborundum Corporation, Latrobe, Pennsylvania (Part no. 95.6001). The metal flange of this feed-through was carefully "aluminum soft-soldered" to the chamber shell. The annular flange used for mounting the chamber on the experiment package surrounded the feed-through. The collector rod was soldered to the feed-through as shown in Figure 3.

It may be pointed out here that considerable difficulty was experienced in soldering the feed-through to the aluminum shell. Often the joint would develop small leaks, and at times would even develop a large crack after the chamber was pressurized. Only a very careful and patient soldering operation yielded satisfactory chambers.

Before welding, the two hemispherical shells were thoroughly cleaned with a detergent and alcohol to remove dirt and grease. After welding the chamber was rinsed with trichloro-vythene and alcohol.

The chamber was subjected to two leak tests to assure that in flight it would maintain its pressurization. First, the residual gas in the chamber when evacuated to 10^{-6} mm of Hg was sampled with a helium leak detector as helium was sprayed on the outside of the chamber to check for vacuum leaks. A second test was for loss of filling gas when the chamber was pressurized. Here, the chamber filled with helium to 60 lbs./in.^{2} pressure was placed in an evacuated bell jar for about 24 hours, and was then tested for leaks into the vacuum by the leak detector. A further test for leaks was actually obtained by
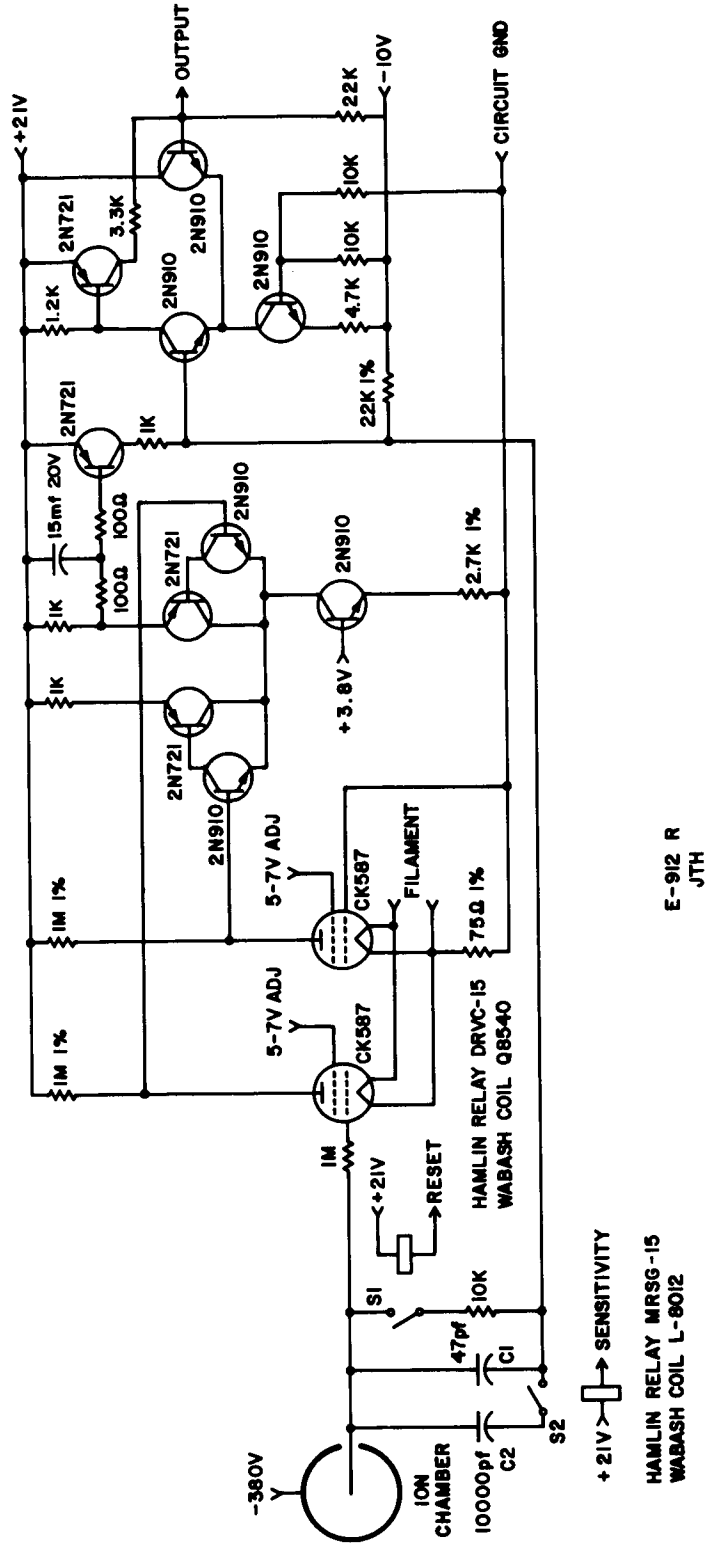
Figure 4

looking for the constancy of the chamber rate with a given radio-
active source when the experiment and the spacecraft were
subjected to thermal vacuum tests.

In preparation for flight, the OGO-I and III chambers were
first evacuated to 7×10^{-7} mm Hg and then filled to a pressure
of 50 lbs./in.^{2} and 60 lbs./in.^{2} of pure argon gas, respectively.
The maximum impurity of the argon gas used for filling was
5 parts per million of oxygen, nitrogen and carbonaceous gases.

(C) ELECTROMETER

As indicated above, the OGO ion chamber differs from those
flown on balloons and satellites in the past in that it did
not use a Neher type pulsing fiber electrometer. Instead, it
used a vacuum tube electrometer to measure the ionization current.

The details of the electrometer are shown in Figure 4. It
is a hybrid amplifier of rather standard design using vacuum
tubes and transistors. It has an internal gain of about 1000,
and gives a positive output for a negative input current. With
the capacitor C_1 connected in the feed-back loop, the amplifier
serves as an integrator, and the input grid of the first
electrometer tube is held near ground potential at all times.
The output as a function of time is a voltage ramp with its
slope proportional to the magnitude of the input current.
When the ramp reaches 5 volts a reset circuit is triggered
which closes the switch S_1. This shorts the output of the amplifier
to its input for a duration of about 3 milliseconds and resets
the output to zero volts. Thus, the output of the electrometer

is a saw-tooth voltage varying between 0 and 5 volts. This
output is fed to a low impedance output amplifier which serves
as a buffer between the electrometer and the analog-to digital
converter in the OGO spacecraft.

The sensitivity of the electrometer is inversely proportional
to the capacity of the condenser C_1. In the OGO experiment
two ranges of sensitivity are available. The condenser C_1
(47 pf) is permanently connected and provides the "high sensitivity"
mode. A much larger condenser C_2 (0.01μf) is automatically
connected in parallel with C_1 whenever the ionization current
is high, thus providing the "low sensitivity" mode.

A careful selection of the components and proper layout of
the amplifier circuit are essential for the successful
operation of the electrometer. The selection of the components
was based on required electrical characteristics and stability
with respect to variations in temperature. The integrating
condensers C_1, C_2 and the reed-relay switches S_1, S_2, being
connected between the input and the output, must have very
low leakage. Glass capacitors and reed-relays with contacts
in vacuum were found to be satisfactory. Both the reed-relays
had glass casings with a leakage resistance of $\approx 10^{15}$ ohms and
were driven by suitable solenoids. The details regarding the
type and the manufacturers are given in Figure 4. The
integrating condensers C_1, C_2 were respectively 47 pf $\pm$ 1%
(dielectric glass) and 0.01μf $\pm$ 2% (dielectric teflon) and
were manufactured by Corning Glass and Component Research
respectively.

OGO-A ION CHAMBER EXPT.
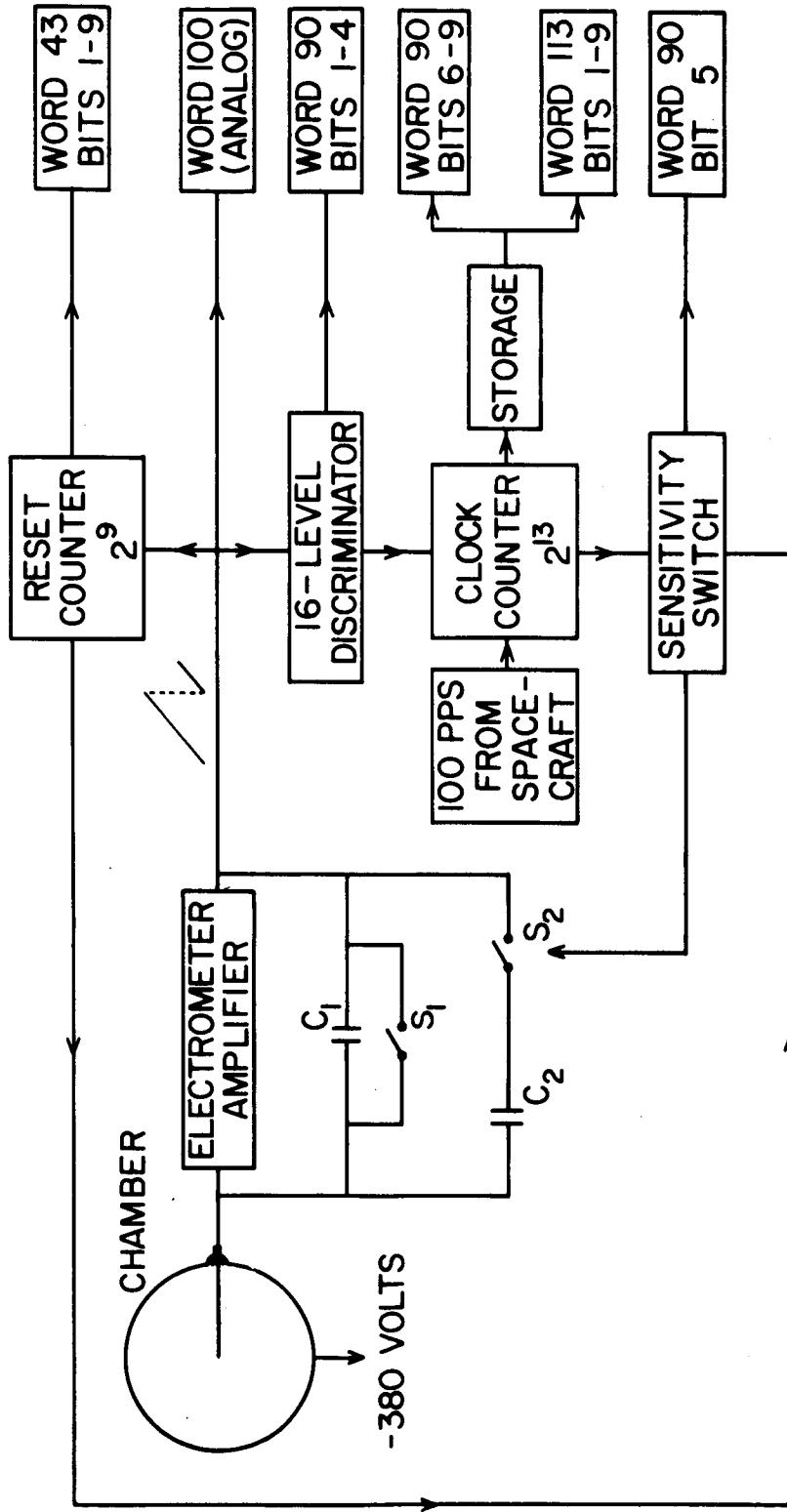
Figure 5 a

The vacuum tubes, type CK587, were chosen for low grid current, ability to withstand vibration, and long-term stability. To make a 1 percent measurement of cosmic rays which produce a current of about 10^{-12} amperes in the chamber, the electrical leakage of the chamber and electrometer system had to be $\sim 10^{-14}$ amperes. The actual leakage for both OGO-I and III chambers was $<2 \times 10^{-14}$ amperes.

(D) OPERATION AND METHODS OF DATA COLLECTION

The general arrangement is shown in Figure 5A. The shell of the chamber is connected to -380 volts and the central collector is connected to the electrometer described in the previous section. All the necessary voltages are obtained from a regulated power supply (not shown in the figure). The output ramp voltage from the electrometer is fed to a spacecraft analog-to-digital converter which reads 0 to 5 volts in 256 bits and is then telemetered through the analog word "100" of the OGO telemetry system.* Each reset of the ramp voltage is counted by a 2^9 counter and the counts are telemetered as the digital word "43" of the spacecraft telemetry system. The ramp voltage is also analyzed by a 16 level voltage discriminator and the highest level passed by the ramp at any particular moment is telemetered as the first four bits of the digital word "90". Thus, even if the ramp voltage is not directly available, it is possible to study the fine structure of the ramp with the help of the discriminator.

Time reference is available from the OGO spacecraft clock

* Computer plot of a sample "ramp" output of the OGO-III ion chamber outside the radiation belts is shown in Fig. 5b. An "ionization burst" occurred at 1404:25 UT.

OGO – II   ION   CHAMBER
15   JULY   1967

IONIZATION   BURST

14: 3: 3.24   14: 3:40.10   14: 4:16.97   14: 4:53.83

TIME   (UT)
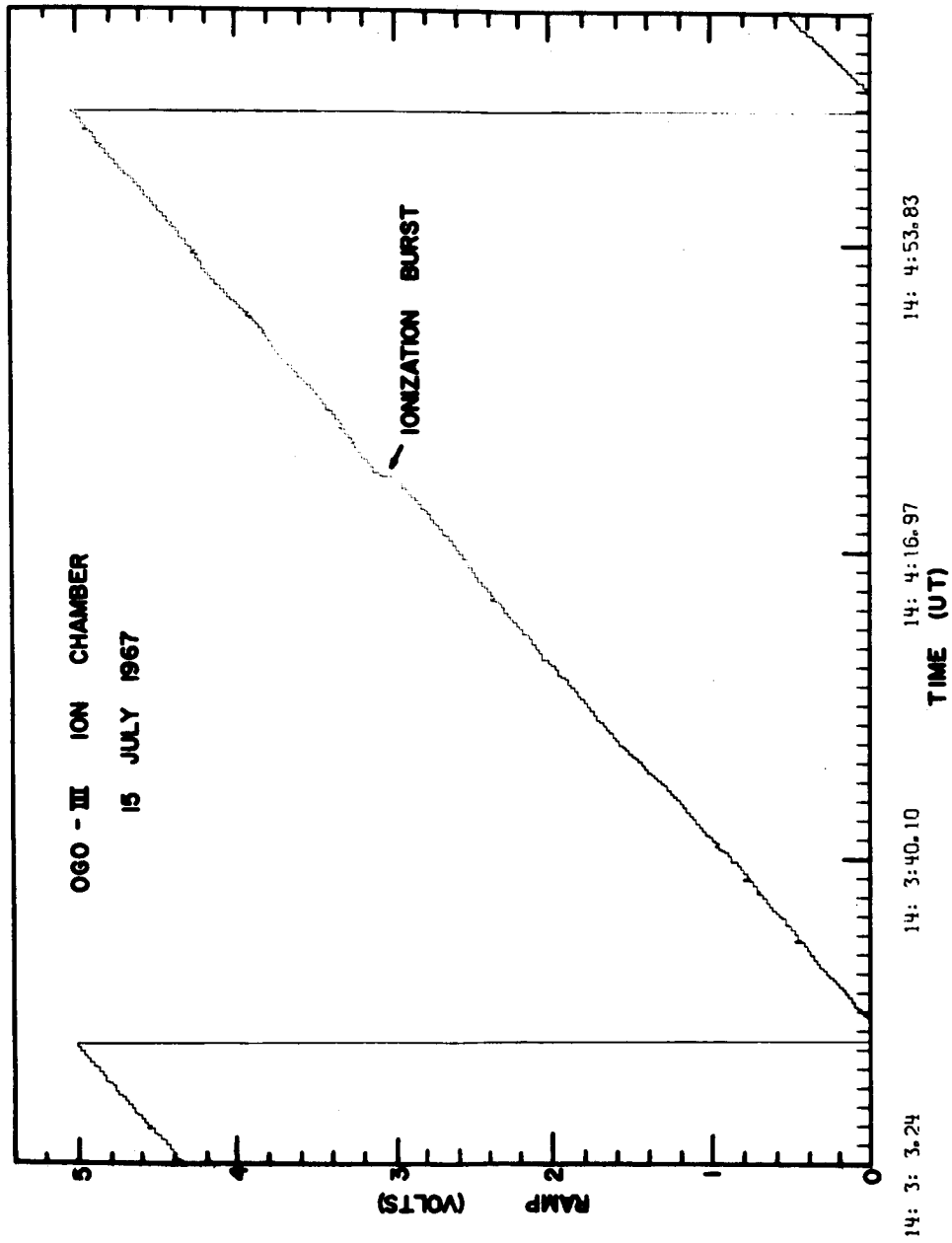
RAMP   (VOLTS)

Figure 5b

at a frequency of 100 pulses/sec. These clock pulses are
pre-scaled by a factor of 2, and are continuously counted by a
2^{13} counter. When the ramp voltage passes through the first
discriminator level, the clock counter is momentarily reset
to zero. When the ramp.reaches the 16th discriminator level,
the counts registered at that moment by the clock counter go
to the "storage" and are available through the bits 6-9 in word
"90" and the bits 1-9 in word "113". These counts are
"stored" until the ramp next passes through the 16th discriminator
level. The number of clock pulses stored at any time is thus
proportional to the time taken by the previous ramp to go
from the 1st to the 16th discriminator levels.

When the rate of ionization in the ion chamber is so large
that the ramp resets at a rate greater than 100 resets/sec,
a reset occurs between two successive clock pulses (not pre-scaled).
This condition, sensed by the "sensitivity switch", triggers
a circuit which closes the switch S_2 and connects the
condenser C_2 in parallel to the condenser C_1. Since C_2 is
about 200 times larger than C_1, the rate of resets immediately
decreases by a factor of 200, thus extending the dynamic range
of the instrument by this factor. The critical rate of 100
resets per sec was so chosen as to insure optimum performance
and long life of the reed-relay switch S_1. The switch S_2 stays
closed until the rate of ionization decreases and the ramp rises
so slowly that the clock counter is completely filled up before
the ramp reaches the 16th level. Such a condition is sensed
by the sensitivity switch which then opens the switch S_2, thus

leaving only the condenser C_1 connected across the electrometer amplifier. The information about the "ON" or "OFF" position of the switch S_2 is telemetered through the bit 5 of the word "90". The "ON" and "OFF" conditions occur at different rates of ionization. Such a "hysteresis" is purposely incorporated so as to avoid frequent switching of the condenser C_2 when the spacecraft is passing through a region where the rate of ionization is barely enough to satisfy the "ON" or "OFF" condition.

The data from the experiment is available in the form of two completely independent outputs (equipment groups), except the word 100 which is available on one equipment group only. It is therefore possible that while one output is being telemetered in real time, the other output can be connected to the tape recorder aboard the spacecraft.

(E) PRINCIPAL DIFFICULTIES ENCOUNTERED

The principal difficulties involved in the design of the experiment were:

1. Electrical leakage between the collector rod in the chamber and the chamber shell, and also between the input to the electrometer amplifier and the circuit ground.

2. Damage to the electrometer tubes during the vibration tests.

The difficulties with the electrical leakage were removed in three ways - First, by using the "feed-through" with a guard-ring to isolate the collector rod from the chamber. The

design and the use of this feed-through has been discussed
earlier. Secondly, to reduce the electrical leakage between
the input of the electrometer and the circuit ground, which
was principally due to poor electrical resistance of the
reed-relays S_1 and S_2 (see Figure 4), several available
reed-relays were tested for electrical resistance at temperatures
between -20°C and +60°C, and only those which maintained a
high resistance ($\approx 10^{15}$ ohms) throughout this temperature range
were used in the experiment. Thirdly, the entire electrometer
amplifier and the feed-through on the chamber were potted with
polyurethane foam to keep out humidity during the testing and
calibration of the experiment on the ground. The foam was
found to have excellent electrical characteristics, and the
operation of the electrometer was quite satisfactory.

The polyurethane foam also insured stability of the
components against vibration. However, when the electrometer
was mounted directly on the chamber so as to have shortest possible
input leads, the electrometer tubes (CK5889) were found to change
their electrical characteristics after the vibration tests.
After several trials this difficulty was removed by using
CK587 electrometer tubes, which are more rugged than CK5889
tubes, and by mounting the electrometer on the main box instead
of on the chamber itself as was done earlier.

(F) THE COMPLETE EXPERIMENT

The complete experimental package is shown in Figure 6.
From the left side of the figure are successively the chamber
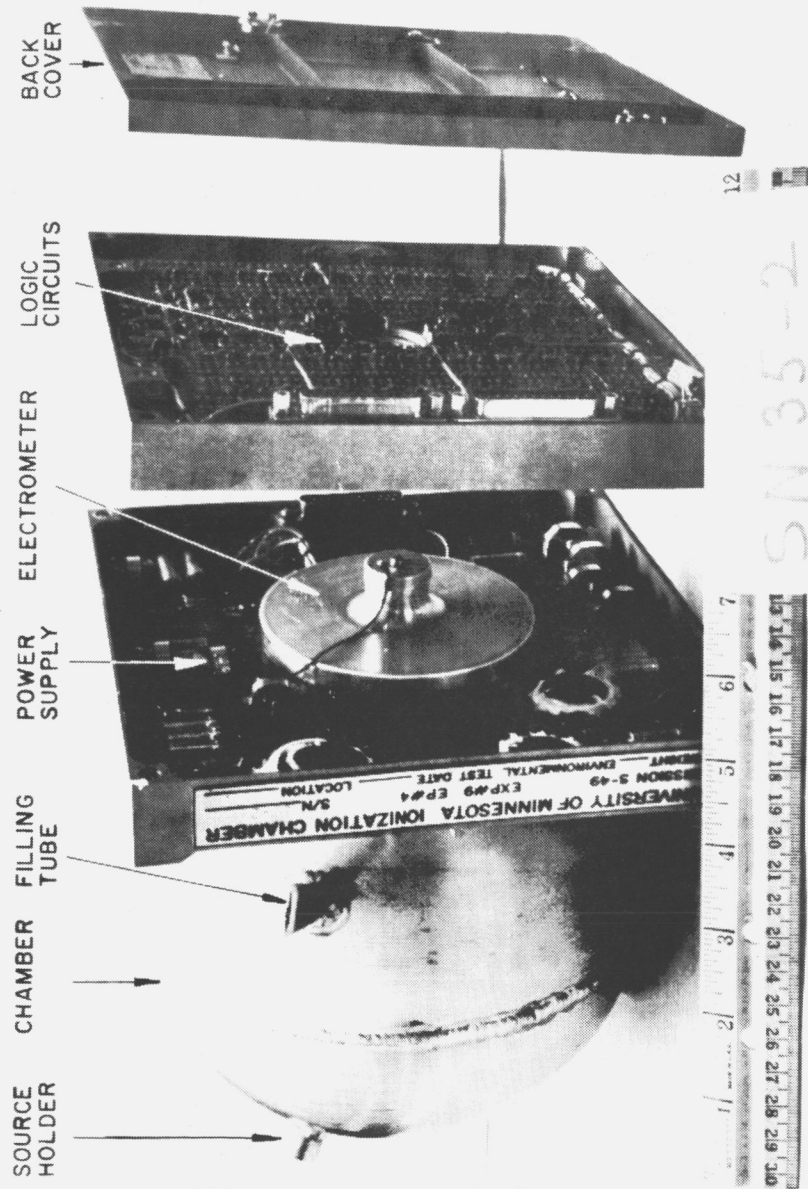
Figure 6

itself, the section of the box containing the power supply
and the electrometer amplifier (shielded by an aluminum cover),
the section containing logic circuits, and the bottom cover
with the heater and thermistor mounted on it.

The metal box (dimensions 7.5 in. x 7.5 in. x 2.5 in.)
was milled from magnesium blocks and was "anadised" to
prevent oxidation. The chamber, which was mounted on the top
section of this box, was insulated from it with the help of
teflon rings. Experience showed that this material provided
an excellent insulation between the chamber shell, which was
at a potential of -380 volts, and the magnesium box, which was
at the ground potential, even under humid conditions.

In the flight configuration the experimental package is
surrounded by a thermal blanket constructed from several layers
of aluminum mylar and plastic sheets. The total thickness of
the material is equivalent to about 0.003 inches of aluminum.
The innermost layer of the thermal blanket consists of a plastic
sheet so that the chamber shell is electrically insulated from
the aluminum mylar. In order to further prevent possible
electrical arcing between the chamber shell and the thermal
blanket, the former was coated with a thin coating of clear
epoxy.

(G) NORMALIZATION AND CALIBRATION OF THE ION CHAMBER

In the laboratory the experiment was tested with a "test
box" which consists of two parts:

1. Active part: It supplies all the necessary voltages, clock pulses, etc. to the experiment and thus simulates the spacecraft.

2. Passive part: It reads out the data collected by the experiment and displays it on number display tubes so that it can be easily interpreted.

Provisions are also made for displaying the data on a strip-chart recorder and punch-paper tape. Various parameters like supply voltages, and the amplitudes of various types of pulses available from the active part of the test box are variable, and so the test box can be used to check the performance of the experiment under widely different conditions. The various frequencies, including that of the clock pulses, are obtained from a standard crystal oscillator with a stability and accuracy of one part in a million. It was, therefore, possible to calibrate the ion chamber under conditions equivalent to those under which the experiment is operated on the spacecraft.

As stated before, the data are available in three different forms, viz.

1. The time taken by the ramp to go from the first to the sixteenth discriminator level as given by the "clock pulses" from words 90 and 113.

2. The instantaneous ramp voltage given by the analog word 100.

3. The number of ramp-resets as given by the word 43.

Correspondingly, the rate of ionization can be computed by three different methods.

1. Use of the "Clock Pulses"

Under a constant radiation source, the ramp voltage against time is a straight line with constant slope. The time ΔT taken by the ramp voltage to pass from the 1st to the 16th discriminator level is a measure of the average rate of ionization during that time. The quantity $1/\Delta T$ is defined as "number of pulses per second".

The chamber is calibrated with a radium source usually used for calibrating standard ion chambers flown on balloons for the "Continuous Monitoring Project" of the University of Minnesota (May, 1961). The pulsing rate of the OGO ion chamber is normalized so that it gives 33.28 normalized pulses/sec x 10^3 with the radium source (Callender, 1964). This is the rate of a standard continuous monitoring chamber with the same source. The OGO chamber rate normalized in this manner is called "Normalized rate".

Before launching into space the OGO-I and III chambers were calibrated many times in the laboratory with the radium source mentioned above. The results are shown in Table 3*. The time ΔT between the 1st and 16th discriminator levels was clocked manually by a stop-watch and also, whenever possible, by counting the clock pulses. Both values of ΔT are presented in Table 3 for comparison. It can be seen that the agreement is excellent. The average values of ΔT for the OGO-I and III

* Table 3 given on p. 169

chambers are 161.7 and 144.4 sec., respectively. Hence,

the "normalization factors" for the two chambers are given by

$$\text{N.F. (OGO-I)} \quad = \frac{33.28 \times 10^{-3}}{1/161.7} \quad = 5.381$$

$$\text{N.F. (OGO-III)} \quad = \frac{33.28 \times 10^{-3}}{1/144.4} \quad = 4.806$$

Therefore if ΔT be the time in seconds taken by the ramp to go

from the 1st to the 16th discriminator level when the chamber

is exposed to some source of radiation, then the average rate

of ionization in the chamber during the time ΔT is given by

N.F./ΔT Norm. pulses/sec.

Here a word about the stability of the discriminator

levels is in order. The stability of the voltages for individual

discriminator levels is determined essentially by the stability

of the power supply voltage which is regulated to $\simeq 1$ percent.

The lower discriminator levels, because of the small absolute

values of their respective voltages, are more susceptible to

variations due to noise or the changes in component characteristics

than the higher discriminator levels (see, for example, Table 5, p.179).

However, it is important to note that the only parameter used

in this method of computing the ionization is the time ΔT

taken by the ramp to go from the 1st to the 16th discriminator

levels. The accuracy of the method, therefore, depends only

on the stability of the difference between the voltages of the

1st and the 16th discriminator levels and is completely

independent of the precise values of these voltages. This method is therefore used for computing the ionization due to cosmic rays where 1% accuracy is required. This method fails at high rates of ionization because of the fast rise time of the ramp and the subsequent short time ΔT. The method yields the rate of ionization averaged over time ΔT.

2. Use of the Analog Word

Using the method (1) as the basis, the instantaneous rate of ionization can be calculated from the knowledge of the ramp voltage as a function of time. Since the difference between the voltages of the first and 16th discriminator levels is known to be 3.86 volts, we find from method (1) for OGO-I

$$\frac{3.86 \text{ volts}}{161.7 \text{ sec.}} \equiv 33.28 \times 10^{-3} \text{ norm. pulses/sec}$$

or 1 volt/sec $\equiv$ 1.39 norm. pulses/sec.

Similarly for OGO-III we get

1 volt/sec $\equiv$ 1.25 norm. pulses/sec.

This method also fails when the rate of ionization is high because of the fast rise time of the ramp.

3. Use of the "Number of Resets"

Since the ramp is known to go from 0 to 5.1 volts, for OGO-I we find from method (2),

1 ramp reset/sec $\equiv$ 7.09 norm. pulses/sec

Similarly for OGO-III one finds

1 ramp reset/sec $\equiv$ 6.37 norm. pulses/sec.

The accuracy of this method depends on the exact knowledge of the end voltages of the ramp which were found to vary by less than 3% over the entire temperature range (0°-40°C) over which the experiment operated in actual flight. This uncertainty of 3% is of little consequence because this method of computing the ionization is used only when the rate of ionization is very high as in the Van Allen radiation belts or solar proton events.

As mentioned earlier, the OGO ion chamber experiments were calibrated several times with the standard radium source used for calibrating the ion chambers flown on balloons. To obtain the normalized pulsing rate one or more of the above methods were used. However, the use of clock pulses was preferred whenever possible because of their higher accuracy. Results of some of the calibrations for the OGO-I ion chamber experiment made after it had passed the "flight acceptance test" at the Goddard Space Flight Center, Greenbelt, Maryland are presented in Table 4. It can be seen that all the radium source calibrations are within $\pm$ 0.65% of the standard rate of 33.28 norm. pulses/sec x 10^3.

In order to insure that the characteristics of the electrometer amplifier did not change with time, the drift of the electrometer was measured frequently up to the time of launching the satellite. Some of the measurements are listed in Table 4.

TABLE 4

OGO-I ION CHAMBER CALIBRATION

| DATE | *NORM. PULSES/SEC x 10^3 | | ELECTROMETER DRIFT |
	STANDARD Ra	Sr^{90}	10^{-14} AMP.
30 Aug. 1963		40.06	
3 Sept. 1963		39.01	
23 Sept. 1963	33.15		1.49
30 Sept. 1963	33.39		1.62
9 Oct. 1963	33.26		1.45
11 Oct. 1963		38.61	1.00
14 Oct. 1963		39.23	
15 Oct. 1963	33.49		
19 Oct. 1963	33.38	39.31	1.85
22 Oct. 1963	33.24	39.28	1.29
28 Oct. 1963	33.26	38.98	1.00
2 Nov. 1963	33.13	38.98	
5 Nov. 1963		39.23	2.00
10 Dec. 1963		39.05	1.00
21 Jan. 1964		37.93	1.56
15 May 1964	33.42	39.29	
15 July 1964		39.67	1.04
21 July 1964		38.03	
28 July 1964		38.88	1.56
7 Aug. 1964		38.38	0.52
29 Aug. 1964		40.47	0.52

COSMIC RAY IONIZATION IN SPACE $\approx 2 \times 10^{-12}$ AMP.

*Rates deduced from the "clock" time.

It can be seen that during the course of about one year the electrometer drift was fairly constant, and at all times the drift was less than 1% of the ionization current due to cosmic rays in free space (2×10^{-12} amperes). On the ground the ionization current due to the cosmic ray background radiation is about 6×10^{-15} amperes (deduced from measurements by Shamos and Liboff, 1966) which is about 40 percent of the average electrometer drift. The background due to radio-activity in the vicinity of the chamber is also believed to be of the same order. Thus, for the OGO-I electrometer the above two background radiations account for most of the drift.

In general, a drift of 10^{-14} amperes is inherent in an electrometer of the type described here. The drift could be either negative or positive. The principal requirements for an acceptable electrometer are that the drift should be of this order and must remain constant over long periods of time.

A Sr^{90} source was used as a "secondary" standard for calibrating the OGO-I ion chamber. This source could be fitted right on the chamber and was, therefore, convenient for calibration during the various pre-launch check-outs. The results of some of these calibrations are also presented in Table 4. It can be seen that during the one year period (a) the change in the chamber calibration was <3.5%, and (b) there was no systematic decrease in the chamber rate as would occur if the chamber shell developed a small leakage. Fortunately, simultaneous measurements with OGO-I and OGO-III ion chambers in actual flight are available and are found to agree within 0.1% although OGO-III was launched 21 months after the launch

of OGO-I (see Chapter IV, Sec. (D)). This indicates that it has been possible to achieve the desired accuracy of 1 percent for the chamber calibration as stated in the objectives of the OGO experiment (see Chapter I, Sec. (A)).

(H) RELIABILITY TESTS

In order to insure reliable operation of the OGO-I and III ionization chamber experiments, they were subjected to several reliability and performance tests. These tests were based on the requirements set up by the OGO Project Office at the

Goddard Space Flight Center (GSFC), Greenbelt, Maryland.
They represented the environmental variations under which the
experiments were expected to operate during the actual flight
of the spacecrafts. The principal tests were

    1. Interface

    2. Vibration

    3. Thermal vacuum

    4. Interference

In each of these tests the ion chamber experiment was electrically
connected to a "spacecraft simulator" and the experiment was
operated with a suitable radioactive source located at a fixed
position relative to the chamber. In most cases a Sr^{90} source
was placed in the holder on the chamber shell especially provided
for this purpose. While checking the electrometer leakage
(drift) this source, of course, was removed. The "clock time",
ramp time, minimum and maximum values of the ramp voltage, and
the voltages corresponding to the 16 discriminator levels were
recorded by the spacecraft data system during each test. This
data was then printed out and checked for variations of the
characteristics of the experiment during the test. The tests
themselves are briefly described below.

The interface test was made to determine if the electrical
interface between the main spacecraft and the ion chamber
experiment was satisfactory. During the test the various
electrical parameters available from the spacecraft (for
example, magnitude of the supply voltage, shape and size of

the clock pulses) were varied and the effect of these variations on the performance of the experiment was determined.

In the vibration test the experimental package was mounted on a "vibration-table" and was subjected to sinusoidal (10-2000 cps) and random vibrations inducing accelerations up to a peak value of 20 g. The experiment was checked for normal operation before and after the test.

In the thermal vacuum test the experiment was placed inside a sealed enclosure. The latter was evacuated to a pressure of 10^{-6} mm of Hg and its temperature was first maintained at 0° C and then at 40° C. At both these temperatures the experiment was tested for normal operation.

The interference test was designed to determine if the presence or operation of other experiments on the spacecraft or the operation of the spacecraft systems themselves affected the performance of the ion chamber experiment. The experiment was operated continuously while the other experiments or the spacecraft systems were turned on and off one by one and the ion chamber data was examined for the possible interference.

The exact specifications of the above tests are given in the relevant GSFC (NASA) bulletins. Due to lack of space it is not possible to give here the results of all these tests. For illustration we give in Table 5* the results of the thermal vacuum test for the OGO-I chamber experiment. The total test lasted for about 24 hours. During this time the data was read out several times at some suitable intervals. Each such read-out is called a "data run" in Table 5. From that table the following facts may be noted.

* Table 5 given on p. 189.

1. The vacuum does not affect the performance of the experiment.

2. At a particular temperature, the different data runs made over a period of several hours are self-consistent.

3. At the two extreme temperatures the average "clock time", i.e. the time between the 1st and 16th discriminator levels as determined from the counted "clock pulses", agrees within 1.2 percent. The ramp time (the time between the ramp resets) agrees within 2.8 percent and the various discriminator level voltages agree within 6.4 percent. The agreement between the differences in these levels is much better.

The above tests were conducted both at Minneapolis and at GSFC, Greenbelt, Maryland, and were considered as "flight acceptance tests". The tests conducted at Minneapolis were somewhat more severe than those at GSFC. For example, although the "official" thermal vacuum test described above included a variation of temperature from 0°C to 40°C, during the tests conducted at Minneapolis the experiment was operated in the range -10°C to 50°C and the performance was found satisfactory.

In addition to the above tests, the experiment was subjected to an "endurance test". This was designed to investigate the following aspects:

1. Effect of switching the experiment ON inside the radiation belts where the radiation is so intense that

the ionization current in the OGO chamber is about
one micro-ampere.

Because of the large ionization current the voltage across
the capacitor at the input of the electrometer was expected to
increase rapidly and tend to attain the full voltage (-380 volts)
applied to the chamber unless it was periodically reset to zero
by the electrometer. It was feared that if the experiment is
turned on in the radiation belts and the high voltage happens to
be applied to the chamber before the electrometer starts functioning,
the large voltage across the capacitor may cause a breakdown in
its dielectric.

2. Effect of frequent switching ON and OFF.

In this test the chamber was disconnected from the electrometer.
Instead a 10^9 ohm resistance was connected between the high
voltage (-380 volts) and the input to the electrometer. This
was equivalent to an ionization current of 0.38 micro-amperes.
The supply voltage (28 volts) to the entire experiment was
then switched ON and OFF periodically with the help of a timing
circuit. No damage to the experiment was noticed as a result
of this test. This is further borne out by the fact that the
OGO-I and III ion chamber experiments have operated successfully
in space for more than 30 and 9 months respectively and have
not yet developed any malfunction.

III. RESPONSE CHARACTERISTICS

(A) DYNAMIC RANGE AND LINEARITY OF RESPONSE

Although the principal objective of the OGO ion chamber experiment was to measure the ionization due to primary cosmic rays outside the magnetosphere, it was thought desirable to design the experiment in such a way that useful measurements could be made also in the radiation belts. This was particularly important because the University of Minnesota has also an electron spectrometer aboard the same satellite (Kane et al., 1966). Therefore, there existed an interesting possibility of comparing and complementing the measurements made with these two completely independent experiments.

To achieve this aim, it was necessary for the ion chamber experiment to have a large dynamic range. On the basis of previous measurements by workers at this University and elsewhere, the peak ionization in the radiation belts was expected to be about 10^6 x the cosmic ray ionization in free space. A "sensitivity switch", described earlier, was therefore incorporated in the experiment. Total dynamic range attainable with this device is over six orders of magnitude. It should be mentioned here that this large dynamic range of the ion chamber does in no way affect its basic accuracy of about 1% for the cosmic ray measurements.

To test the dynamic range and linearity of the OGO ion chamber, it was exposed to a wide range of radiation dosage at the γ-ray facility of the University of Minnesota. The
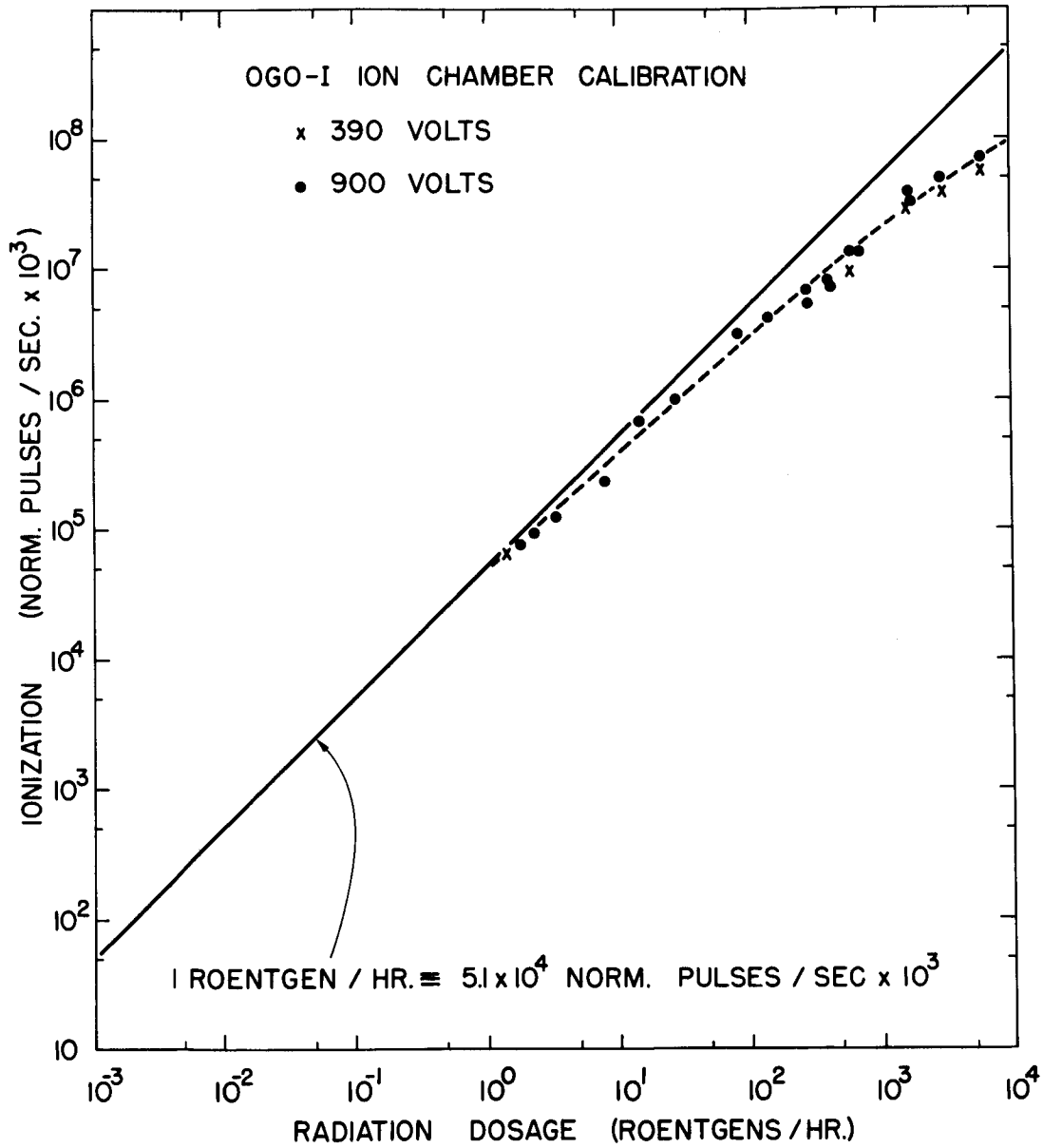
Figure 7

results obtained are shown in Figure 7. Here the normalized
pulsing rate of the ion chamber is plotted against the
radiation dosage as measured by suitable Victoreen R-meters.

The relation between the ion chamber rate and the dosage
as expected on the basis of the definition of "roentgen" is
shown in Figure 7 by the solid line. This relation is obtained
in the following manner. Let

w = 26.4 eV = energy required to produce an ion pair in argon,

M = 38.4 g = total mass of the argon in the standard ion chamber,

q_o = 0.67 x 10^{-10} coulombs/normalized pulse for the standard chamber (May, 1961),

e = 1.61 x 10^{-19} coulombs = electronic charge.

Then an energy loss E ergs/g in argon would give rise to

$$\frac{M\,E\,e}{1.6 \times 10^{-12}\,w\,q_o} \quad \text{norm. pulses} \qquad (3\text{-}1)$$

Now, 1 roentgen implies an energy loss of 84 ergs/g in air at
STP. If we assume that at the γ-ray energies of interest the
mass absorption coefficient of air and argon are nearly equal,
we get

1 roentgen/hr. $\equiv$ 51 norm. pulses/sec. $\qquad (3\text{-}2)$

This linear relationship is shown by the solid line in Figure 7.
It can be seen that for a radiation dosage of 1 roentgen/hour, the
observed and computed response are in good agreement. However, at
higher dosages the observed response is non-linear and falls
below the expected value. This is believed to be due to the loss

of ions because of the "volume recombination" in the chamber gas. The rates measured in the radiation belts are corrected for this effect in the following manner.

Let I_c and I be, respectively, the "correct" (solid line in Figure 7) and the observed ion chamber rate corresponding to a radiation dosage D. Then, from Figure 7, for D in roentgens/hr.,

$$I_c = 5.1 \times 10^4 \, D \text{ norm. pulses/sec} \times 10^3 \qquad (3\text{-}3)$$

For rates $\leq 4 \times 10^4$ norm. pulses/sec $\times 10^3$, $I = I_c$, but for rates $\geq 4 \times 10^4$ norm. pulses/sec $\times 10^3$,

$$I \simeq 4.7 \times 10^4 \, D^{0.87} \text{ norm. pulses/sec} \times 10^3. \qquad (3\text{-}4)$$

Eliminating D, between (3-3) and (3-4) we get the corrected rate

$$(3\text{-}5)$$
$$I_c = 5.1 \times 10^4 \left[\frac{I}{4.7 \times 10^4} \right]^{1.16} \text{ norm. pulses/sec} \times 10^3.$$

Note that this correction is necessary only for the observed ion chamber rates $\geq 4 \times 10^4$ norm. pulses/sec $\times 10^3$.

If the ionization is produced by charged particles with energies only slightly higher than the minimum energy for penetrating the chamber wall, most of the ions are formed close to the wall where the electric field is very low. Consequently, a considerable fraction of the ions may be lost due to recombination. Unfortunately, this effect would not be expected to show in the high dosage γ-ray calibration discussed

previously, because the γ-ray ionization is produced uniformly throughout the volume of the chamber. In the outer radiation belt, however, where one encounters a steeply falling spectrum of electrons, the effect may be very important. So far, no direct laboratory measurements have been made with electron fluxes similar to the radiation belts.

(B) RESPONSE TIME

In order to make an estimate of the response-time characteristics of the OGO ion chamber a rotating wheel was interposed between the ion chamber and a beam of electrons with energies between 0.1 and 2.2 MeV obtained from a Sr^{90} source. The wheel was made of 1 cm thick aluminum and had a small hole which would periodically expose the chamber to the Sr^{90} source. Thus the chamber could be exposed to a burst of electrons, the duration of the burst being about 0.2 seconds. The response of the chamber was determined from the instantaneous slope of the output ramp voltage. The results obtained are shown in Figure 8. Here the relative response of the chamber is plotted against time after the beginning of the electron burst. It can be seen that most of the chamber response to the burst is concentrated at times $t \leq 2$ seconds.

An opportunity to determine the time resolution possible with the OGO ionization under actual flight conditions in space was provided by the solar x-ray burst which occurred at 0954 UT on 20 March 1966 and was detected by the OGO-I ion chamber.
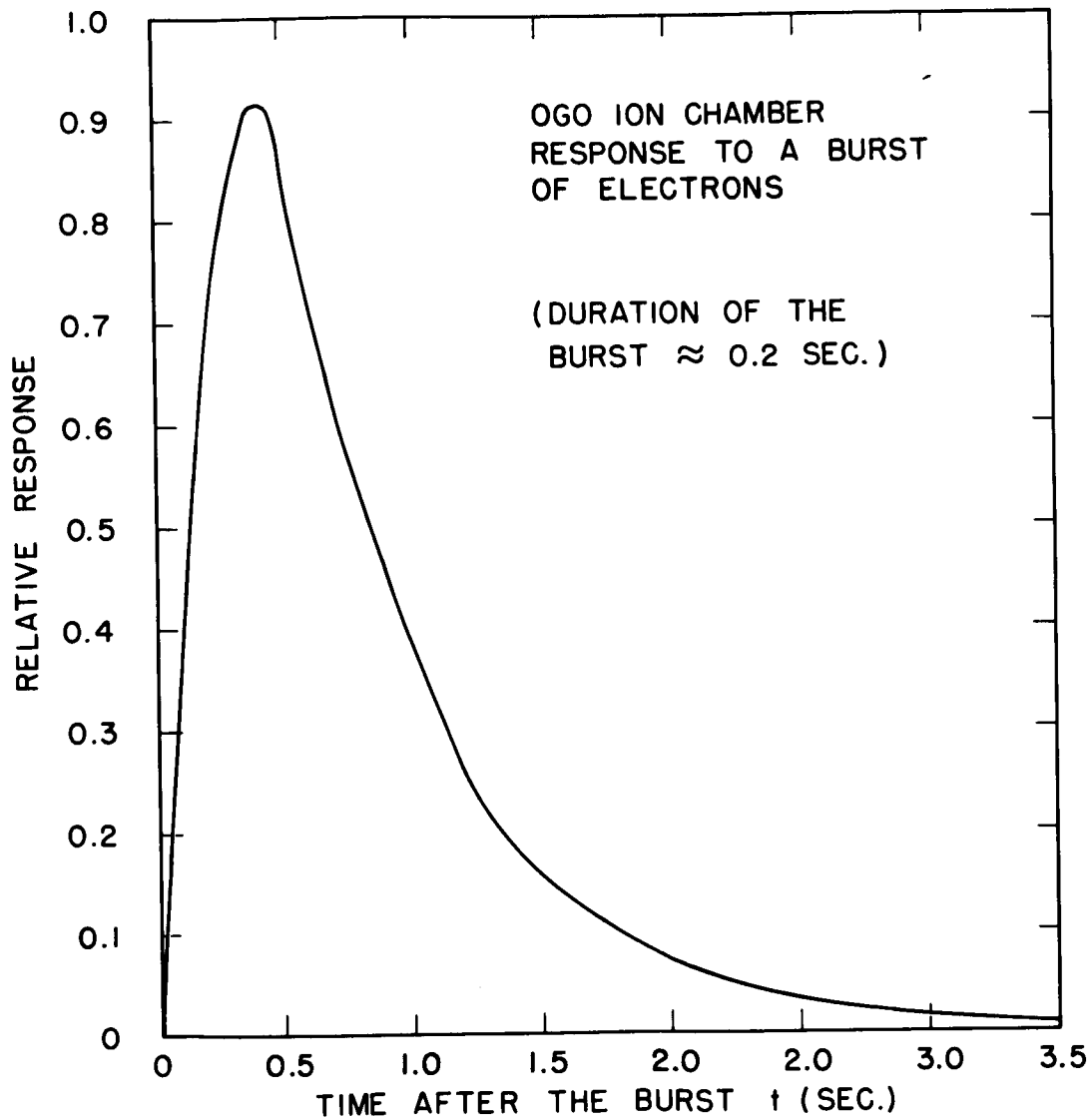
Figure 8

As stated earlier the ion chamber experiment is mounted on a boom which extends 4 feet from the OGO spacecraft in a direction nearly perpendicular to its spin-axis. Therefore, so far as the ion chamber is concerned, a beam of x-rays moving in a direction perpendicular to the spin axis of the spacecraft will be completely occulted by the main body of the spacecraft once in every spin revolution. If the direction of the beam is not exactly perpendicular to the spin-axis, the occultation may be partial, except when the beam is nearly parallel to the spin-axis, in which case there will be no occultation at all. Thus, in general, a part of the x-ray beam is occulted from the chamber once in each spin revolution. Therefore, during a solar x-ray burst the pulsing rate of the chamber is expected to show sudden decreases once every spin period, i.e. once in 12 seconds.

The observed pulsing rate of the OGO-I ion chamber during the x-ray burst on 20 March 1966 is shown in Figure 9. Here the 1.15 second averages obtained from the analog data are plotted against Universal Time (UT). It can be seen that during the event the chamber rate did show a roll modulation with a period of 12 seconds. We may therefore conclude the following:

1. During the time period 0954-1006 UT on 20 March 1966 the OGO-I ion chamber was responding to a (uni-directional) beam of radiation as is expected in a solar x-ray burst.

54
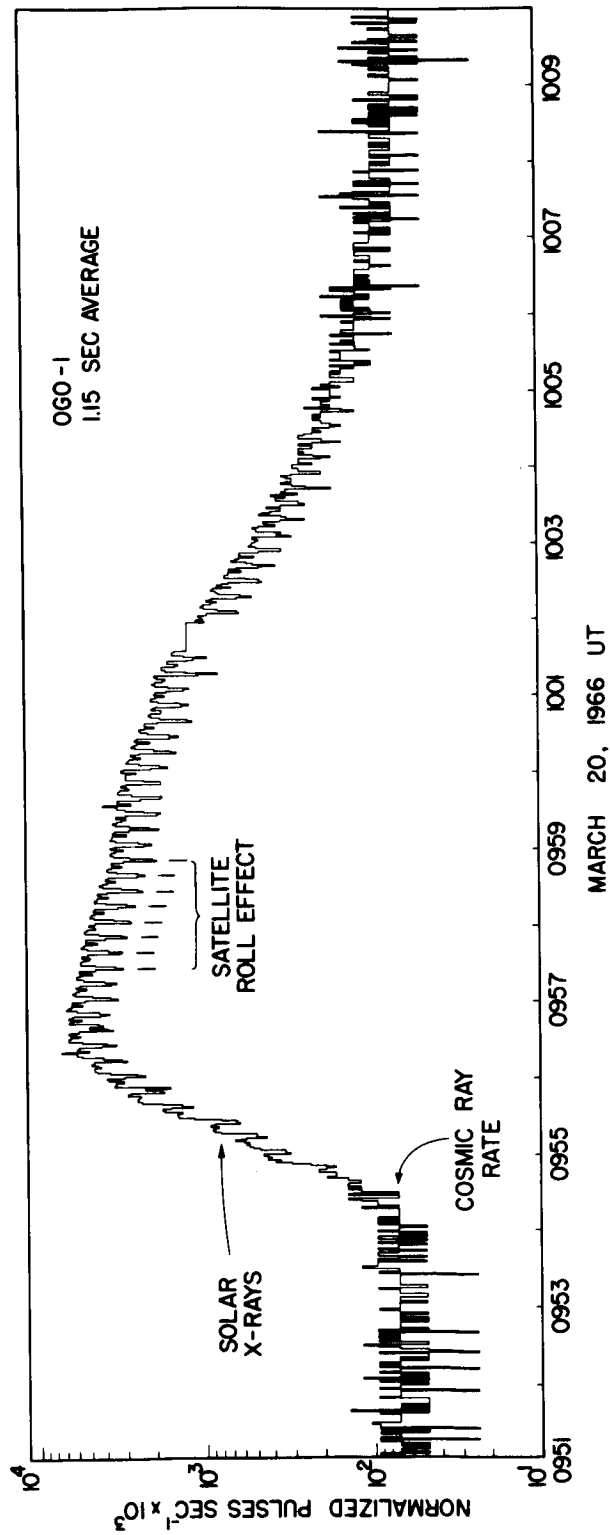
Figure 9

2. The time resolution of the chamber is such that it
    can respond to variations with a period ≥ 12 seconds.

(C) CORRECTION FOR THE DEAD-TIME OF THE RESET SWITCH

As mentioned earlier, the ramp is reset by a reed relay
switch which remains closed for about 3 milliseconds. This
introduces an error in the observed time between resets. The
error can be estimated in the following manner.

Let T_o sec be the dead-time and T sec the observed time
between resets. Then the true time between resets is

$$T_c = T - T_o \text{ sec.}$$

Since the ionization rate is known as a function of the time
between resets, one obtains the correction curve shown in
Figure 10. Here, the corrected ("true") rate is plotted against
the observed rate.

In this connection it is important to note the following:

1. No correction is needed when the chamber rate is
    computed from the clock pulses, as in the case of
    cosmic ray measurements.

2. The correction is significant ($>3\%$) for ramp times
    $\leq$ 100 milliseconds which usually occur inside the
    radiation belts and only in the high sensitivity mode.
    The correction is highest ($\approx 30\%$) when the sensitivity
    is about to switch from "high" to "low" mode, (shown
    by dashed line in Figure 10), no correction being needed
    after the switching takes place.

OGO – A ION CHAMBER
(HIGH SENSITIVITY MODE)

TRUE RATE 10^5 (NORM. PULSES / SEC x 10^3)

OBSERVED RATE 10^5 (NORM. PULSES/SEC x 10^3)
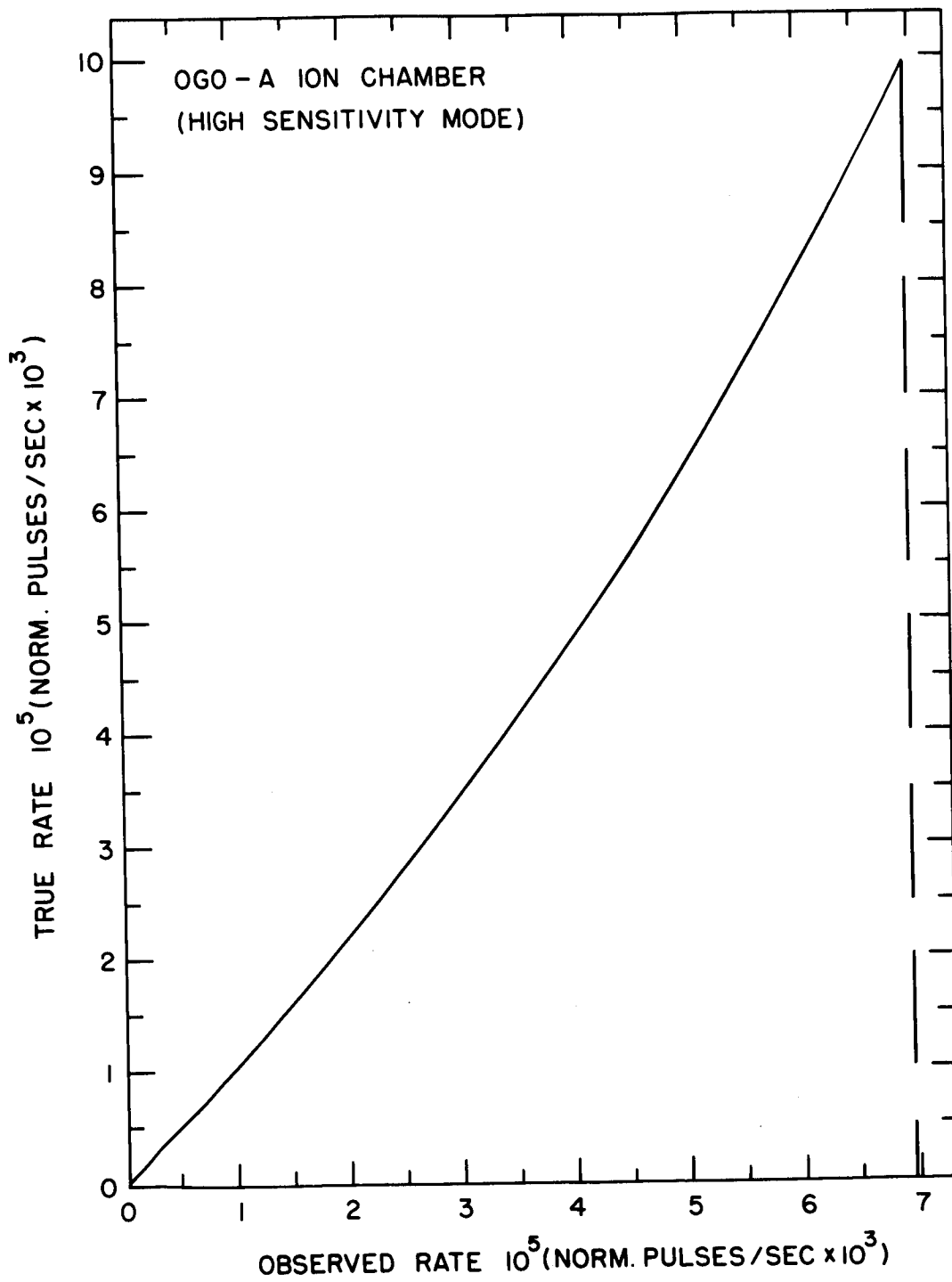
Figure 10

(D) RELATION BETWEEN PULSING RATE AND ENERGY DEPOSITED

Let I norm. pulses sec^{-1} be the pulsing rate of the OGO-I

ion chamber when it is exposed to some radiation. If ΔE MeV sec^{-1}

be the rate at which energy is deposited in the chamber, we

wish to find the relationship between I and ΔE.

Now the OGO-I ion chamber contains argon at a pressure

of 50 lbs/in^2 while the standard ion chamber, to which all

the observed ion chamber rates are normalized, contains argon

at a pressure of 115 lbs/in^2. Hence the equivalent energy

deposited in the standard chamber is $\frac{115}{50}$ ΔE MeV sec^{-1}. Since

an energy of 26.4 eV is required to form an ion pair in argon,

the resulting production of ion pairs is

$$\frac{115 \times 10^6}{50 \times 26.4} \ \Delta E \ \text{ion pairs} \ sec^{-1}$$

Hence the rate of charge collection is

$$\Delta q = \frac{115 \times 10^6}{50 \times 26.4} \ \Delta E \times 1.6 \times 10^{-19} \ \text{coulombs} \ sec^{-1} \quad (3-6)$$

where $e = 1.6 \times 10^{-19}$ coulombs is the electronic charge.

Since the "normalized charge per pulse" for the standard chamber

is 0.67×10^{-10} coulombs (May, 1961) the normalized pulsing

rate is given by

$$I = \frac{\Delta q}{0.67 \times 10^{-10}}$$

$$= 0.208 \times 10^{-3} \ \Delta E \ \text{norm. pulses} \ sec^{-1} . \quad (3-7)$$

Note that ΔE MeV sec^{-1} is the rate at which energy is deposited

TABLE 6

ION CHAMBER	a (NORM. PULSES MEV^{-1} x 10^3)	I_O (NORM. PULSES x 10^3)	E_O (BEV)
OGO-I	0.208	5381	25.9
OGO-III	0.173	4806	27.8

in the OGO-I chamber. The desired relation between the observed ionization and energy deposited is given by

$$a = \frac{I}{\Delta E} = 0.208 \times 10^{-13} \text{ norm. pulses/MeV} . \qquad (3-8)$$

A quantity of interest is the total energy deposition required to cause the ramp voltage to go from the first to the sixteenth discriminator level. Let T be the "clock" time, i.e. the time taken by the ramp to go from the first to the sixteenth level, when the OGO-I ion chamber is exposed to the radiation considered above. Then the pulsing rate of the chamber is given by (see Chapter II, Section (G))

$$I = \frac{5.381}{\Delta T} \text{ norm. pulses sec}^{-1} .$$

Hence, we get

$$0.208 \times 10^{-3} \Delta E = \frac{5.381}{\Delta T}$$

Therefore the total energy deposited during the time ΔT is

$$E_O = \Delta E \, \Delta T = 2.59 \times 10^4 \text{ MeV} \qquad (3-9)$$

and the total ionization is

$$I_O = I \, \Delta T = 5.381 \text{ norm. pulses} \qquad (3-10)$$

Note that the quantities a, E_O, and I_O are constants for a given chamber experiment. Their values for the OGO-III ion chamber can be evaluated in a similar manner. For later reference these three constants for the OGO-I and OGO-III ion chambers are given in Table 6.

(E) RESPONSE TO PROTONS AND HEAVIER NUCLEI

Since the primary object of the OGO ion chamber experiment
is to measure the ionization due to primary cosmic rays, it
is of interest to compare the observed ionization with the one
that we would expect on the basis of a simple calculation of
the ionization loss of these particles in the sensitive volume
of the ion chamber. As a first step in this direction we
proceed to calculate the pulsing rate of the ion chamber due
to an isotropic flux 1 particle/cm^2 sec of mono-energetic particles
of a particular charge Ze. We begin by considering the
ionization due to such a flux of protons. To simplify the
calculation we will assume that the relation between the
range (g cm^{-2}) and energy (MeV/nucleon) of a particle is
nearly the same in argon as in aluminum.

1. Response to Protons

(a) The Energy Loss of an Individual Particle:

Figure 11 shows the schematic diagram of an ion
chamber in free space. Let t_o cm be the thickness of the
chamber wall and r cm the inner radius of the chamber. Suppose
a proton with kinetic energy E MeV is incident on the chamber
in a direction such that the perpendicular distance between
the center of the chamber and the path of the particle is y.
We can call y the "impact parameter". The effective thickness t
of the chamber wall and the maximum possible path length 2x cms
in the chamber gas depend on y and are given by:

$$t(y) = \sqrt{(r + t_o)^2 - y^2} - x(y) \quad cm \qquad (3\text{-}11)$$

$$2x(y) = 2\sqrt{r^2 - y^2} \qquad (3\text{-}12)$$

61
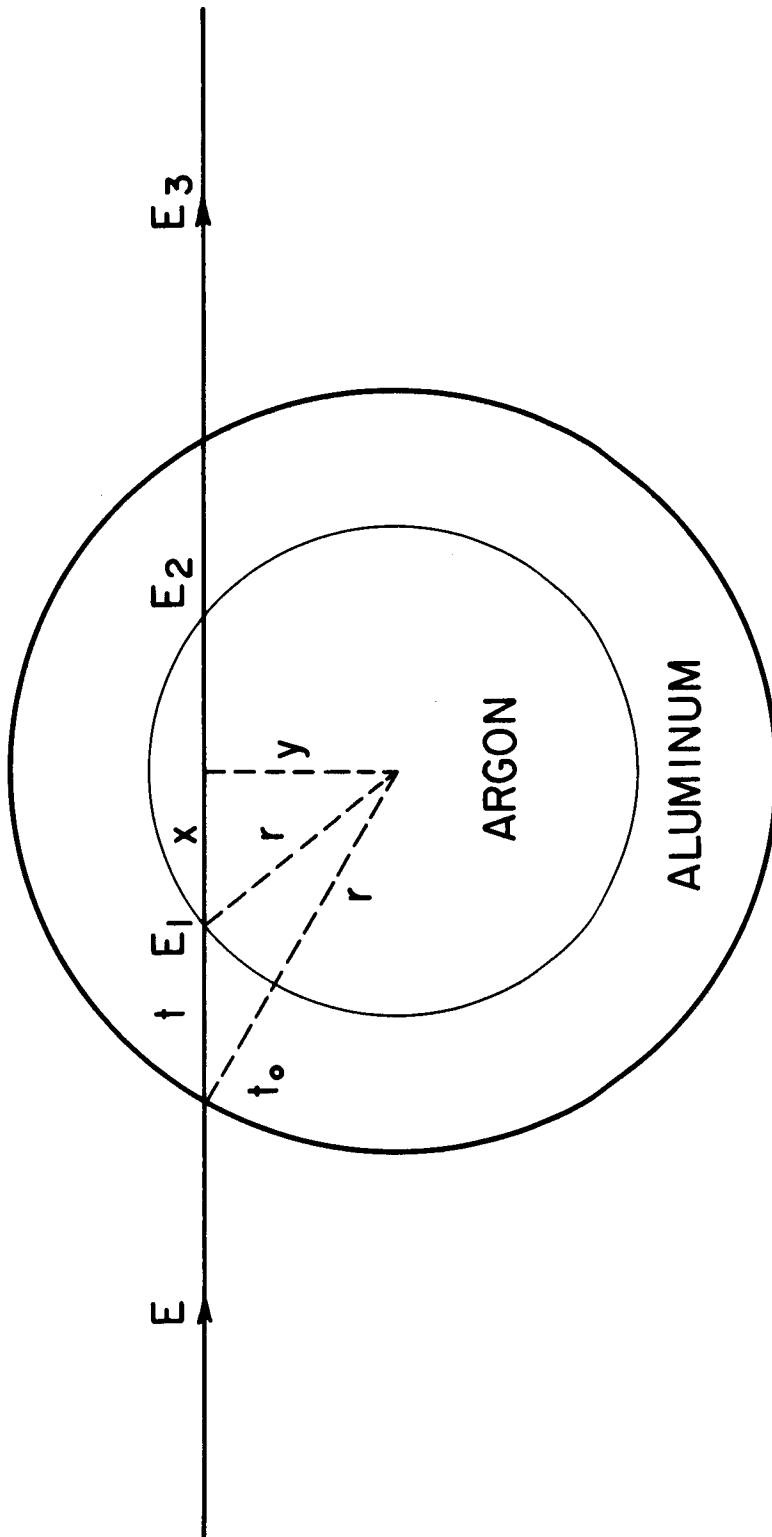
t_o = THICKNESS OF THE ALUMINUM WALL

r = INNER RADIUS OF THE CHAMBER

Figure 11

The residual range of the proton after penetrating the wall is given by:

$$R_1(E,y) = R(E) - \rho_{Al} \, t(y) \quad g \, cm^{-2} \qquad (3\text{-}13)$$

where R is the initial range of the incident proton and ρ_{Al} is the density of aluminum in $g \, cm^{-3}$. Let E_1 be the energy of the proton corresponding to the range R_1. E_1 can be found from the range-energy tables given, for example, by Yuan and Wu(1961a).

Let ρ_{Ar} be the density in $g \, cm^{-3}$ of the argon gas in the ion chamber. If $R_1 < 2x\rho_{Ar} \, g \, cm^{-2}$ the proton will not be able to go all the way across the chamber, and its energy loss in the chamber gas will be E_1 MeV. Even if $R_1 = 2x\rho_{Ar} \, g \, cm^{-2}$ the proton will be just able to go across the chamber gas and so the energy loss will still be E_1 MeV. However, if $R_1 > 2x\rho_{Ar} \, g \, cm^{-2}$, the particle will go beyond the chamber gas and may even come out of the chamber. In this case, the "residual range" R_2 of the proton after it crosses the chamber gas is given by:

$$R_2(E,y) = R_1(E,y) - 2\sqrt{r^2-y^2} \cdot \rho_{Ar} \, g \, cm^{-2} \qquad (3\text{-}14)$$

If E_2 be the corresponding "residual energy" of the proton, its energy loss in the chamber gas is given by:

$$\Delta E(E,y) = E_1(E,y) - E_2(E,y) \quad MeV \qquad (3\text{-}15)$$

Thus, with the help of the range-energy tables it is possible to calculate the energy loss of a proton for various values of

E and y.

In the above discussion the minimum value of E is the
one for which the range is equal to $t_o \rho_{A\ell} g \ cm^{-2}$. This is the
cut-off energy of the chamber and its value for the OGO ion chamber
is 12 MeV. For $E \geq 25$ MeV the thickness of the wall and
the chamber gas is small compared to the range of the
incident proton. The energy loss ΔE in this case can be
more directly calculated by the relation:

$$\Delta E(E,y) = \left(\frac{dE}{dx}\right)_{argon} 2 \sqrt{r^2 - y^2} \ \rho_{Ar} \ MeV$$

where $\left(\frac{dE}{dx}\right)_{argon}$ MeV g^{-1} cm^2 is the rate of energy loss in

argon for protons with kinetic energy E MeV. It can be
computed from Bethe's energy loss formula as given by Rossi (1956):

$$-\frac{dE}{dx} = \frac{2Cm_e c^2 z^2}{\beta^2} \left[\ell_n \frac{4m_e^2 c^2 \beta^4}{(1-\beta^2)^2 I^2(z)} - 2\beta^2 \right] MeV(g \ cm^{-2})^{-1}$$

where

   $m_e c^2$ = rest energy of electron = 0.51 MeV

   Ze = charge of incident particle

   β = velocity of the particle/velocity of light

   z = atomic number of argon = 18

   A = mass number of argon = 40

   I(z) = ionization potential for argon = 190 eV

   E = energy of the incident particle (MeV)

   x = path length in argon (g cm^{-2})

   C = 0.154 $\frac{z}{A}$ g^{-1} cm^2

(b) Average Energy Loss Per Particle:

Consider a flux $J(E)$ particles/cm^2 sec of mono-energetic protons with energy E incident on the chamber. Then the total rate of energy loss in the chamber due to such a proton flux is given by:

$$(\Delta E)_{total} = \int_{0}^{r} J(E) \Delta E(E,y) \, 2\pi y \, dy$$

$$= 2\pi J(E) \int_{0}^{r} \Delta E(E,y) \, y \, dy \text{ MeV/sec} \qquad (3-18)$$

The total number of particles passing through the chamber is:

$$N_{total} = \int_{0}^{r} J(E) 2\pi y \, dy = \pi r^2 J(E) \text{ particles/sec.} \qquad (3-19)$$

Hence, for protons of a given energy E we can define an average energy loss $\overline{\Delta E}$ per particle in the chamber

$$\overline{\Delta E}(E) = \frac{(\Delta E)_{total}}{N_{total}} = \frac{2}{r^2} \int_{0}^{r} \Delta E(E,y) \, y \, dy \text{ MeV/particle} \qquad (3-20)$$

In case of protons with energy <25 MeV, there is no simple expression for $\Delta E(E,y)$. Consequently the integral on the right hand side has to be evaluated numerically. This is done by dividing the cross-section of the chamber into eight zones corresponding to the intervals of the values of y: 0-2, 2-4, 4-6, 6-7, 7-7.5, 7.5-8.0, 8.0-8.5, and 8.5-8.9 cms.

For protons with energy >25 MeV, the energy loss has the form obtained earlier, viz.

$$\Delta E(E,y) \simeq \left(\frac{dE}{dx}\right)_{argon} 2 \sqrt{r^2 - y^2} \; \rho_{Ar}$$

where $\frac{dE}{dx}$ = constant along the path in argon.

Therefore the average energy loss is

$$\overline{\Delta E}(E) \simeq \frac{2\rho_{Ar}}{r^2} \left(\frac{dE}{dx}\right)_{argon} \int_0^r \sqrt{r^2 - y^2} \; 2y \; dy$$

$$= \frac{4r}{3} \; \rho_{Ar} \left(\frac{dE}{dx}\right)_{argon} \quad \text{MeV/particle} \tag{3-21}$$

It may be noted here that

$$\frac{4r}{3} = \frac{\displaystyle\int_0^r 2\sqrt{r^2 - y^2} \; 2\pi y \; dy}{\displaystyle\int_0^r 2\pi y \; dy}$$

= average path length (in cm) inside the chamber. In g cm^{-2} the average path length in the chamber gas is 0.068. Hence

$$\overline{\Delta E} \simeq 0.068 \left(\frac{dE}{dx}\right)_{argon} \quad \text{MeV} \tag{3-22}$$

(c) Average Ionization due to Unit Isotropic Flux:

Consider an isotropic flux 1 particle cm^{-2} sec^{-1} of mono-energetic protons with energy E incident on the chamber.
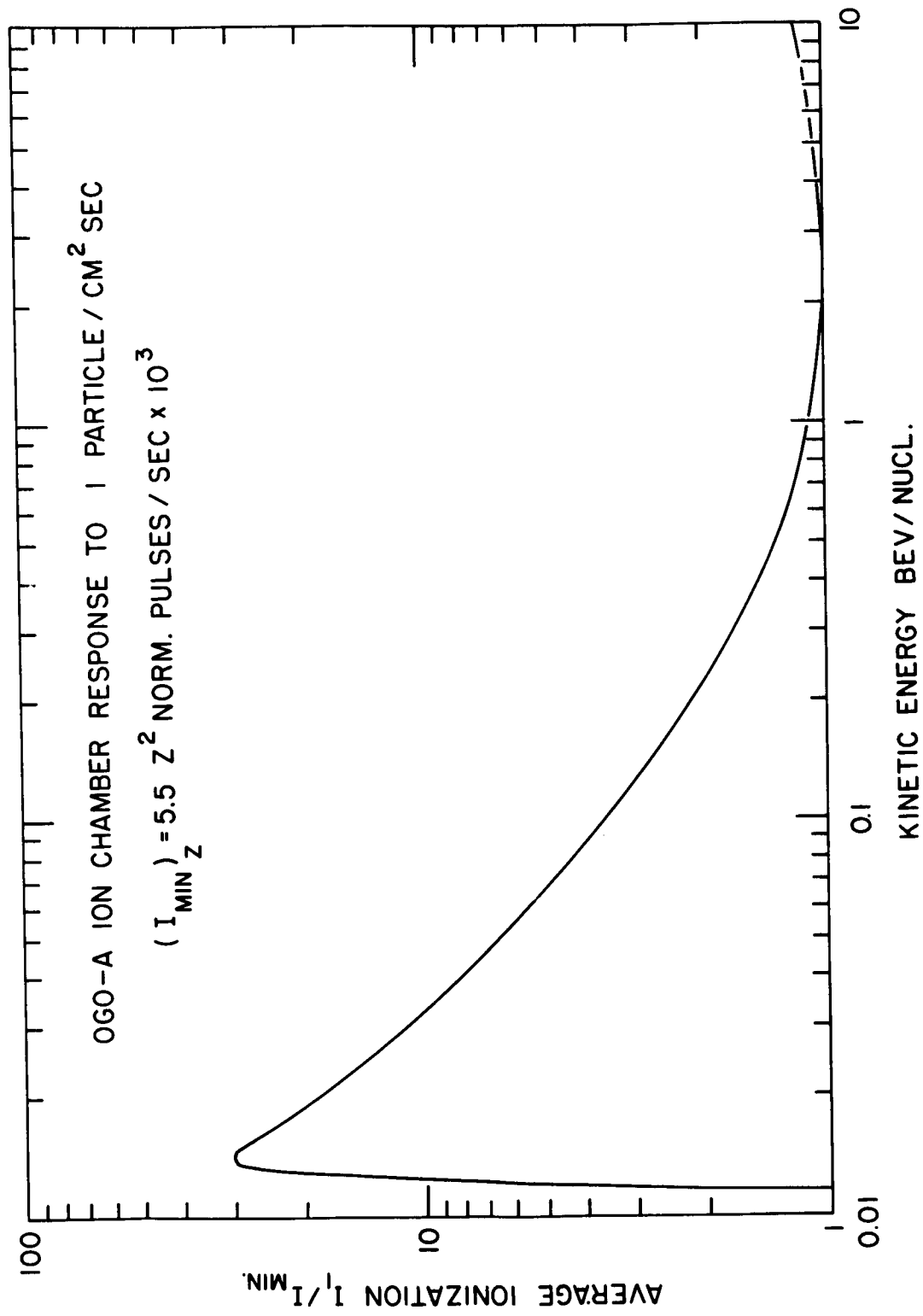
Figure 12

If $A = \pi r^2$ be the omnidirectional projected area of the OGO ion chamber, the total number of particles passing through the chamber is A particles/sec and the total average energy loss is $A \ \overline{\Delta E}$ (E) MeV/sec. Therefore from section (D) we get the resulting ion chamber rate

$$I_1(E) = 0.208 \times 10^{-3} A \ \overline{\Delta E} \ (E) \ \text{norm. pulses sec}^{-1}.$$

With $A = 250 \ \text{cm}^2$ this gives

$$I_1(E) = 52 \ \overline{\Delta E} \ (E) \ \text{norm. pulses sec}^{-1} \times 10^3. \qquad (3-23)$$

Note that here $\overline{\Delta E}$ is in MeV. For minimum ionizing protons

$$\left(\frac{dE}{dx}\right)_{\text{argon}} = 1.56 \ \text{MeV g}^{-1} \ \text{cm}^2 \qquad (3-24)$$

Since the average path length in the chamber gas is $0.068 \ \text{g cm}^{-2}$, we get

$$\overline{\Delta E} = 1.56 \times 0.068 = 0.106 \ \text{MeV}$$

Hence,

$$I_{\text{Min}} = 5.5 \ \text{norm. pulses/sec} \times 10^3 \qquad (3-25)$$

and

$$\frac{I_1(E)}{I_{\text{Min}}} = 9.5 \ \overline{\Delta E} \ (E) \ . \qquad (3-26)$$

The computed ionization using the above relation is shown in Figure 12.

2. Response to α-Particles or Heavier Nuclei

In terms of kinetic energy per nucleon the range-energy relationship for α-particles is the same as that for protons, particularly in the range of energies of present interest. Therefore, the curves $I_1(E)/I_{Min}$ for protons and α-particles are identical, although

$$(I_{Min})_\alpha = 4 \, (I_{Min}) \text{ protons}$$

$$= 22 \text{ norm. pulses/sec} \times 10^3 \qquad (3\text{-}27)$$

Beyond about 40 MeV/nucleon the same curve can also be used for nuclei heavier than α-particles, the corresponding I_{Min}, being given by

$$(I_{Min})_Z = Z^2 \, (I_{Min}) \text{ protons}$$

$$= 5.5 \, Z^2 \text{ norm. pulses/sec} \times 10^3 \qquad (3\text{-}28)$$

where Ze is the charge of the nuclei. However, the cut-off energy for heavy nuclei is higher than that for protons. For example, for 0^{16} the cut-off energy due to the presence of chamber wall is about 25 MeV/nucleon. Consequently, the low energy end of the curve shown in Figure 12 is not applicable to heavy nuclei. However, it is important to note that this limitation is of no consequence to the present analysis because in the calculation of ionization due to primary cosmic rays, we will be concerned with only those heavy nuclei which have kinetic energies above about 40 MeV/nucleon.

OGO ION CHAMBER
RESPONSE TO ELECTRONS
(NORMAL INCIDENCE)
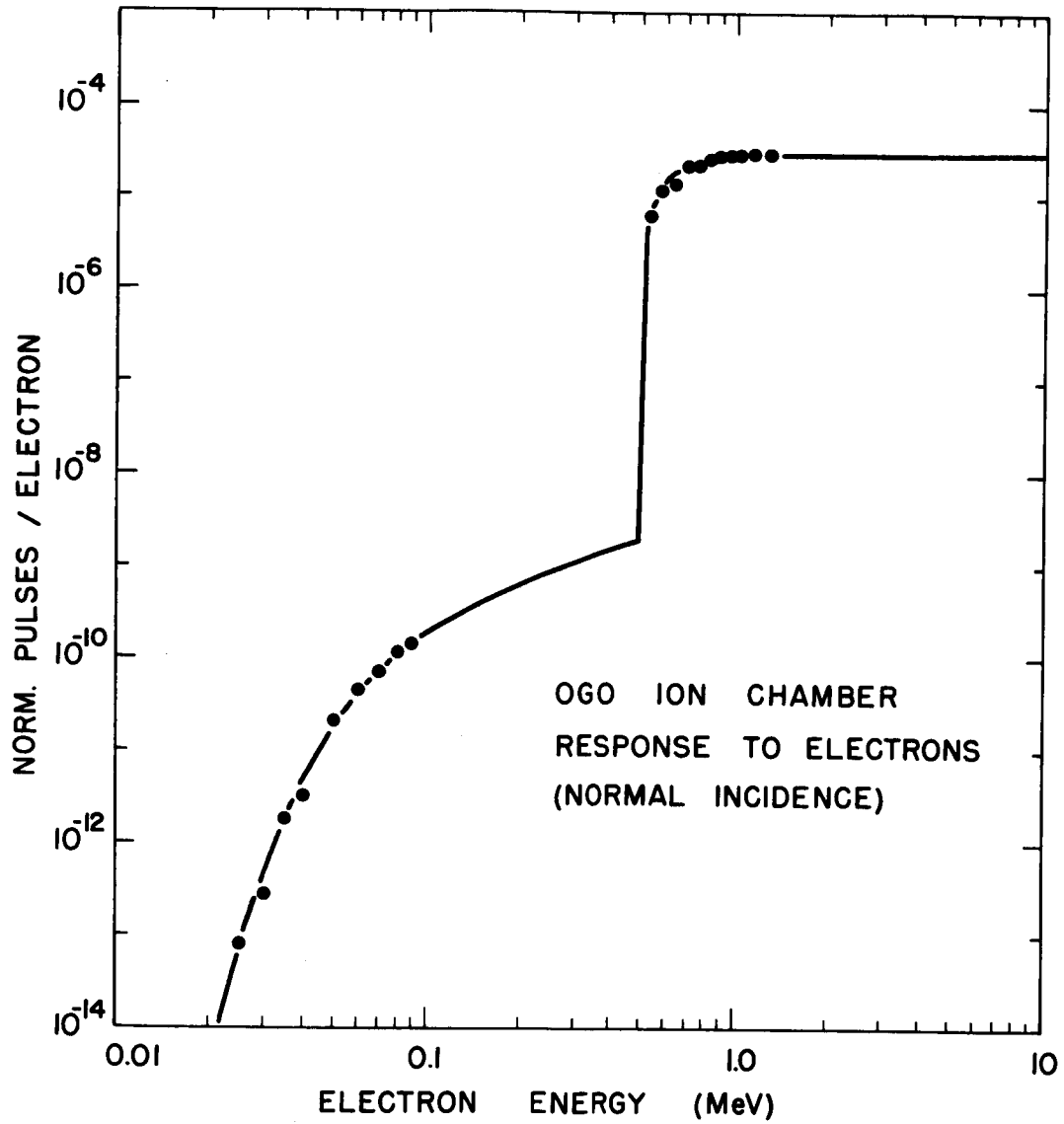
Figure 13

(F) RESPONSE TO ELECTRONS

The response of the OGO ion chamber to a narrow beam of penetrating (E $\geq$ 0.6 MeV) and non-penetrating electrons has been obtained experimentally. The chamber responds to the penetrating electrons by the ionization they produce in the chamber gas. To the non-penetrating electrons, the chamber responds through the bremsstrahlung they produce in the chamber wall.

In the energy range 20-100 KeV, the electron beam was obtained from an accelerator available in the laboratory. The beam current was monitored by interposing a thick target between the chamber and the accelerator and measuring the target current with an electrometer amplifier.

In the energy range 0.5 - 1.2 MeV, the electron beam was obtained with the help of a Sr^{90} source and a magnetic analyzer similar to the one used in the University of Minnesota OGO electron-spectrometer experiment (Kane et al., 1966). Electrons of various energies could be obtained by varying the current through the electromagnet. The intensity and the energy of the electrons in the beam were measured with the help of a solid state detector.

The results obtained for a narrow beam of electrons incident normally on the OGO chamber are shown by circles in Figure 13. The solid line is an extrapolation based on these experimental results. It can be seen from Figure 13 that the response of the chamber to non-penetrating electrons (E $\approx$ 40 KeV) is several orders of magnitude below that
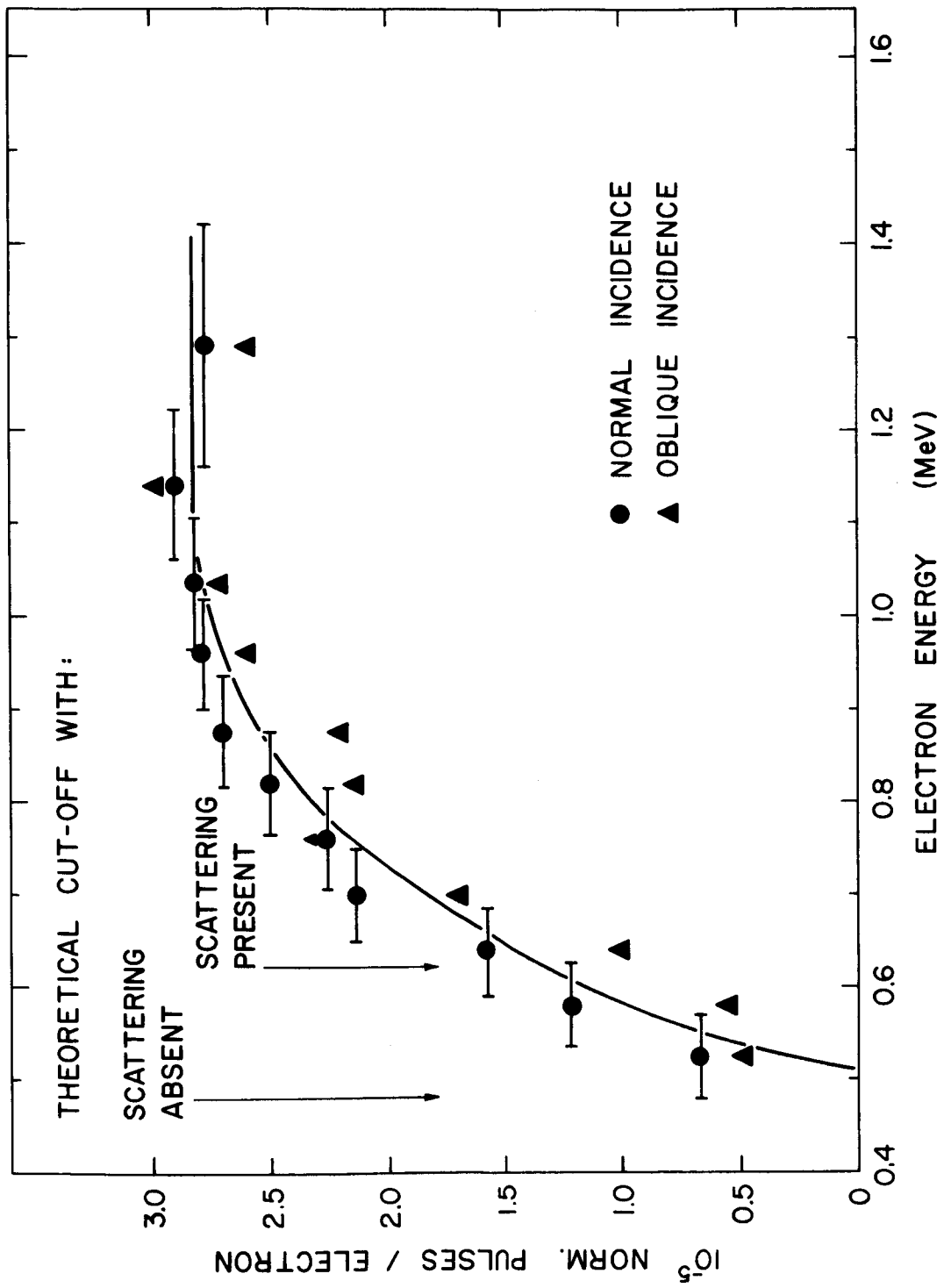
Figure 14
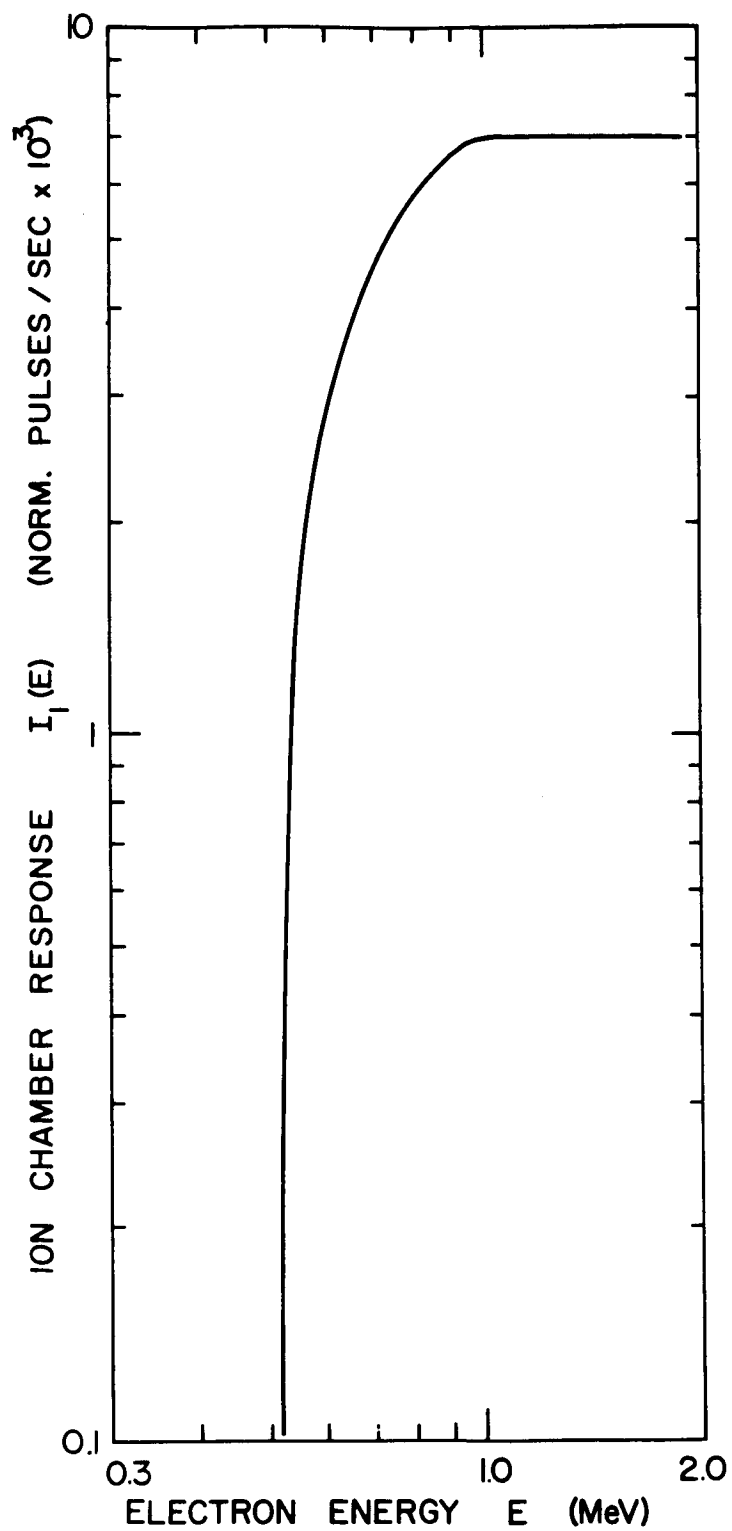
Figure 15

due to penetrating (E ≃ 1 MeV) electrons.

In order to make an estimate of the chamber response
to an isotropic flux of penetrating electrons, the response
of the chamber was also measured for a narrow electron beam
incident obliquely (≃40°) on the chamber wall. The results
for normal as well as oblique incidence are shown in Figure 14.
It can be seen that for electrons above about 1 MeV the
chamber response is nearly independent of the angle of
incidence of the electrons. This seems to indicate that the
electrons are considerably scattered in the chamber wall,
as is to be expected, and after crossing the chamber wall
their directions inside the chamber gas are distributed in a manner
independent of their initial direction. Below 1 MeV, the
response to the electrons depends on their angle of incidence.
For the sake of a rough estimate, we may assume that the
mean response for all directions of incidence lies in-between
the response for normal and oblique incidence as shown by the
solid curve in Figure 14. The response of the chamber to an
omnidirectional flux will then be directly proportional to this
response curve. Such a response for an omnidirectional
flux of 1 electron/cm^2 sec is shown in Figure 15. Also
shown in Figure 14 is the cut-off energy of the chamber for
a straight electron path in the wall and also one in which the
scattering of the electron is included.

(G) RESPONSE TO X-RAYS

In order to determine the response of the chamber to x-rays, nearly monoenergetic photons were obtained by fluorescent scattering of the x-rays available from a conventional x-ray tube. To determine the number-energy spectrum, a narrow beam of the scattered photons was allowed to fall normally on a Na I scintillation counter. When molybdenum, silver and tin were used as scattering materials, the scattered photons have an energy distribution peaked near the K x-ray energies of the scattering materials, viz. 17, 22 and 26 KeV respectively.

With narrow beams of 17, 22 and 26 KeV x-rays incident normally on the chamber, the corresponding chamber rate was recorded and the incident photon flux was measured each time by replacing the chamber with the scintillation counter. The results obtained are shown in Figure 16. Also shown is the chamber response computed in the following manner.

Let N_o photons/sec of energy E KeV be incident normally on the chamber. Let $\alpha(E)$ and $\beta(E)$ be respectively the mass attenuation coefficient of aluminum and mass absorption coefficient of argon for these photons. Then the number of photons entering the argon gas is

$$N_1 = N_o \exp\left(-\alpha(E)\ \rho_{A\ell}\ t_o\right) \text{ photons/sec} \qquad (3\text{-}29)$$

where t_o cms is the thickness of the chamber wall and $\rho_{A\ell}$ g/cm^3 is the density of aluminum. The number of photons leaving the gas after crossing the diameter of the

OGO ION CHAMBER
RESPONSE TO NARROW
BEAM THROUGH CENTER
OF CHAMBER
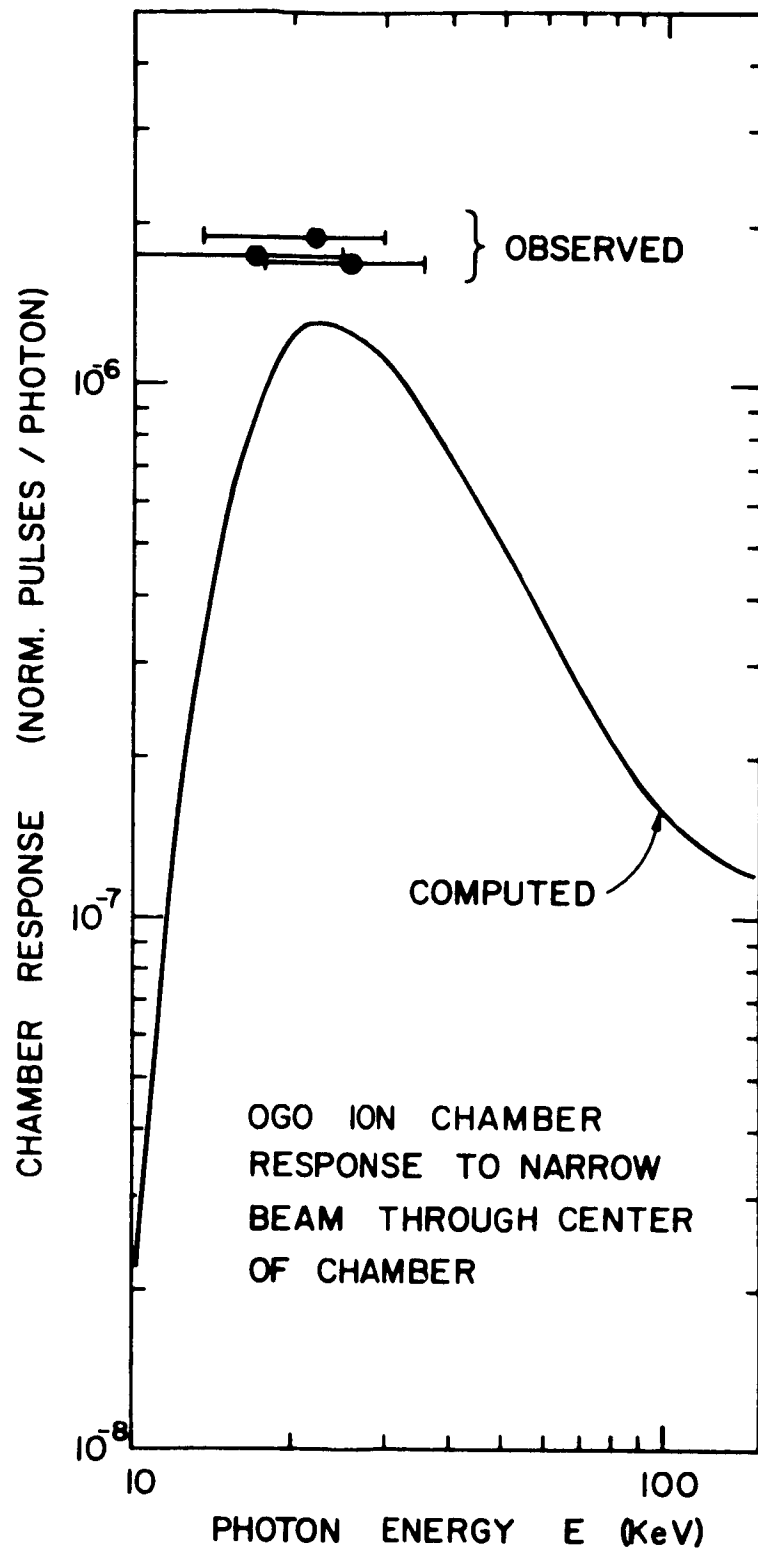
Figure 16

chamber is

$$N_2 = N_o \exp{(-\alpha(E)\rho_{A\ell} t_o)} \exp{(-\beta(E)\rho_A 2r)} \text{ photons/sec } (3-30)$$

where r cms is the radius of the chamber and ρ_A g/cm^3 is the density of argon in the chamber. Hence, the number of photons absorbed in the gas is

$$\Delta N = N_1 - N_2$$

$$\Delta N = N_o \exp{(-\alpha(E)\rho_{A\ell} t_o)} \quad [1 - \exp{(-\beta(E)\rho_A 2r)}] \text{ photons/sec.}$$

Therefore, the energy absorbed per incident photon is

$$\Delta E = \frac{E \Delta N}{N_o}$$

$$\Delta E = E \exp{(-\alpha(E)\rho_{A\ell} t_o)} [1 - \exp{(-\beta(E)\rho_A 2r)}] \times 10^{-3}$$

(3-31)

MeV/photon.

If all this energy is ultimately absorbed in the gas in the chamber, the resulting ion chamber rate is given by (from Section (D)) $I_1(E) = 0.208 \times 10^{-3} \Delta E$ norm. pulses/photon

$$= 2.08 \times 10^{-7} E \exp{(-\alpha(E)\rho_{A\ell} t_o)} [1 - \exp{(-\beta(E)\rho_A 2r)}]$$

(3-32)

norm. pulses/photon .

This relation is shown in Figure 16 by the solid line. The response of the chamber to a broad beam of x-rays with a flux of 1 photon/cm^2 sec can be similarly obtained by
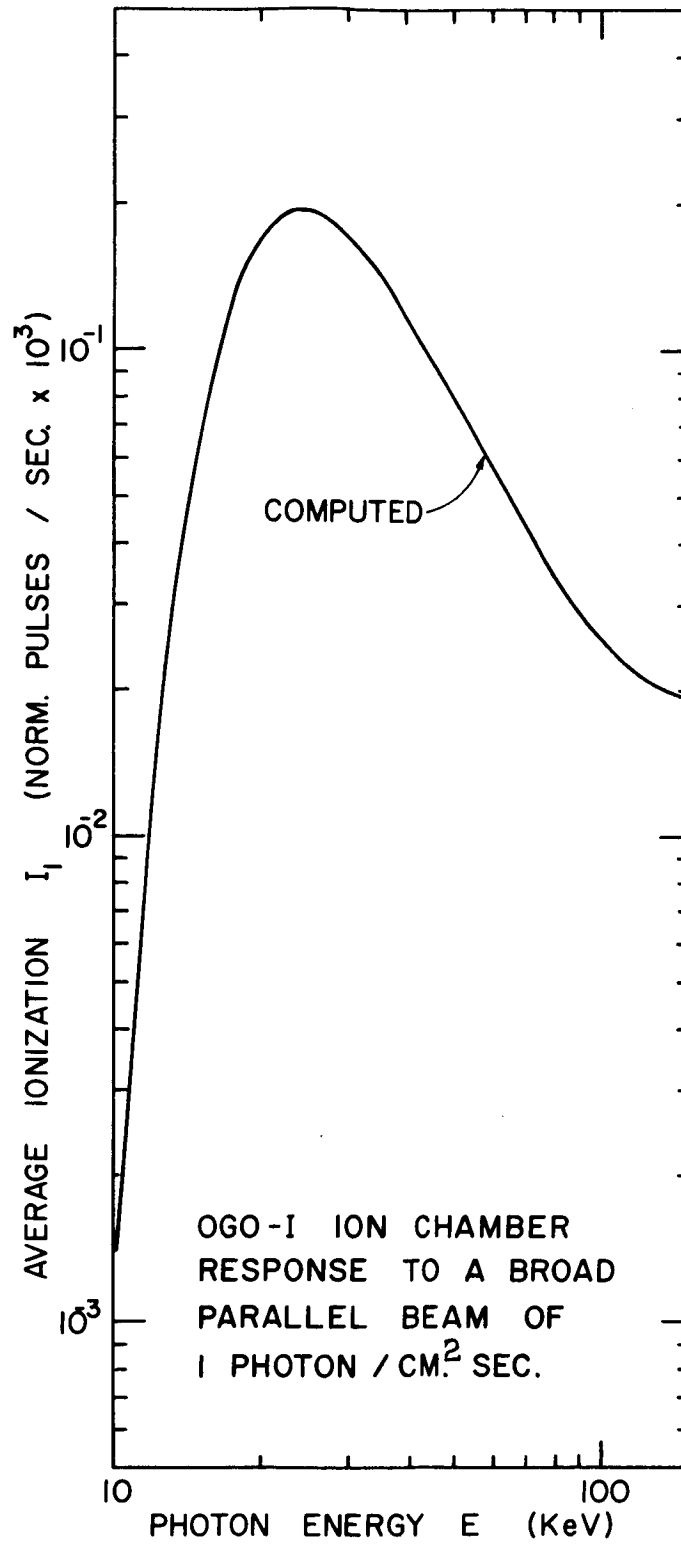
Figure 17

integrating over the cross-sectional area of the chamber.
The result of such a computation is shown in Figure 17. The
values of α and β were obtained from Evans, 1955 and
National Bureau of Standards Handbook 62, 1956.

For verifying directly the x-ray absorption in the
chamber, it was interposed between the source and the scintillator.
For ≈ 22 KeV photons the observed attenuation factor was
≈ 0.24 which is comparable to the factor 0.17 expected on the
basis of exponential attenuation by the two chamber walls
and the argon gas. This agreement within 30 percent is considered
adequate for the present purpose because the response
characteristics evaluated here are used mainly to interpret
the observed solar x-ray bursts during which the pulsing
rate of the OGO ion chamber increases by several orders of
magnitude.

IV. PRESENTATION OF DATA

(A) NATURE OF THE DATA

As described in Chapter III the basic data for the
OGO ionization chamber experiment is available in three forms,
viz.

Analog word 100 — Instantaneous ramp voltage.

Word 90 + 113 — Number of clock pulses counted between
1st and 16th discriminator levels.

Word 43 — Serial number of the ramp reset.

These three pieces of information can be independently converted
to the "normalized rate" in the manner described in Chapter III.
However, it is important to note that the normalized pulsing
rates obtained in these three different ways represent rates
averaged over different time intervals as can be seen from
Figure 18. Here the ramp voltage $V(t)$ is plotted against time
t for a constant source of radiation. Since the instantaneous
slope of the ramp $\frac{dV}{dt}$ is proportional to the rate of
ionization, in this particular case the slope is constant at
all times. The analog word 100, which gives the instantaneous
ramp voltage $V(t)$ can therefore yield normalized chamber rates
averaged over an arbitrarily small interval, the limitation
being the time between the successive data readouts in the
OGO satellite telemetry. On the other hand, the rates
deduced from "clock pulses" are averaged over time spent by
the ramp voltage between 1st and 16th discriminator levels,
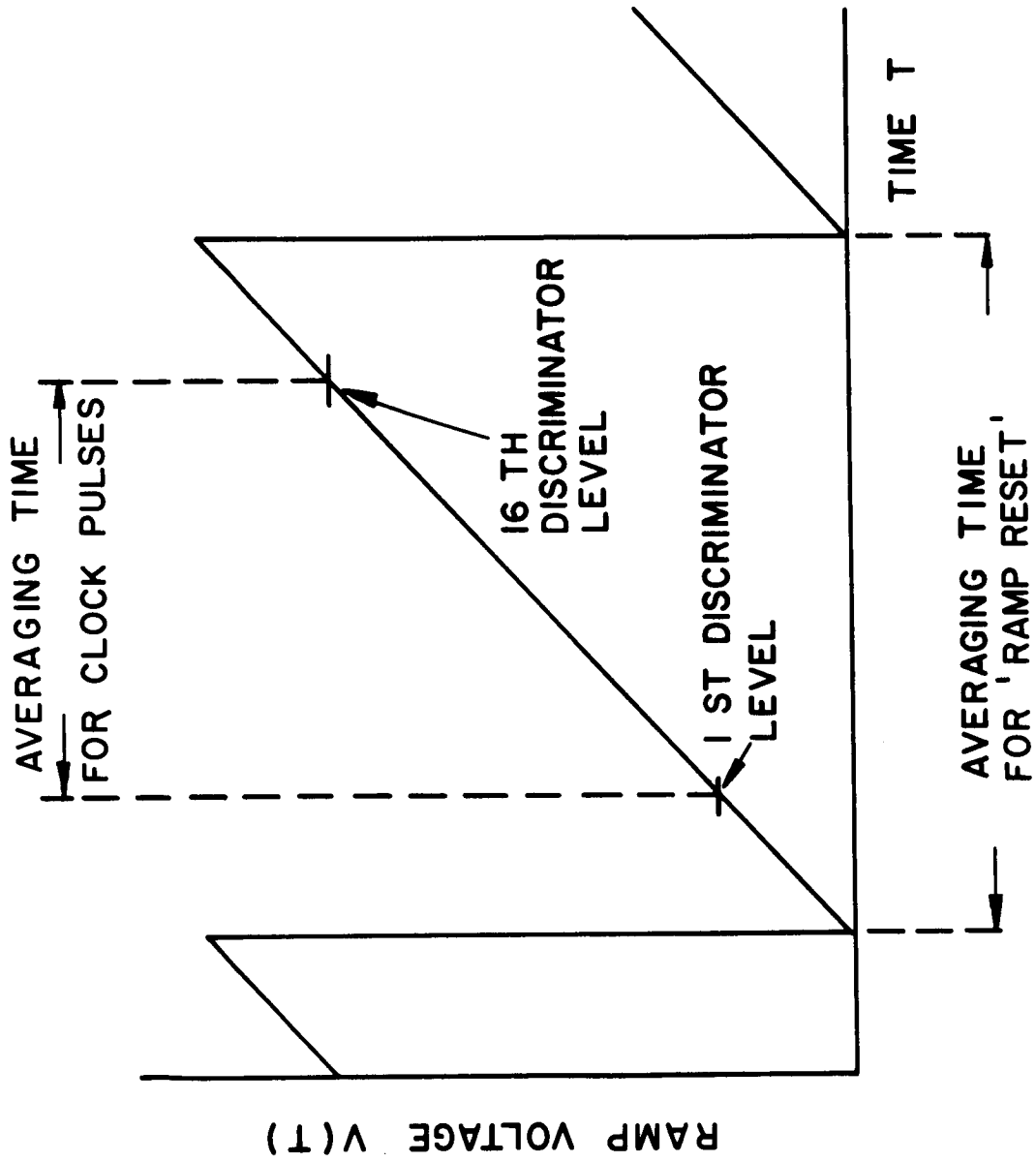
Figure 18

and therefore the time of averaging is inversely proportional
to the ion chamber rate. Similarly the rates deduced from
the ramp resets are averages over the time between successive
resets and therefore the time of averaging is inversely
proportional to the ion chamber rate. From Figure 18 it can
be seen that the averaging time for the rate deduced from
"ramp reset" is somewhat larger than the corresponding time
for "clock pulses". .

In order to organize in a standard form the data obtained
during the actual flight of the OGO ionization chamber experiment,
the observed rates are tabulated as averages over integral
number of minutes. When the rates are low, the following
procedure is used. The occurrence of a ramp reset is
recorded to the nearest integral minute. The rates are
computed as usual from the clock pulses and the ramp reset,
but the two rates are tabulated as if the averaging time for
the clock pulses was the same as that for the ramp resets.
It must be noted that this procedure does not introduce any
error in the computation of the chamber rates. It only
introduces an uncertainty of about half a minute in the precise
location of that particular rate in time. For most purposes
this small uncertainty in time is of little consequence. Moreover,
whenever higher precision in time is required the time can be
deduced from the original data.

Table 7 shows a sample computer print-out of the "one
minute averages" of the OGO-I ion chamber data processed in
the manner described above. The data covers the period

TABLE 7

12DEC66 OGO-A PLAYBACK DECOM 49 REEL 01 ID NO. Y=3R25 FILE NO. 0 RECORD NO. 174 EG 1 1KB TAPE PAGE NO. 102

Date			UNFILTERED WORD 43 PULSES	RAMPS	DT	FILTERED WORD 43 PULSES	RAMPS	DT	CLOCK PULSES PULSES	RAMPS	DT	ANAL ORU PULSES	RAMPS	DT
MAR 12, 1965	0	B 1	62.03E-03	0	114	62.03E-03	0	114	62.98E-03	0		66.11E-03*	1	51
MAR 12, 1965	0	B 2		0	115		0	115		0	85	67.09E-03	0	31
MAR 12, 1965	0	B 3	61.61E-03	1	115	61.61E-03	0	115	63.45E-03	1	84	59.22E-03*	1	54
MAR 12, 1965	0	B 4		0	120		0	120		0	90	60.64E-03	1	20
MAR 12, 1965	0	B 5	59.24E-03	1	120	59.24E-03	1	120	59.56E-03	0		57.61E-03	0	45
MAR 12, 1965	0	B 6		0	115		0	115		0	86	59.90E-03	0	44
MAR 12, 1965	0	B 7	61.41E-03	1	115	61.41E-03	0	115	62.35E-03	1		71.59E-03*	1	30
MAR 12, 1965	0	B 8		0	113		0	113		0	85	62.13E-08*	0	30
MAR 12, 1965	0	B 9	62.75E-03	1	113	62.75E-03	1	113	62.77E-03	1		61.61E-03	1	43
MAR 12, 1965	0	B 10		0	116		0	116		0	85	63.51E-08	0	34
MAR 12, 1965	0	B 11	61.00E-03	1	116	61.00E-03	0	116	63.01E-03	1		68.24E-03	1	40
MAR 12, 1965	0	B 12		0	117		0	117		0	87	60.71E-02*	0	39
MAR 12, 1965	0	B 13	60.40E-03	1	117	60.40E-03	0	117	61.55E-03	1		61.98E-03	1	40
MAR 12, 1965	0	B 14		0	114		0	114		0	86	62.45E-03	0	31
MAR 12, 1965	0	B 15	62.15E-03	1	114	62.15E-03	0	114	62.45E-03	1		69.56E-03*	1	49
MAR 12, 1965	0	B 16		0	115		0	115		0	85	61.96E-03*	0	21
MAR 12, 1965	0	B 17	61.50E-03	1	115	61.50E-03	1	115	63.11E-03	1		59.98E-03	1	22
MAR 12, 1965	0	B 18		0	117		0	117		0	86	63.04E-03	0	23
MAR 12, 1965	0	B 19	60.40E-03	1	111	60.40E-03	1	111	62.50E-03	0	84	63.59E-03	1	50
MAR 12, 1965	0	B 20	63.96E-03	1	111	63.96E-03	1	111	63.88E-03	0	84	63.44E-03	0	21
MAR 12, 1965	0	B 21		0			0		61.79E-03	0	87	64.44E-03	1	58
MAR 12, 1965	0	B 22	61.38E-03	1	115	61.38E-03	1	115		0	85	63.18E-03	0	24
MAR 12, 1965	0	B 23	61.73E-03	1	115	61.73E-03	1	115	62.90E-03	0		59.73E-08	0	53
MAR 12, 1965	0	B 24		0			0			0	87	64.54E-08	1	20
MAR 12, 1965	0	B 25	62.03E-03	1	114	62.03E-03	1	114	61.75E-03	0		61.15E-08	0	51
MAR 12, 1965	0	B 26		0			0			0	85	63.70E-03	0	30
MAR 12, 1965	0	B 27	61.61E-03	1	115	61.61E-03	1	115	62.95E-03	0		62.90E-03	1	57
MAR 12, 1965	0	B 28		0			0			0	87	56.59E-03	0	36
MAR 12, 1965	0	B 29	59.24E-03	1	120	59.24E-03	1	120	61.27E-03	0		58.42E-03	0	57
MAR 12, 1965	0	B 30		0			0			0	89	60.62E-03	1	30
MAR 12, 1965	0	B 31	59.82E-03	1	118	59.82E-03	1	118	59.81E-03	0		64.17E-03	1	51
MAR 12, 1965	0	B 32		0			0			0	86	63.32E-03	0	30
MAR 12, 1965	0	B 33	61.41E-03	1	115	61.41E-03	1	115	61.93E-03	0		65.10E-03	0	42
MAR 12, 1965	0	B 34		0			0			0	84	61.77E-03	1	30
MAR 12, 1965	0	B 35	62.23E-03	1	114	62.23E-03	1	114	63.81E-03	0		62.64E-03	0	42
MAR 12, 1965	0	B 36		0			0			0	84	64.59E-03	1	31
MAR 12, 1965	0	B 37		0			0		64.53E-03	0	83	63.48E-03	0	0
MAR 12, 1965	0	B 38	62.75E-03	1	113	62.75E-03	1	113		0	0		0	50
MAR 12, 1965	0	B 39		0			0			0	0	46.24E-03*	0	50
MAR 12, 1965	0	B 40	59.42E-03	1	118	59.42E-03	1	118	60.87E-03	0	84	59.48E-03*	0	33
MAR 12, 1965	0	B 41	62.66E-03	1	113	62.66E-03	1	113	62.68E-03	0	85	62.42E-03	1	49
MAR 12, 1965	0	B 42		0			0			0		62.52E-03	0	37
MAR 12, 1965	0	B 43	62.87E-03	1	113	62.87E-03	1	113	63.72E-03	0	84	65.16E-03	1	40
MAR 12, 1965	0	B 44		0			0			0		63.53E-03	1	26
MAR 12, 1965	0	B 45	62.75E-03	1	113	62.75E-03	1	113	63.21E-03	0	85	61.34E-03	0	50
MAR 12, 1965	0	B 46		0			0		62.76E-03	0	85	62.66E-03	0	23
MAR 12, 1965	0	B 47	62.03E-03	1	114	62.03E-03	1	114		0		61.77E-03	1	50
MAR 12, 1965	0	B 48		0			0		61.83E-03	0	87	61.85E-03	0	23
MAR 12, 1965	0	B 49		0			0			0		59.83E-03	1	50
MAR 12, 1965	0	B 50	61.40E-03	1	117	60.40E-03	1	117	64.33E-03	0	87	59.86E-03	0	21
MAR 12, 1965	0	B 51	62.11E-03	0	114	62.11E-03	0	114		0	84	61.56E-03	1	55
MAR 12, 1965	0	A 52		0			0			0		63.95E-03	0	24
MAR 12, 1965	0	A 53	58.79E-03	0	120	58.79E-03	0	120	60.15E-03	0	89	60.65E-03	0	56
MAR 12, 1965	0	A 54		0			0			0		66.74E-03*	1	25
MAR 12, 1965	0	B 55	63.30E-03	1	112	63.30E-03	1	112	64.26E-03	0	83	63.58E-03	1	51

Figure 19

0800-0850 hours on 12 March 1965. At this time the OGO-I satellite was at a geocentric distance of 23.3 earth radii on the sunward side. The chamber rates in Table 7, therefore, are the rates in interplanetary space. In addition to the rates deduced from the ramp resets (unfiltered word 43), clock pulses, and the analog word, the rates are also deduced from the "filtered word 43". This filtering is achieved by requiring that the word 43 (ramp reset counter) should increase monotonically and that its value should be constant for at least two successive readouts. This filtering criterion is found to remove the effects of transient noise to which this data is susceptible.

From Table 7 it can be seen that the rates deduced from the three different sets of information are quite consistent. In order to visualize the fluctuations in the chamber rate in free space, the rates deduced from clock pulses and presented in Table 7 are plotted against time in Figure 19. In this particular sample of data the chamber rate fluctuated by about 5 percent about the average value. Fluctuations as large as 7 percent about the average value are sometimes observed.

From the basic "1 minute averages", rates averaged over 5 minutes and 1 hour are formed. Whenever maximum time resolution is required the analog data is used directly for computing the chamber rate.

For each orbit the various orbital parameters are available
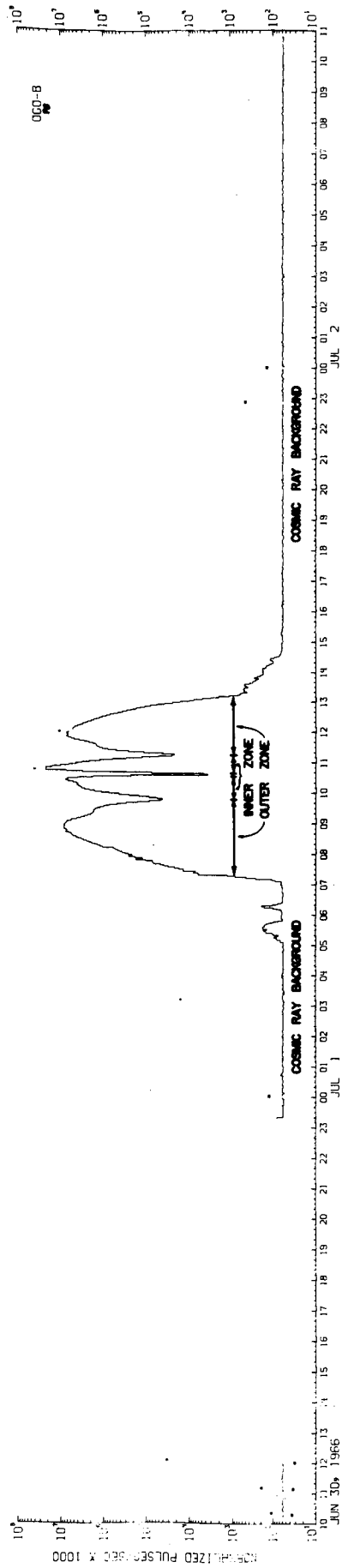
Figure 20

as a function of time. Thus, it is possible to study the dependence of the observed ion chamber rates on different orbital parameters.

(B) VARIATION OF RATES DURING AN ORBIT

A typical computer plot of the one minute average rates against Universal Time during an orbit of the OGO-III satellite is shown in Figure 20. The location of the inner and outer radiation zones as well as the cosmic ray background rate are indicated on the plot.

Figure 21 shows the chamber rates during some inbound passes of the OGO-I satellite. Here the chamber rates are plotted against the geocentric distance of the satellite. For reference, also given are local time ϕ (degrees), the geomagnetic latitude λ (degrees) and the L-parameter (earth radii). At the apogee the rate is about 60 norm. pulses/sec x 10^3. As the satellite comes closer to the earth, the rate stays almost constant up to a radial distance of about 13 earth radii and then begins to increase, first slowly and then rapidly, until it reaches a maximum in the outer radiation zone at $L \simeq 5$. Then the rate goes through a minimum at $L \simeq 3$ and increases to another maximum in the inner radiation zone. Figure 22 shows similar rate vs. geocentric distance profile for some outbound passes of the OGO-I satellite. These profiles are basically similar to those in Figure 21. The apparent compression of the radiation belts in Figure 22 is due to the fact that the geomagnetic latitude of the satellite is,
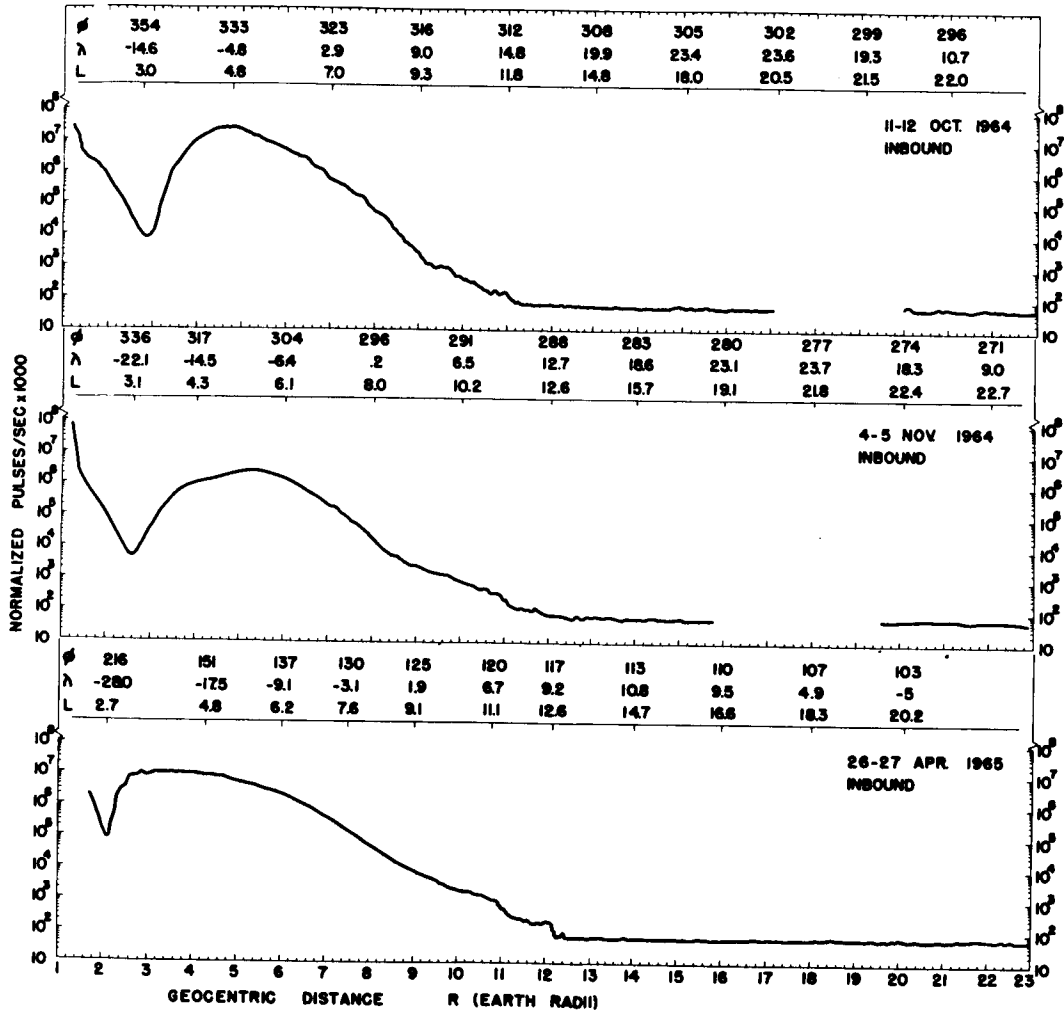
Figure 21
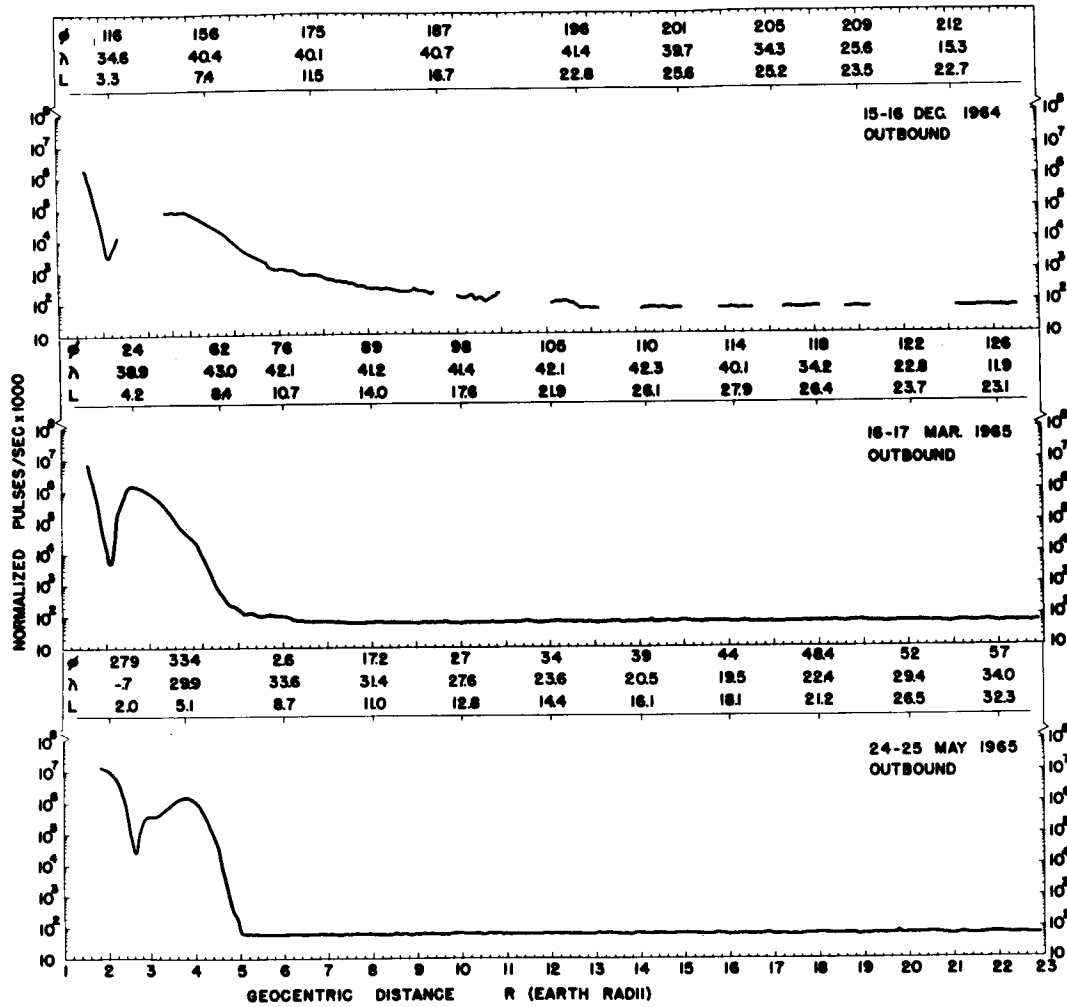
Figure 22

in general, higher during outbound passes than in the inbound passes. Consequently, the radiation belts terminate at a shorter radial distance during the outbound passes.

Large irregular increases are sometimes observed in the ionization chamber rate well beyond the outer radiation zone. An example of such an increase is shown in Figure 23. These increases, which are almost always characterized by a highly irregular behavior, have been observed earlier by various workers (Fan et al., 1964; Frank and Van Allen, 1964; Anderson et al., 1965), and are believed to be due to large transient fluxes of energetic electrons ($E \geq 40$ KeV).

Occasionally large increases in the chamber rate also occur during and after a solar flare. An example of such an increase is shown in Figure 24. Due to the good correlation of such increases in the chamber rates with the radio noise and particles emitted by the sun, such events are easily identified as solar flare events.

From Figures 23 and 24 it can be seen that the transient increases in the ionization chamber rate are superimposed on a relatively steady background rate which, as indicated earlier, is essentially constant for radial distances $R \geq 13$ earth radii. This background rate is identified as that due to primary cosmic rays. Detailed arguments in support of this identification are presented in the next chapter.

(C) SELECTION OF DATA

In view of the discussion in the last section and the
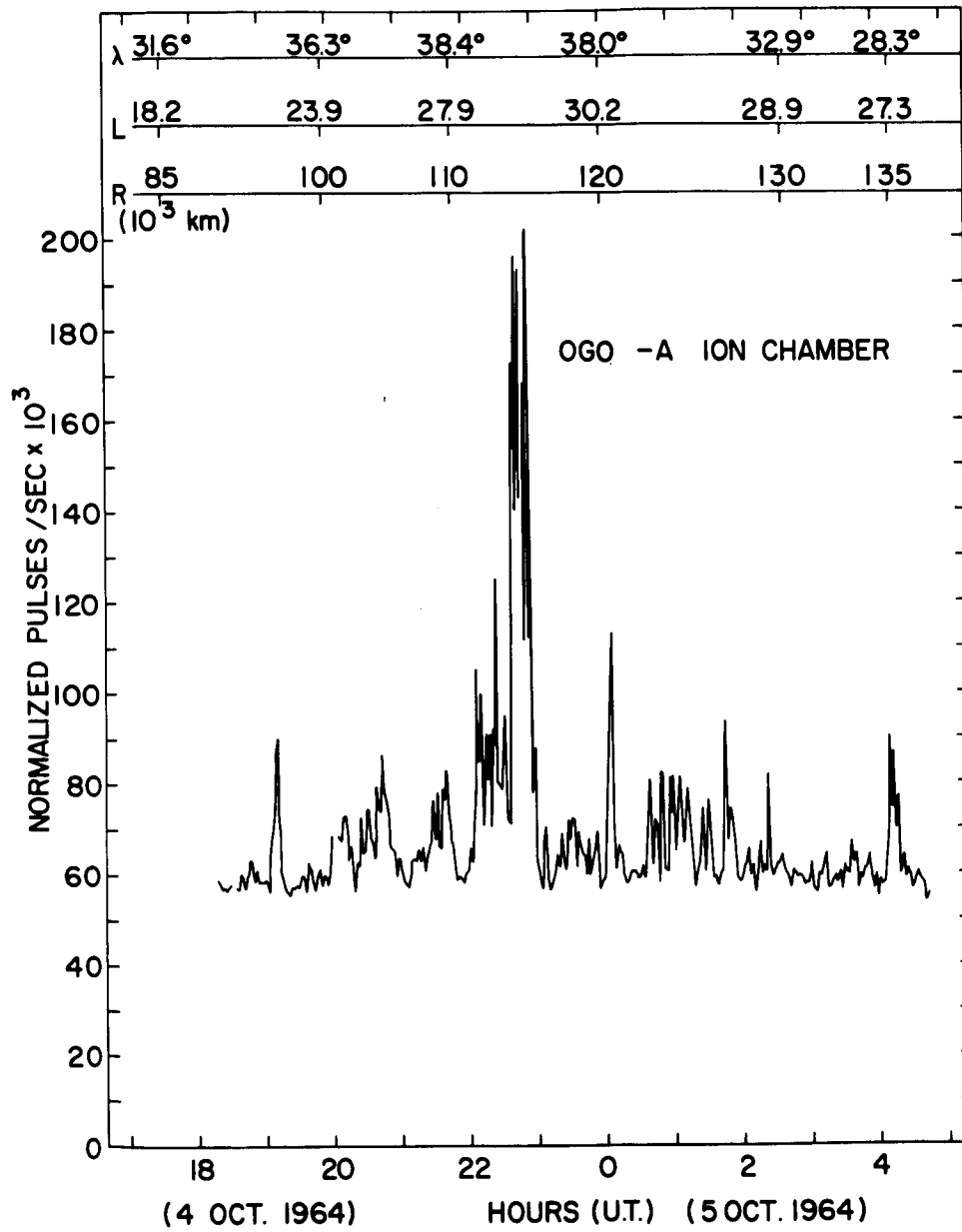
Figure 23
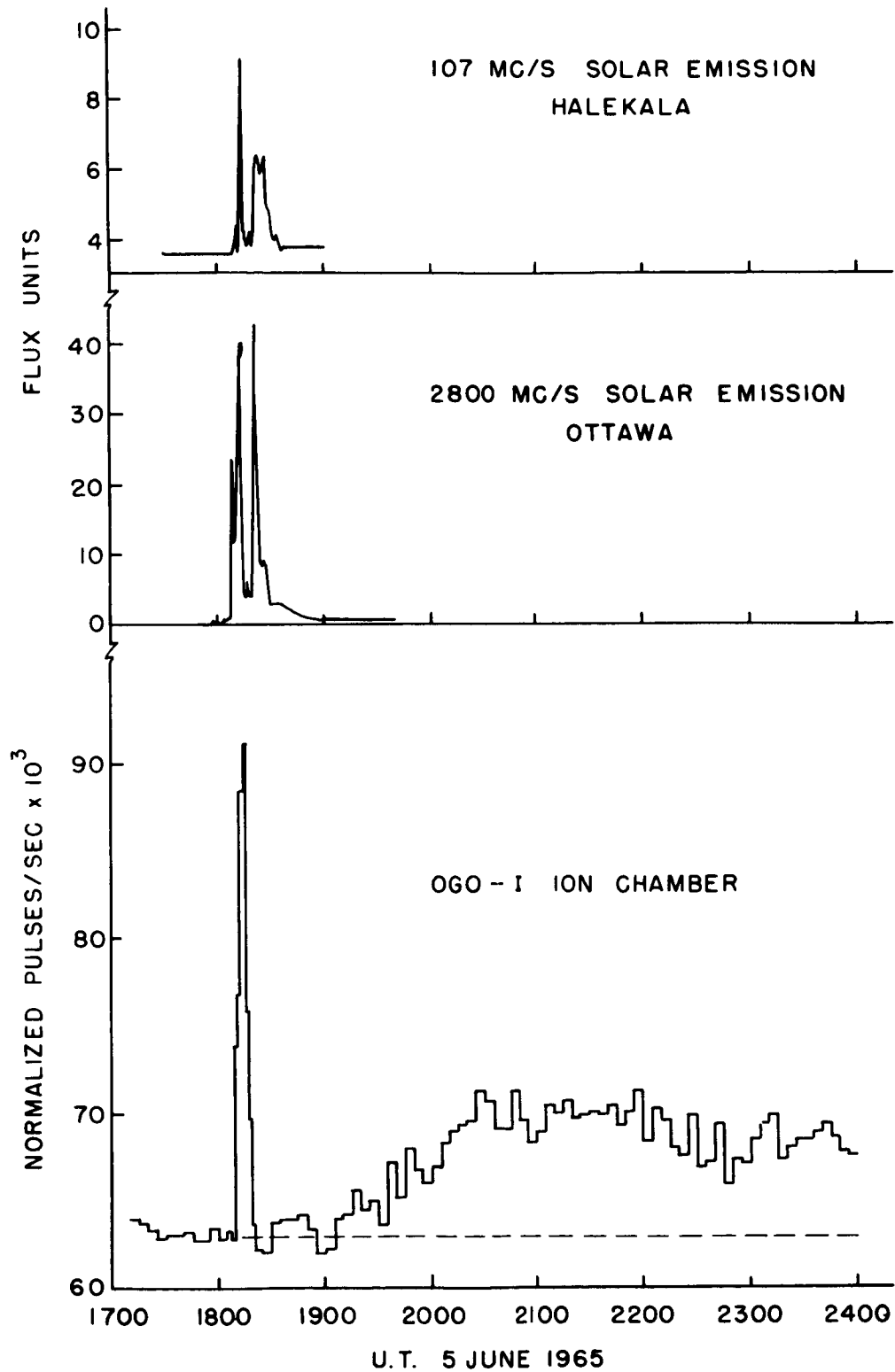
Figure 24

principal objective of the OGO ionization chamber experiment,
viz. measurement of the ionization rate due to primary cosmic
rays in free space, the available data were selected in the
following manner:

1. Only those rates which were derived from the counting
   of "clock pulses" were used. As indicated in
   Chapter II, these yield measurements consistent
   within one percent.

2. From the available "one minute averages" described
   earlier, hourly averages are formed. These are
   treated as the basic data for the present analysis.

3. The measurements for only those times at which the
   satellite was located at a radial distance $\geq$ 15 earth
   radii are considered. This criterion ensured that
   at the time of the measurement the satellite was
   well outside the region of trapped radiation surrounding
   the earth.

4. To avoid the influence of transient fluxes of electrons
   or solar x-ray bursts, the particular hourly
   interval during which such an event occurred is
   completely rejected. As discussed in the previous
   section such events can be identified by their
   characteristic features.

5. In case of a solar particle event the entire period
   following the event during which there was detectable
   effect ($\geq$ 1 percent above the galactic background)

TABLE 8

SOLAR PARTICLE EVENT - 17 SEPT. 1966

TIME (UT)	HOURLY MEAN RATE (NORM. PULSES SEC^{-1} x 10^3)		FRACTIONAL DIFFERENCE $\frac{R_1-R_2}{R_1}$
	OGO-I (R_1)	OGO-III (R_1)	
0130	614	616	-0.003
0230	588	592	-0.007
0330	568	572	-0.007
0430	576	568	0.014
0530	557	549	0.014
0630	513	499	0.027
0730	504	506	-0.004
0830	476	478	-0.004
0930	446	445	0.002
1030	446	442	0.009
1130	466	475	-0.019
1230	493	499	-0.012
1330	458	462	-0.009
1430	440	434	0.014
1530	434	431	00.007
1630	403	403	0.000
1730	382	383	-0.003
1830	371	369	0.005
AVERAGE	485.3	484.6	0.001

on the ionization chamber rates was rejected. This
period varied from half a day to several days from
event to event.

(D) COMPARISON OF OGO-I AND OGO-III IONIZATION CHAMBERS IN FLIGHT

The ionization chambers aboard the OGO-I and OGO-III
satellites were constructed and normalized identically so that
their pulsing rates under the same radiation source were
equal in the laboratory. To check their equivalence during
the actual flight in space it is necessary to compare the
measurements made simultaneously by the two chambers when
they are located in a suitable region of space. On 17 September
1966 between 0100 and 1900 hours UT the two satellites were
close to their apogees where the two chambers normally
respond only to primary cosmic rays. On this particular
day a solar particle event was in progress and the chamber
rates were higher than those due to the galactic cosmic
rays alone. Table 8 shows the simultaneous measurements made
with the OGO-I and OGO-III ion chambers. It can be seen that
the two chambers agree on an average within 0.1 percent.
Considering that the two chambers were in different regions
of space, the agreement between the two chambers is excellent.
In the following discussion the measurements with these
two chambers will therefore be considered equivalent.

(E) VARIATION OF RATES IN FREE SPACE

The hourly average rates, obtained in the manner described
above, are used to form daily mean rates. The number of hourly
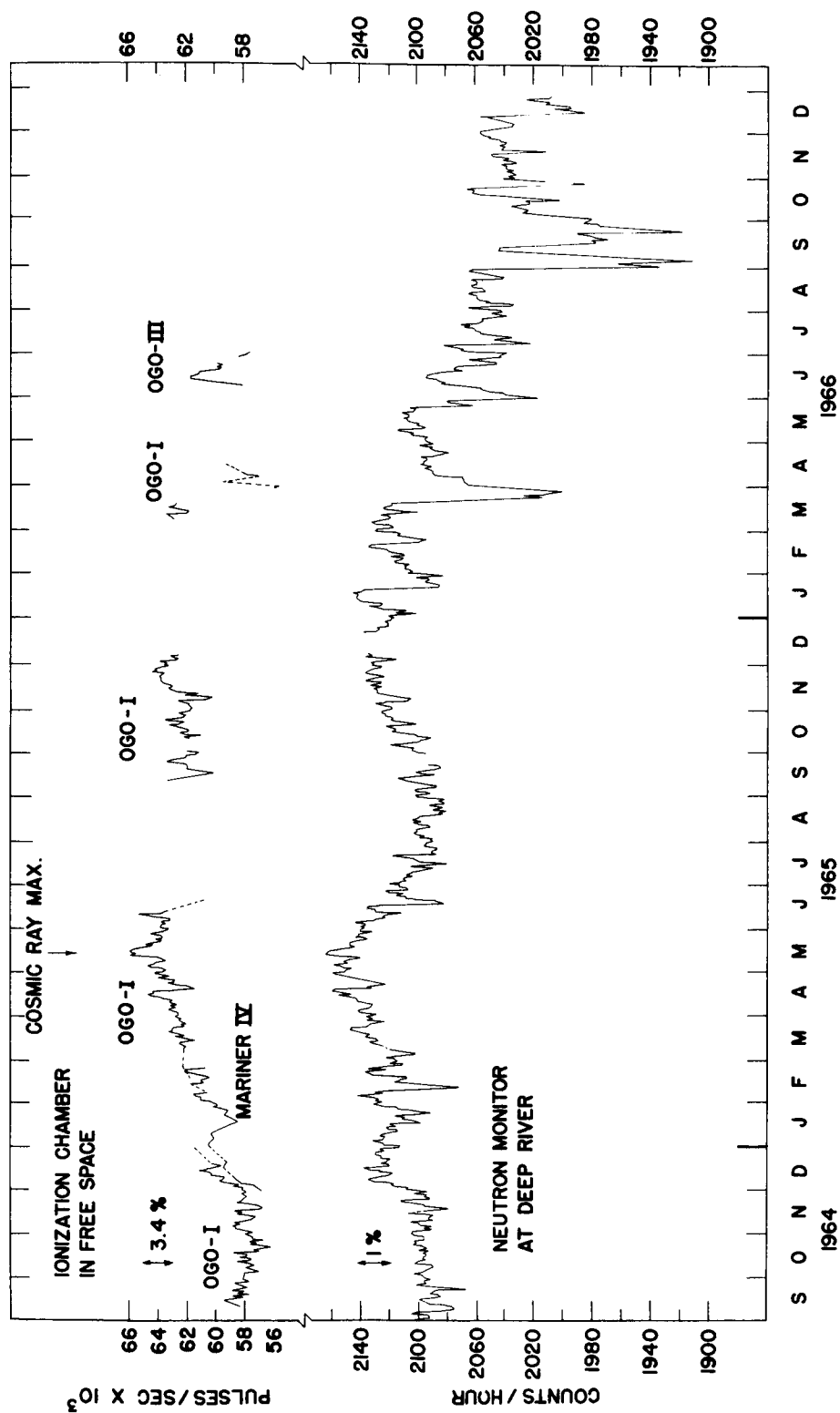
Figure 25

averages available to compute a daily mean rate varied from
1 to 24. Figure 25 shows the daily mean rates plotted against
time for the period September 1964 to June 1966, a period which
covered the cosmic ray maximum in the current solar cycle.
For comparison the daily mean counting rates of the
Deep River Neutron monitor (courtesy of World Data Center A)
and Mariner IV ionization chamber (Dr. Hugh Anderson -
private communication) are also shown in Figure 25. The
pulsing rates of the Mariner IV ionization chamber, which are
originally given in the units of ion pairs/cm^3 sec STP air),
are converted to the units of norm. pulses sec^{-1} x 10^3 by
multiplying the former by the factor 0.0611. This factor is
based on the intercomparison of the rates of two similar
chambers at balloon altitude (Winckler, 1960). The data
plotted in Figure 25 is also presented in Table 9.*

From Figure 25 it can be seen that the absolute rates
of the OGO and Mariner IV chambers agree within about two percent.
The large Forbush decreases, which are so prominent in
the neutron monitor data, are not so conspicuous in the
ionization chamber data because most of these decreases are
preceded by a solar flare and a solar particle event.
Consequently, the ionization chamber rates are in fact higher
than normal during the onset period of a Forbush decrease.
As mentioned earlier, for the present analysis the measurements
on these days are rejected on the ground that they do not
represent the quiescent level of the primary cosmic ray intensity.

---

*Table 9 given on p. 193.

During the period 10 September to 29 November 1964 the
quiescent rates of the ionization chamber and the neutron
monitor were essentially constant. The first prominent
increase in the rates started on 30 November 1964 almost
simultaneously for the ionization chamber and the neutron
monitor. The rates continued to increase until about
15 December 1964 and then fluctuated about this level. For
the period under consideration, the rates of both the
detectors reached their maximum values in the middle of
May 1965. These maximum values were higher than the mean
values in September 1964 by 13.3 percent and 2.1 percent for
the ionization chamber and the neutron monitor, respectively.
After 13 May 1965 the rates of both the detectors began to
decrease gradually. On this long-term decrease are super-
posed several Forbush decreases of varying magnitudes and
duration.

In order to visualize the relationship between the
long-term changes in the ionization chamber in free space and
the Deep River neutron monitor, monthly means are formed from
the daily mean rates of the ionization chamber. Similarly,
monthly mean rates are formed for the Deep River neutron monitor
by including only those days in a month on which the
ionization chamber data are available. These means are
called "correlated" monthly means of the neutron monitor
and are plotted against time in Figure 26, together with the
ionization chamber data. It can be seen that the rates for
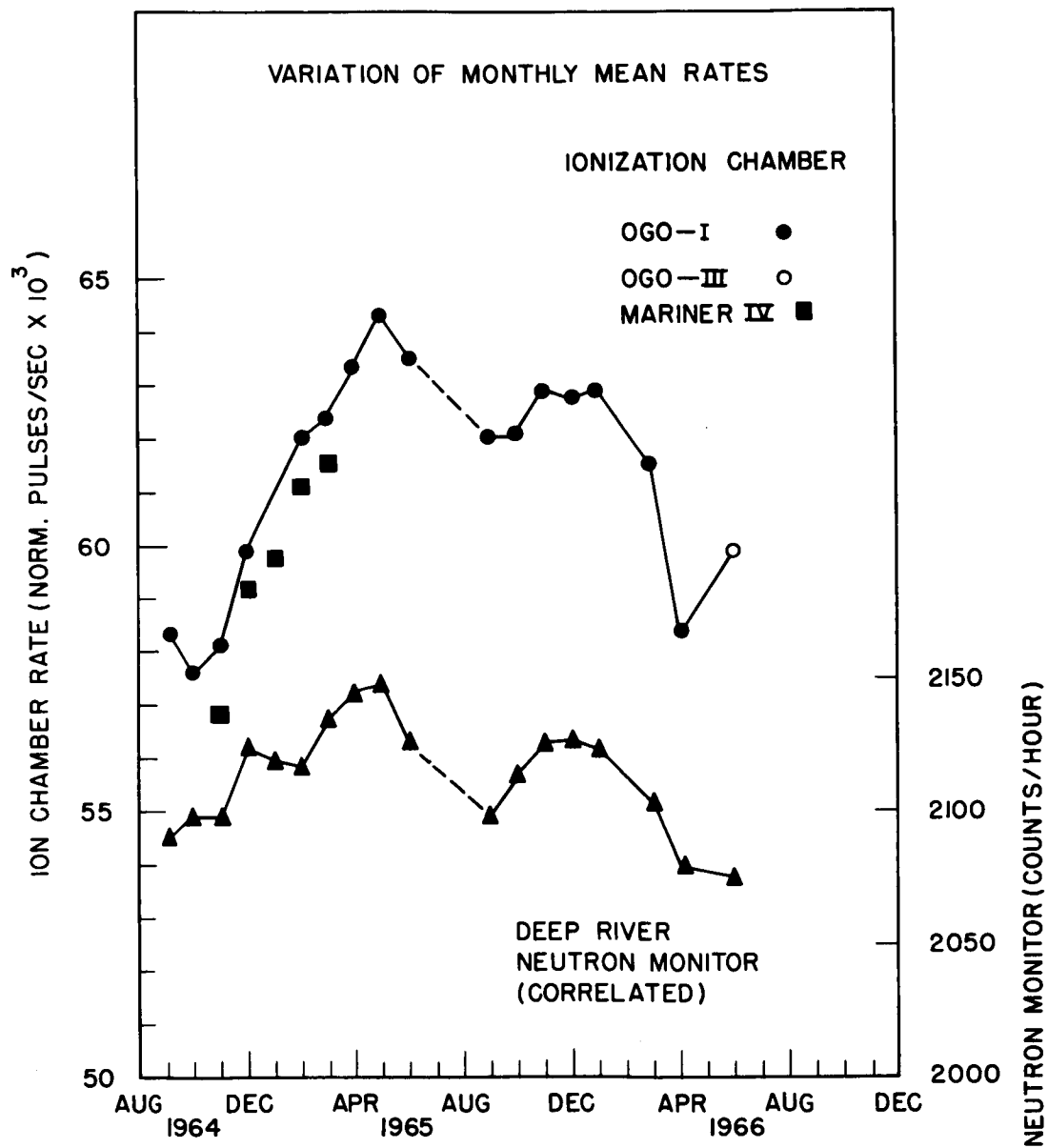
Figure 26

both the ion chamber and the neutron monitor increased
gradually during the period October, 1964 - May, 1965, reached
their maximum values in May, 1965 and then decreased gradually
during the period May - September, 1965. By September, 1965
the rate of the neutron monitor was back to its value in October -
November, 1964, but the ion chamber rate decreased only to
its value in February, 1965. The rates of the two detectors
then went through another peak (December, 1965) somewhat smaller
than the one in May, 1965. After December, 1965, the rates
decreased systematically until April, 1966 at which time the
ion chamber rate is down to its value in September - November, 1964
while the neutron monitor rate in April, 1966 is somewhat
lower than its value in November, 1964. This difference in
the behavior of the ion chamber and neutron monitor rates
after May, 1965 is discussed further in the next section.

The maximum variation in the ion chamber and the Deep River
neutron monitor during the period September, 1964 - May, 1965
is about 11.0 and 2.4 percent respectively. This difference
in the magnitude of the variation in the two detectors is
to be expected because the ion chamber is believed to
respond to primary cosmic rays with rigidity ≈ 2 BV while the
neutron monitor at Deep River responds to primaries with
rigidity ≈ 15 BV.

(F) OTHER MEASUREMENTS IN SPACE

As mentioned in Chapter I, during the period 1960-1965
cosmic ray measurements outside the earth's magnetic field
have been made by ion chambers aboard the Pioneer V deep space

probe, Mariner II and IV space probes, and OGO-I and III satellites. The Pioneer V and Mariner II and IV experiments have been described in detail by Arnoldy et al. (1960, 1964) and Neher and Anderson (1964, 1965), respectively.

Compared to the OGO and Mariner ion chambers, which were essentially in free space, the Pioneer V ion chamber had some material around it, and so the minimum energy of protons to which it could respond was about 25 MeV. To determine the effect of the surrounding material, in April 1960 an ion chamber similar to the Pioneer V ion chamber was calibrated on the ground so that under the "standard" radium source its normalized pulsing rate was the same as that of a standard ion chamber usually flown on balloons. The Pioneer V ion chamber was then mounted on a spare payload identical to the Pioneer V actually flown. This payload was then flown on a balloon at Minneapolis with the standard ion chamber. At the balloon altitude it was found that the ion chamber inside the Pioneer V payload had a pulsing rate of about 17% higher than the pulsing rate of the standard ion chamber flown on the same balloon. This difference in the pulsing rates is believed to be due to the secondaries produced in the Pioneer V payload by the primary cosmic rays. The actual pulsing rate of the Pioneer V ion chamber in space is, therefore, corrected for this effect by multiplying the actual pulsing rate by the factor 0.83. Even though the Pioneer V ion chamber had a higher cutoff energy (25 MeV) for protons than the OGO or Mariner ion chambers (10-12 MeV), this difference can be of

MARCH 1960 – MAY 1965

OGO – I
(SEPT. 1964 – MAY 1965)

MARINER IV
(NOV. 1964 –
FEB. 1965)

MARINER II
(SEPT. – DEC. 1965)

PIONEER V
(MAR. – APRIL, 1960)
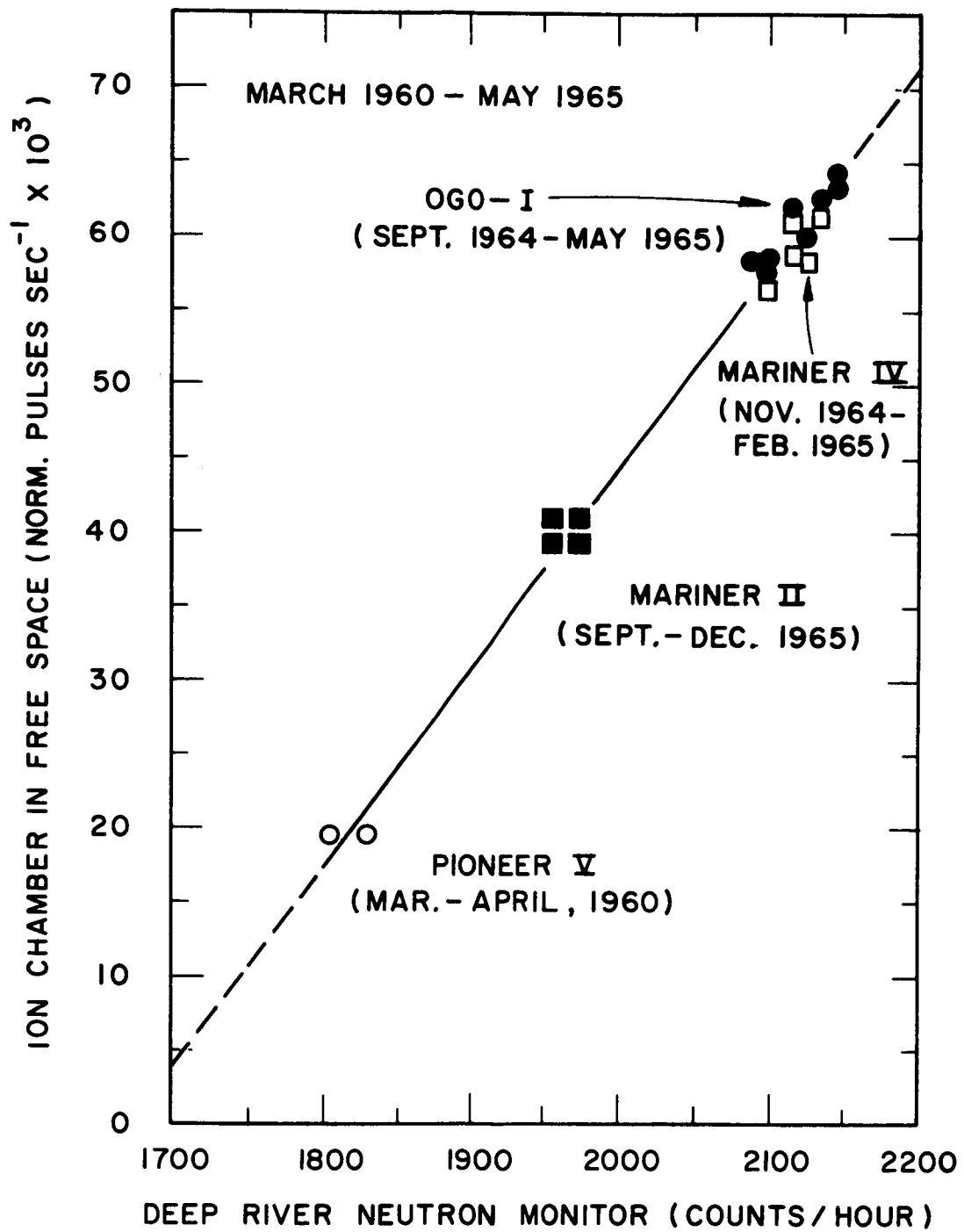
Figure 27

little consequence as far as galactic cosmic rays are concerned,
because during the period of operation (March-April 1960) of
the Pioneer V ion chamber there were very few particles below
1.3 BV, as is indicated by the near equality of the balloon
ion chamber rates at Fort Churchill (atmospheric cutoff ≈0.5 BV)
and at Minneapolis (geomagnetic cutoff ≈1.3 BV) at that time
(see Figure 29). Therefore, apart from the correction factor
of 0.83, the Pioneer V ion chamber can be considered comparable
to the Mariner II and OGO ion chambers.

All the available ionization chamber measurements in free
space made during the period March 1960 - May 1965 are summarized
in Figure 27. Here the monthly means of the ion chamber rates
are plotted against the corresponding "correlated" monthly
means of the Deep River neutron monitor rate. It can be seen
that the relation between the ion chamber and the neutron
monitor rates is very nearly linear.

Figure 28 shows the daily mean rates of the OGO ion
chamber during the period 10 September 1964 - 2 July 1966
plotted against the corresponding rate of the Deep River neutron
monitor. The entire period is divided into two parts,
viz. 10 September 1964 - 14 May 1965 (before the cosmic ray
maximum) and 15 May 1965 - 2 July 1966 (after the maximum).
For reference we have also shown the regression line for the
period March 1960 - May 1965 shown earlier in Figure 27.
From Figure 28 it can be seen that the data points before
15 May 1965 (solid circles) lie fairly close to the regression
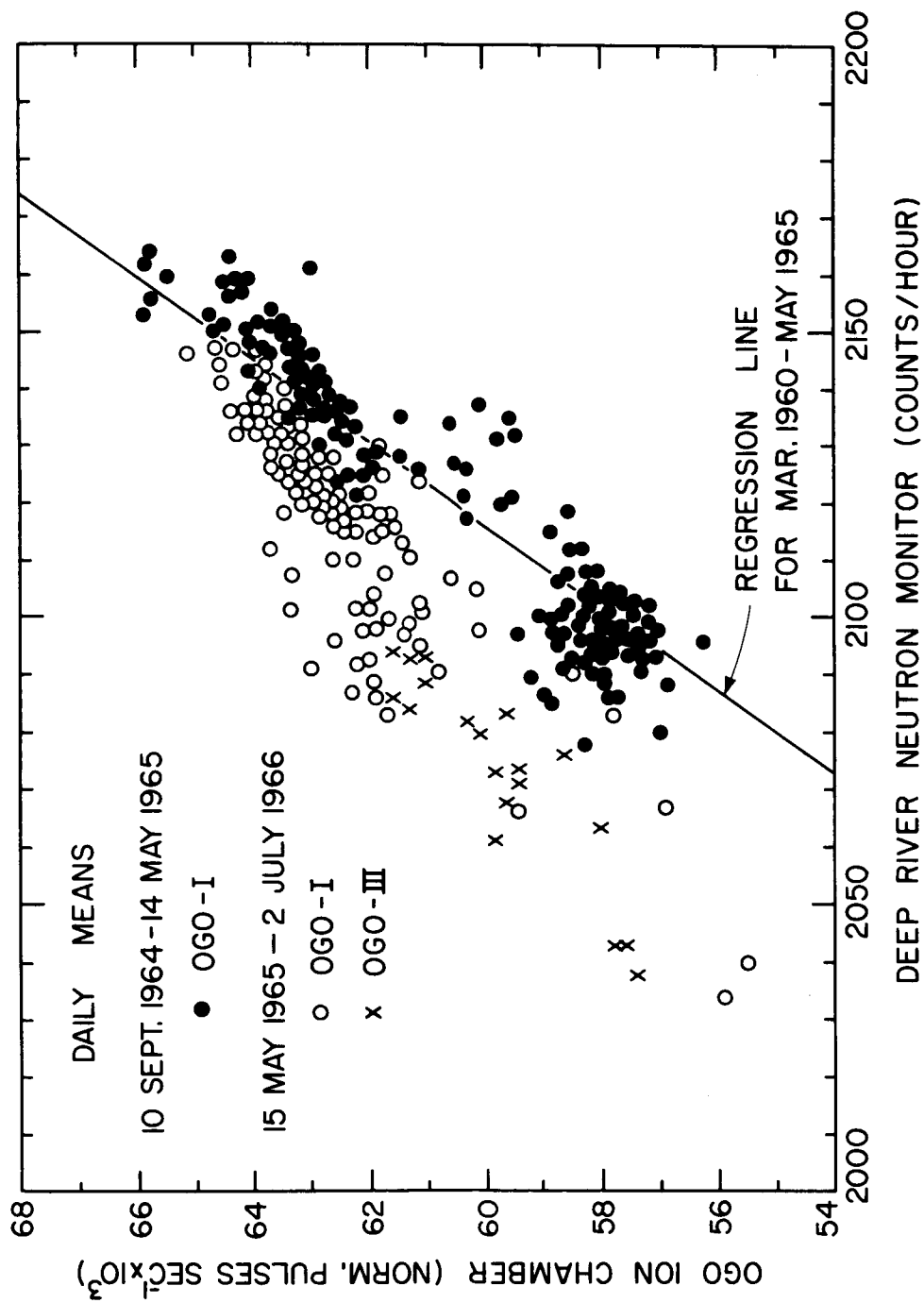
Figure 28

line and are nearly uniformly distributed about that line.
However, the data points after 15 May 1965 lie consistently
above the regression line and are away from it. This shows that
the modulation of the Deep River neutron monitor ($\approx$15 BV
primaries) compared to that of the ion chamber in free space
($\approx$2 BV primaries) is larger after the cosmic ray maximum
than before it.

(G) RELATED MEASUREMENTS WITH ION CHAMBERS ON BALLOONS

Ionization chambers have been flown on balloons by Neher
and Anderson (1962) and by Winckler (1960) for a number of
years in order to monitor the cosmic ray intensity at medium
($\approx$55°) and high ($\geq$70°) geomagnetic latitudes. Such measurements
at 10 millibar altitude made during the period 1954-1965 are
summarized in Figure 29. Also plotted are the sunspot numbers
on a reversed scale so that the sunspot number increases
downward from the top of the figure.

From Figure 29 it can be seen that the solar activity
increased from the year 1954 to 1957, and then decreased from
1957 to 1964. On the other hand, the ion chamber rates,
both at medium (Minneapolis) and high (Churchill) latitudes,
decreased from 1954 to 1958 and then gradually recovered
back to their 1954 values by the year 1965. Thus there is
an overall anti-correlation between the cosmic ray intensity
and the solar activity, although the cosmic ray intensity lags
behind the solar activity by about one year.
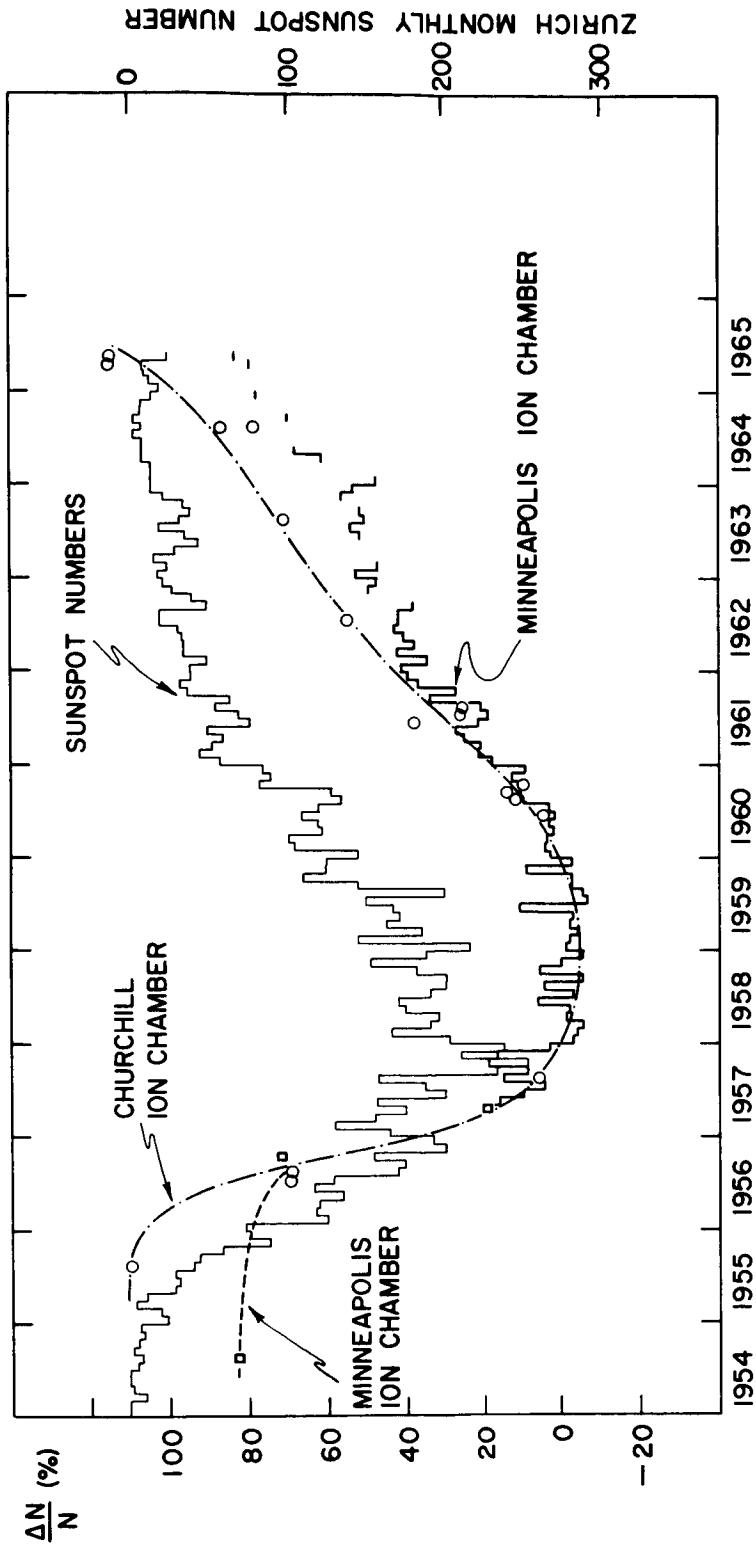
Figure 29
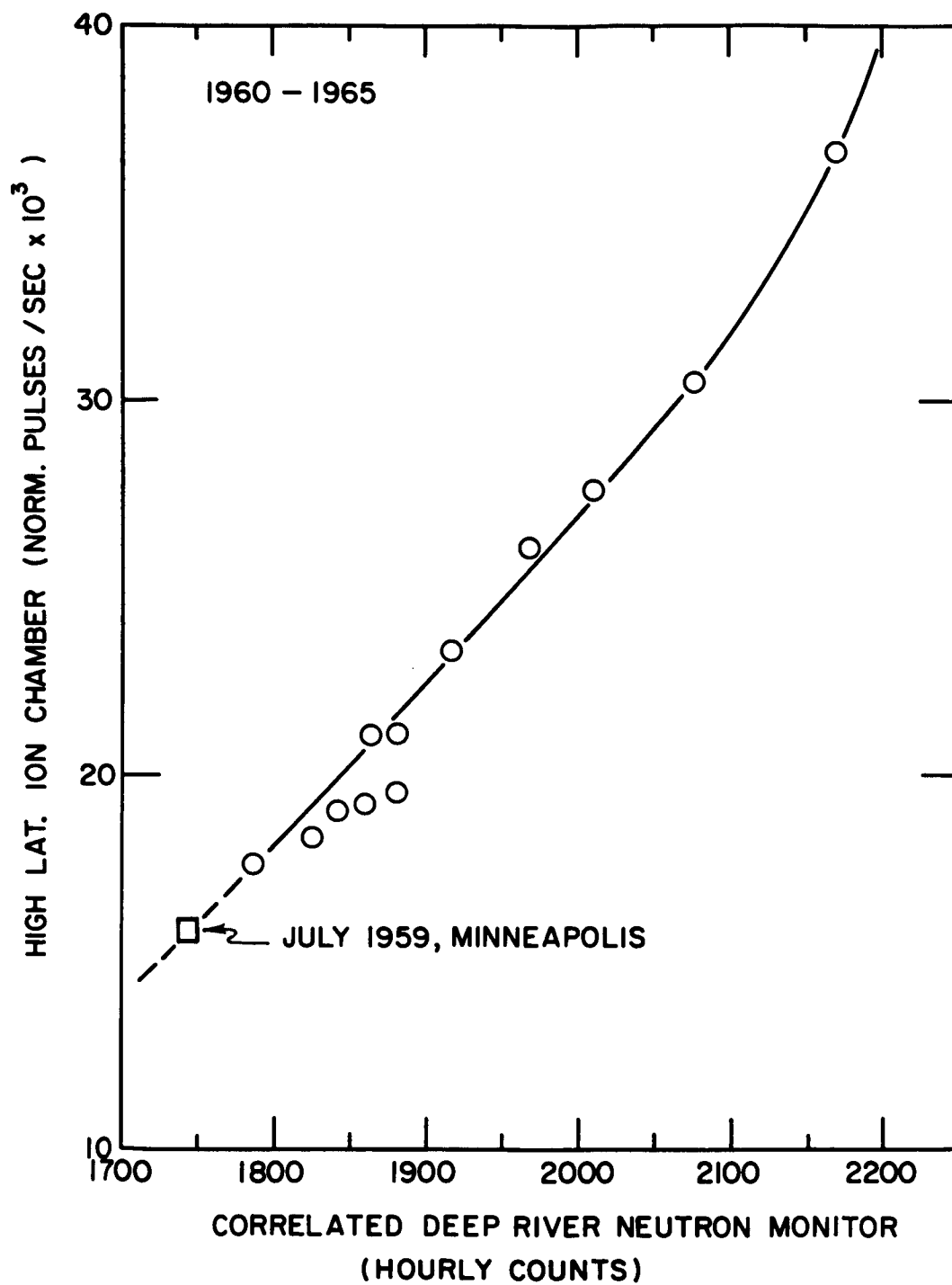
Figure 30

Of particular interest here are the ion chamber measurements
at high latitudes where the minimum rigidity of the primary
protons to which the chamber can respond is determined by the
residual atmosphere above the chamber and has the value ≈0.5 BV.
In order to study the long term variation of these high
latitude chamber rates the time at which the balloon crosses
the 10 mb altitude level during a particular flight is noted.
The ion chamber rate at that time and the corresponding hourly
rate of the neutron monitor at Deep River are tabulated.
This neutron monitor rate is called "correlated" rate. All
such measurements available during a month are averaged to form
monthly mean rates. The regression plot of these rates is
presented in Figure 30. No high latitude chamber measurement
is available near the solar maximum period, (neutron monitor
rate 1700-1775). However, Figure 29 indicates that during
that period the chamber rates at Minneapolis and Churchill
(high latitude) were nearly the same. Therefore the Minneapolis
chamber rate in July 1959 is presumed to be representative
of the high latitude chamber rate at that time and is
therefore included in Figure 30. It can be seen that the
ion chamber and the neutron monitor rates have a definite
relationship which is nearly linear for most of the period
(neutron monitor rate 1700-2075) except near the solar
minimum period (neutron monitor rate 2075-2150) when the ion
chamber rate increases faster than the neutron monitor rate.

A regression plot between the balloon ionization chamber

Figure 31

JAN. 1958— MAY 1965

(Y-axis) CLIMAX NEUTRON MONITOR (HOURLY COUNTS)

(X-axis) DEEP RIVER NEUTRON MONITOR (HOURLY COUNTS)
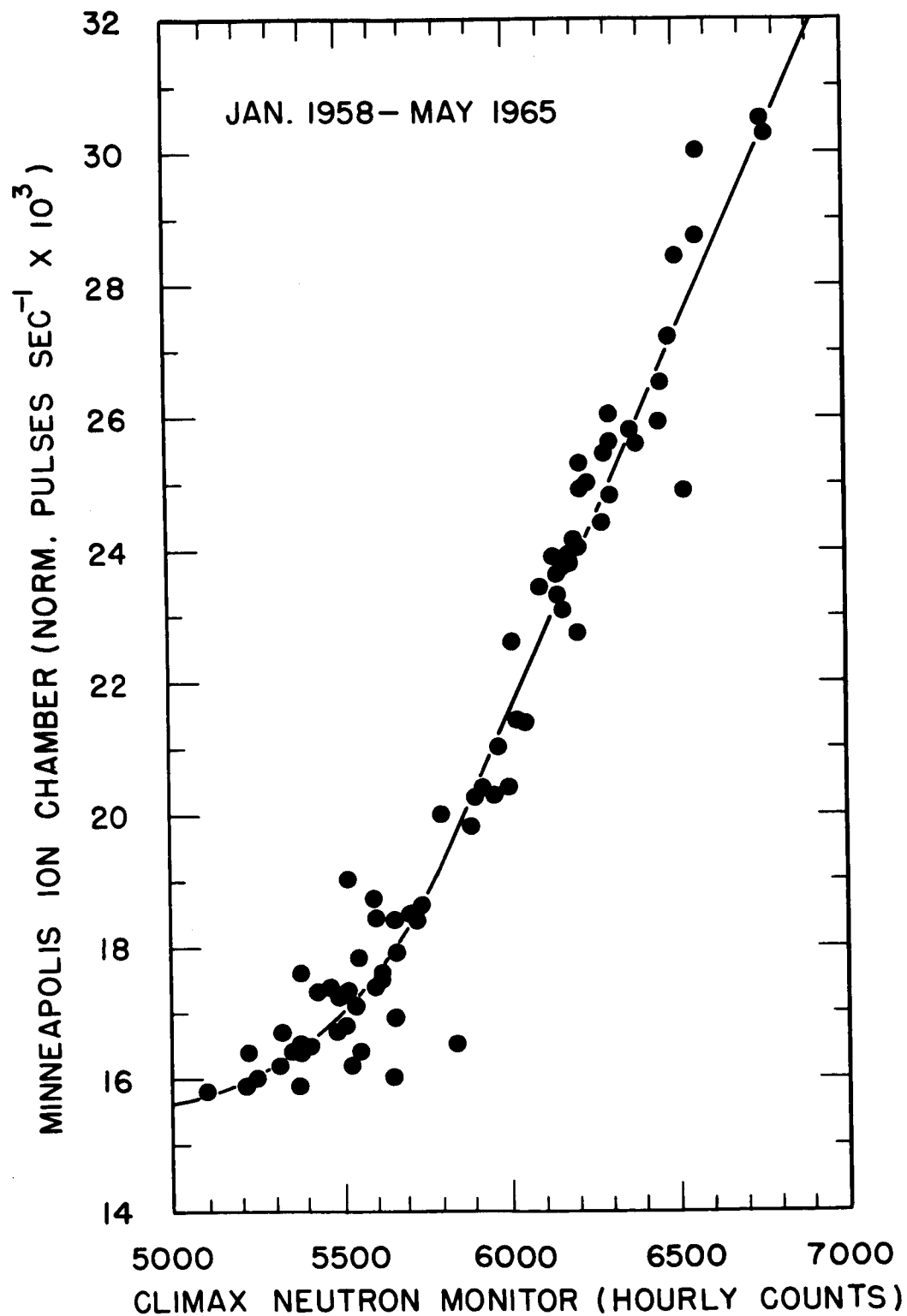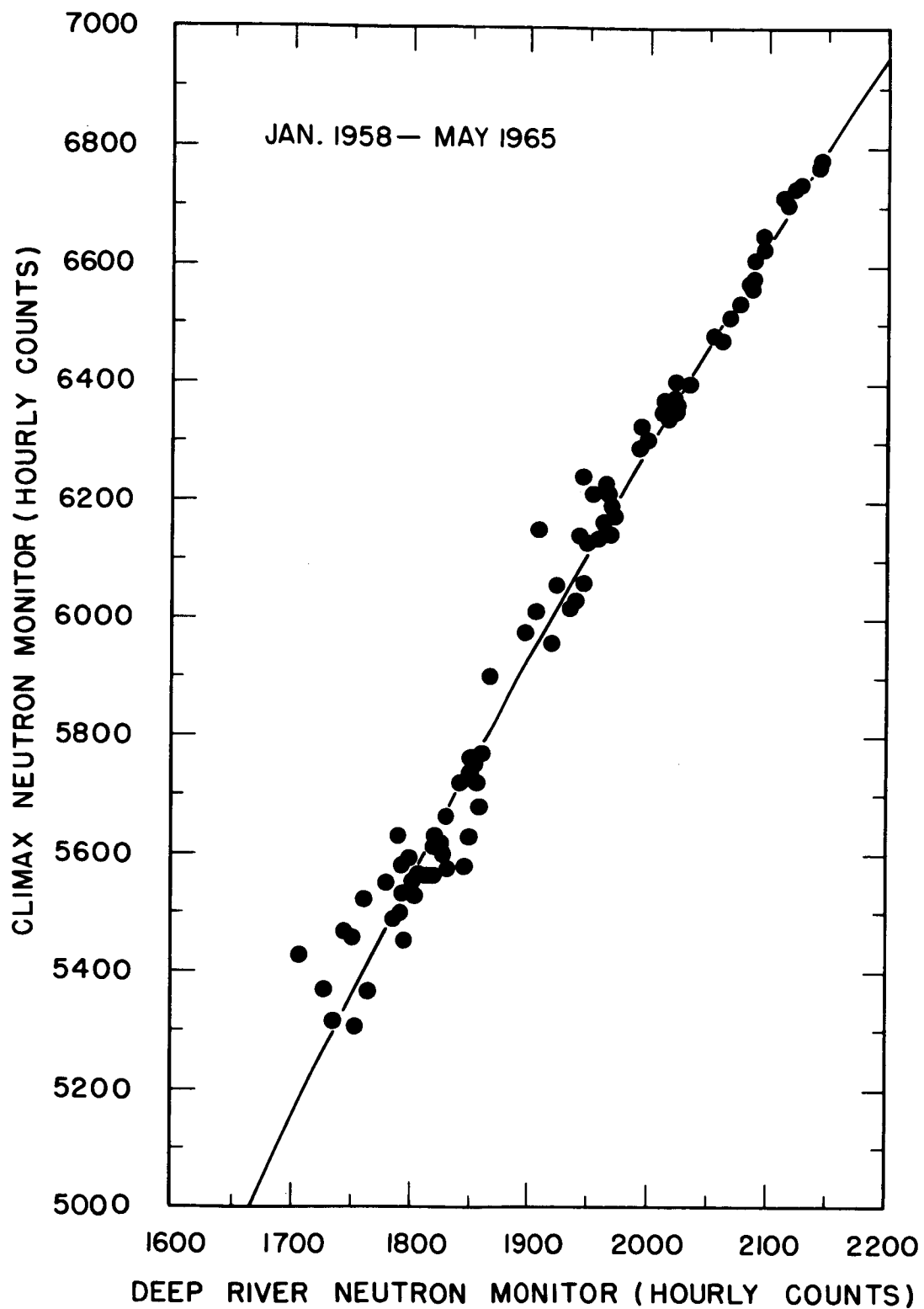
Figure 32

at Minneapolis and the Climax neutron monitor has been presented
by Callender et al. (1965) in Figure 10 of their paper for
the period August 1954 - September 1964. Measurements made
after September 1964 are now available, and so we have re-plotted
their data in Figure 31, which refers to the period January 1958 -
May 1965. The shape of this regression curve is similar to that
for the high latitude ionization chamber. The absolute
pulsing rate of the Minneapolis ionization chamber is somewhat
lower than that of the high latitude ionization chamber. This
is to be expected because the geomagnetic cutoff rigidity
at Minneapolis is about 1.3 BV while at high latitudes
the cutoff rigidity is determined only by the atmosphere above
the balloon and its value for protons is about 0.5 BV.

The regression curves presented earlier in Figures 28 and
30 are based on the Deep River neutron monitor. For the sake
of uniformity, it is desirable to have the Minneapolis
ionization chamber rates also plotted against the Deep River
neutron monitor rates. This can be achieved by using
Figure 32, which gives the regression curve between the
neutron monitors at Climax and Deep River, together with Figure 31.

V. RESPONSE TO COSMIC RAYS

(A) INTERPRETATION OF THE ION CHAMBER MEASUREMENTS IN FREE SPACE

While presenting the measurements made with the ionization

chambers outside the earth's magnetic field, it was tacitly

assumed that the rate of ionization as recorded by these chambers

is entirely due to the primary (galactic) cosmic rays. The

only other energetic particles (proton energy >10 MeV),

which are known to be present in this region of space are

believed to be of solar origin and are produced at the times

of large solar flares. Thus, at times of low solar activity

the chamber in free space can be assumed to respond almost

entirely to primary cosmic rays. That this is very nearly

the case is indicated by the good correlation between the

ion chamber and the ground based high latitude neutron monitor

as shown in Figures 25, 26 and 27. Although the neutron monitor

responds to primaries with rigidity ≈15 BV while the corresponding

rigidity for the ion chamber is ≈2 BV, the long term variation

is known to affect all primaries with rigidity $\leq$ 50 BV, the

magnitude of the variation depending on rigidity (Webber, 1962).

A good correlation between the ion chamber and the neutron

monitor rates is therefore to be expected if both the detectors

respond predominantly to the primary cosmic rays.

However, it is quite possible that even at quiet times

a fraction of the total ionization chamber rate is due to a

small quiescent flux of energetic solar particles. If such

solar particles are indeed present, there is no way of distinguishing
them from the galactic cosmic ray particles except probably
by their directionality or the differences in their variations.
For the present discussion it will be assumed that if such
solar particles are present, their contribution to the total
rate of the ionization chamber is small compared to that due
to the primary cosmic rays and hence the former may be neglected.

(B) THE LONG-TERM VARIATION

As indicated in Chapter I, the galactic cosmic ray
intensity is known to undergo large variations with time.
These variations may be irregular and short-lived, like the
Forbush decreases, or the variations may be systematic long-
term variations like the 11-year variation. Both types of
variation are usually referred to as the "modulation" of the
galactic cosmic rays.

Extensive measurements with particle detectors, ion chambers
flown on balloons and satellites, and neutron monitors indicate
that the modulation is most pronounced at low rigidities.
The charge-discriminating particle detectors measure the
modulation of the individual primary charge components within
specific rigidity intervals, but they are limited to a certain
range of rigidities because of the rather poor statistical
accuracy and the difficulties in the identification and
energy measurement of the particles. On the other hand, ion
chambers and neutron monitors have good statistical accuracy.
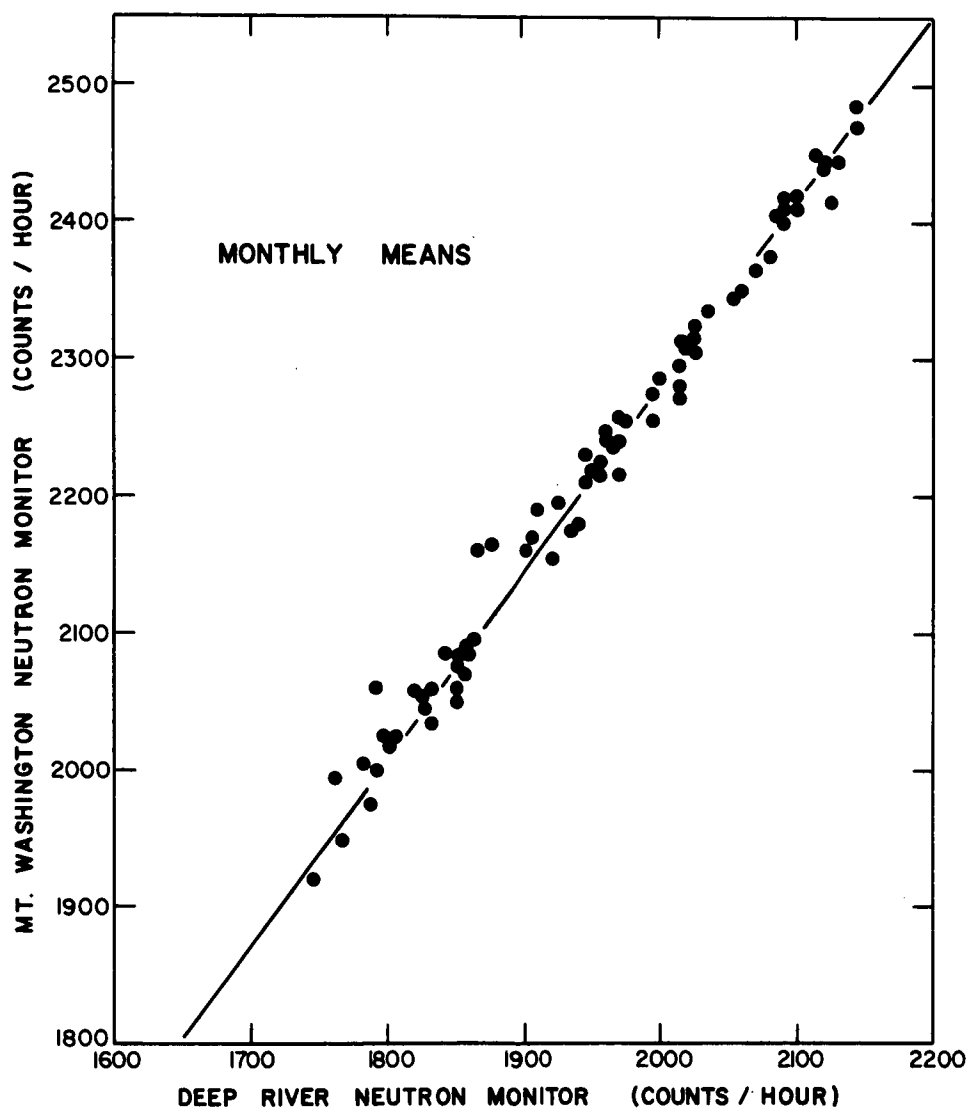
Figure 33

In fact, because of the careful calibration and construction procedures, the ion chamber measurements are consistent to within 1%. However, both ion chambers and neutron monitors respond to the total primary radiation over a wide range of rigidities, and their observed counting rates are related to the primary radiation in a complicated manner. Hence, in order to study and interpret the modulation of the primary cosmic rays over a large range of ridigities, it is advantageous to use all three kinds of detectors.

Although neutron monitors are operated continuously the measurements with the ionization chambers or charge discriminating particle detectors are not made on a continuous basis. The three kinds of measurements are thus made at different times and so it is necessary to define some common reference so that the three kinds of measurements can be compared with each other. It has been found that so far as the long-term variation is concerned the rate of a high latitude neutron monitor can be used interchangeably with time. This has already been illustrated for the ion chambers in free space and on balloons by the regression curves between these detectors and the Deep River neutron monitor presented in Figures 27, 30, 31 and 32. Regression curves for the intensity of He nuclei and protons in various rigidity intervals plotted against the Mt. Washington neutron monitor rate have been presented by Webber (1967) and Freier and Waddington (1965). With the help of the regression curve between the Mt. Washington and the Deep River neutron monitors shown in Figure 33, it is

TABLE 10

CORRELATED RATES OF VARIOUS DETECTORS

NEUTRON MONITOR (Hourly Counts)			He NUCLEI $\frac{}{M^2}$ SEC. STR.			ION CHAMBER (Norm. Pulses Sec^{-1} x10^3)		
Deep River	Mt. Washington	Climax	0.9-1.3 BV	1.3-2.0 BV	2.0-3.0 BV	FREE SPACE	HIGH LAT.	MINNEAPOLIS
1750	1940	5360	3.5	15.2	22.5			16.4
1800	2010	5550	4.5	18.0	25.7	17.5	18.1	17.3
1850	2075	5750	5.8	23.2	30.5	24.0	20.3	18.7
1900	2145	5930	9.0	31.0	36.8	30.7	22.4	20.6
1950	2215	6110	15.0	40.7	43.7	37.5	24.7	22.7
2000	2280	6290	23.0	51.5	50.0	44.2	27.0	24.8
2050	2350	6455	33.7	65.2	57.2	51.0	29.3	26.8
2100	2415	6630	44.5	80.2	64.2	57.7	31.7	28.6
2150	2485	6790	58.5	98.7	72.0	64.8	35.0	30.4

possible to use the Deep River neutron monitor rate as the
"level" of cosmic ray intensity and compare the changes in the
ion chamber rates and the intensities of He nuclei and protons
with the changes in the level of the cosmic ray intensity.
For the purpose of computations the various regression curves
mentioned above are summarized in Table 10 where the counting
rates of the ion chambers and the intensity of He nuclei in
various rigidity intervals are given for the various levels
of cosmic ray intensity represented by the neutron monitor rates.

An attempt made to correlate the observations made with
various detectors is shown in Figure 34. It relates to the
part of the solar cycle between March 1960 and May 1965 when
the monthly mean rate of the neutron monitor at Deep River
increased from 1830 to its maximum value 2150 for the last
solar cycle. If we take the rate in May 1965 as the
reference level N_0 of the cosmic ray intensity and compute
the fractional change $[I(N_0) - I(N)]/I(N_0)$ in the intensity
of He nuclei, the ion chamber rates and the neutron monitor
rate as the intensity increases toward the maximum rates
corresponding to N_0, we obtain the curves shown in Figure 34.
Here the fractional increases in He nuclei intensity
and the ion chamber rates are plotted against the corresponding
increase in the Deep River neutron monitor rate. It can
be seen that the various curves are quite distinct, and the
successive curves differ from each other in a systematic manner.
This indicates that, even though ion chambers respond to
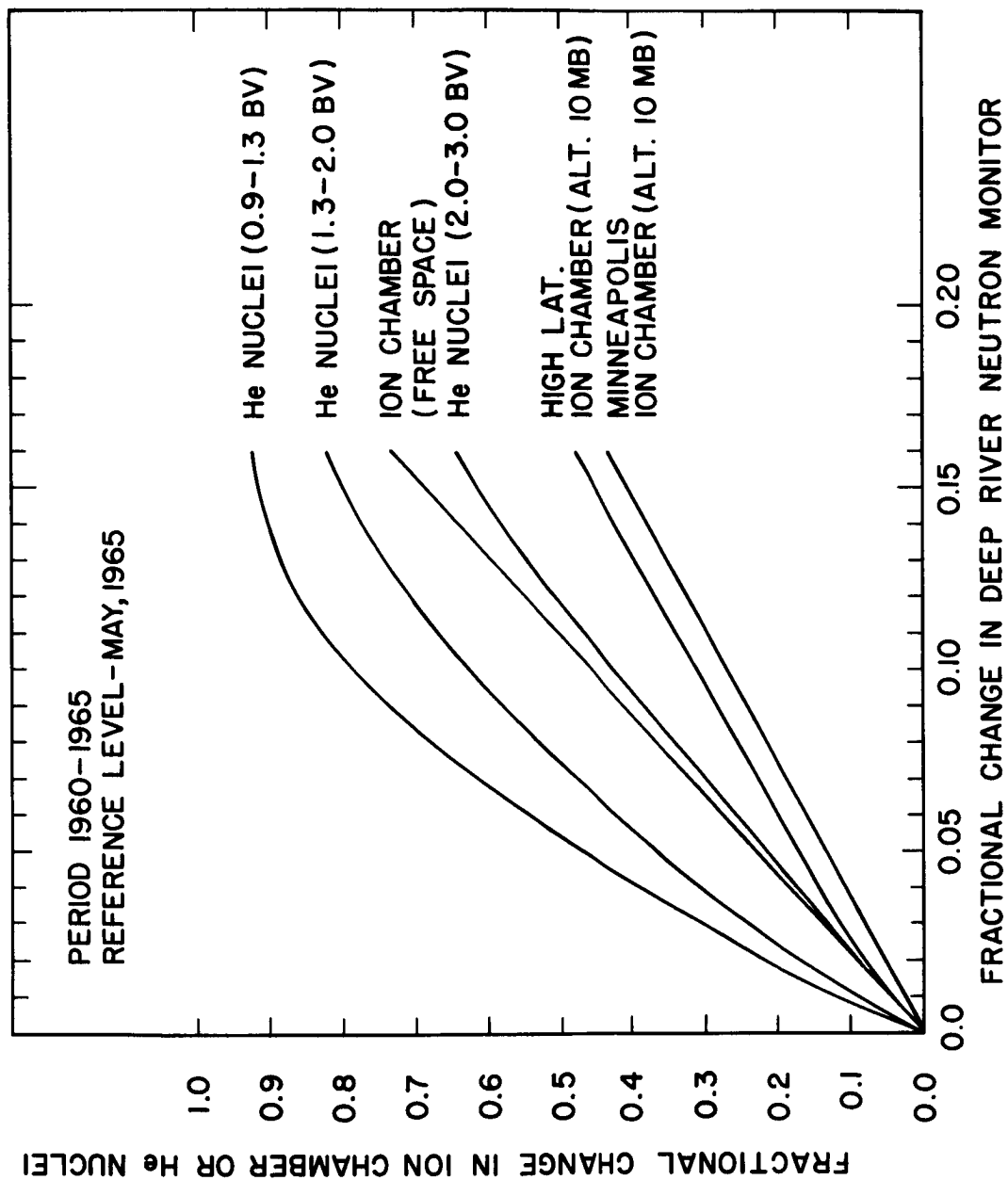
Figure 34

the total primary radiation over a wide range of rigidities, so far as the long-term variation is concerned, the response of an ion chamber in free space is predominantly confined to a comparatively small rigidity interval centered about 2 BV. Similarly, the ion chambers flown on balloons at high latitudes and at Minneapolis apparently respond mainly to the primary variations at rigidities somewhat higher than 3 BV.

In the light of this observation, we proceed to define a "characteristic" rigidity of response for an ion chamber on a balloon or in free space. Our object will be to make a rough estimate of such a characteristic rigidity in a manner completely independent of the above observation. Then we compare the computed rigidity with that expected on the basis of Figure 34 and other observations. It will turn out that, so far as the long-term variation is concerned, we do, indeed, expect a fairly well defined characteristic rigidity of response for an ion chamber and that the estimated value of the characteristic rigidity agrees fairly well with the available observations.

(C) RESPONSE CHARACTERISTICS OF CHAMBERS FLOWN ON BALLOONS

Variations observed with an ion chamber can be related to the variations in the primary cosmic rays with the help of the differential response curves. Callender et al. (1965) have recently discussed the response characteristics of high-altitude ion chambers. They have shown that at a time t the differential response $\partial I/\partial P(P,x,t)$ of an ion chamber at

a depth x in the atmosphere is related to the primary rigidity spectrum $D(P,t)$ by the relation:

$$(\partial I/\partial P) \ (P,x,t) = D(P,t) \ S(P,x) \qquad (5\text{-}1)$$

where $S(P,x)$ is the specific yield function.

Now, if we take the variation of this expression with respect to time, we get

$$\frac{(\partial I/\partial P) \ (P,x,t_o) - (\partial I/\partial P) \ (P,x,t)}{(\partial I/\partial P) \ (P,x,t_o)}$$

$$= \frac{D(P,t_o) - D(P,t)}{D(P,t_o)} \qquad (5\text{-}2)$$

where t_o is the time of reference. The above expression implies that the fractional change in the differential response at a given rigidity is directly comparable to the fractional change in the primary differential spectrum at the same rigidity.

Thus, if differential response curves of an ion chamber at two different times in the solar cycle are available, it is possible at least in principle to measure the fractional modulation of the primary spectrum at each rigidity between about 1 and 15 BV. However, an inspection of Figure 35 taken from Callender et al. (1965), shows that in practice the useful range of rigidities is considerably smaller, because of the relatively poor response of an ion chamber measuring total cosmic radiation to the variations in the high energy primaries. Moreover, ion chamber latitude surveys, from which

ION CHAMBER
IO Mb

1954

1958

R_λ GV

$\frac{dI}{dP}$ % OF I AT 15 GV
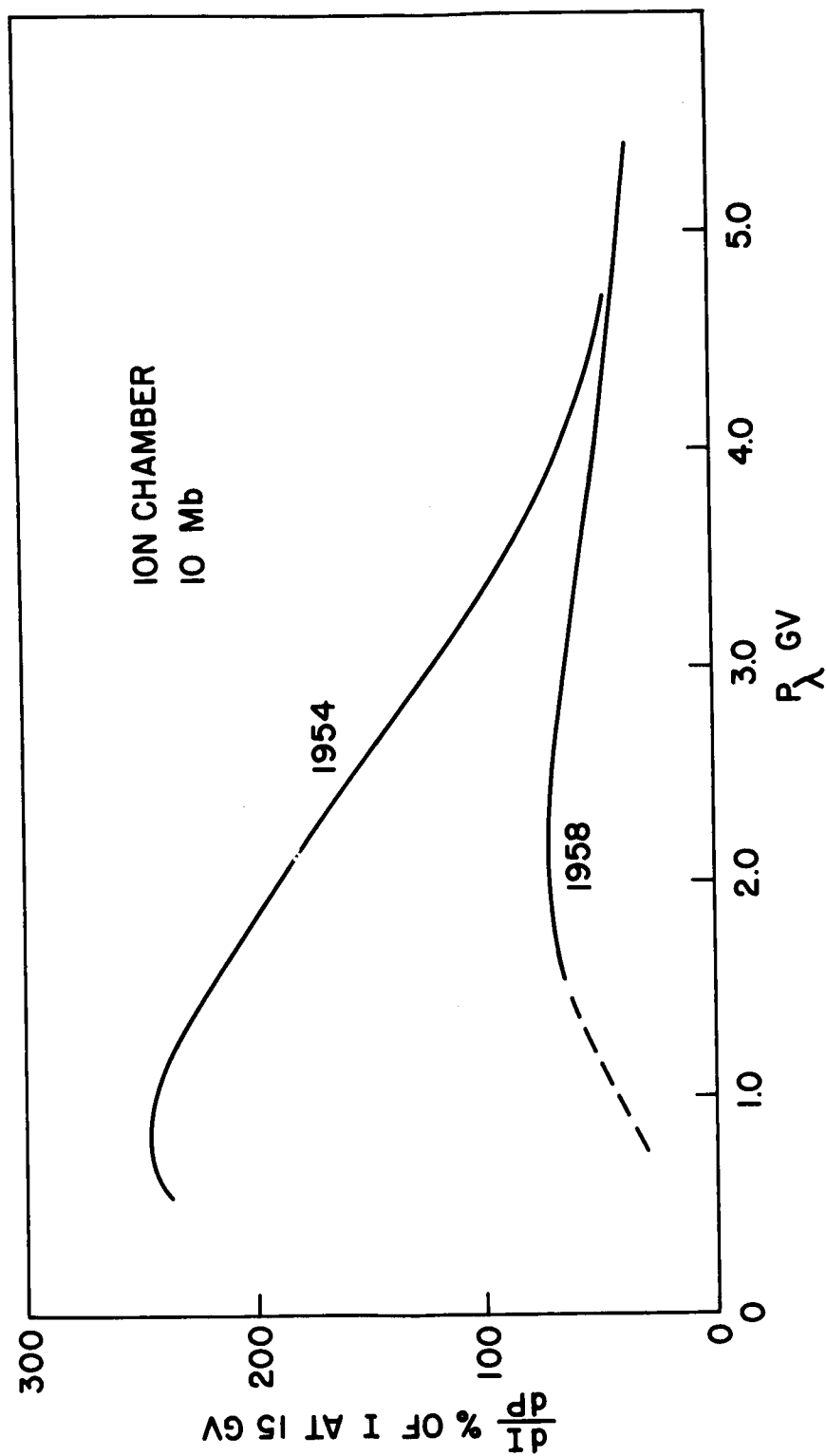
Figure 35

the differential response curves are obtained, are not available for all times in a solar cycle. It is therefore of interest to see if it is possible to express the gross features of the response characteristics of an ion chamber in terms of quantities which do not vary appreciably during a solar cycle.

As a first step in this direction, we define a mean rigidity of response

$$\overline{P}(P_\lambda,x,t) \quad = \quad \frac{\displaystyle\int_{P_\lambda}^{\infty} P(\partial I/\partial P)\ (P,x,t)\ dP}{\displaystyle\int_{P_\lambda}^{\infty} (\partial I/\partial P)\ (P,x,t)\ dP} \tag{5-3}$$

where P_λ is the vertical cutoff rigidity at the point of observation. At a given point of observation, P_λ and x are constant, and therefore $\overline{P}$ depends only on time or level of solar activity. The variation in $\overline{P}$ in the course of a solar cycle can be estimated with the help of the differential response curves in Figure 35. If we assume that beyond 5.5 BV the curves in Figure 35 maintain the same slope as at 5 BV, we can numerically calculate the mean rigidity of response $\overline{P}$ for the balloon ion chambers at 10 mb at high latitudes (P_λ = atmospheric cutoff $\simeq$ 0.5 BV) and at Minneapolis (P_λ = geomagnetic cutoff $\simeq$1.3 BV). The values obtained are, respectively, 2.5 and 3.2 BV at solar
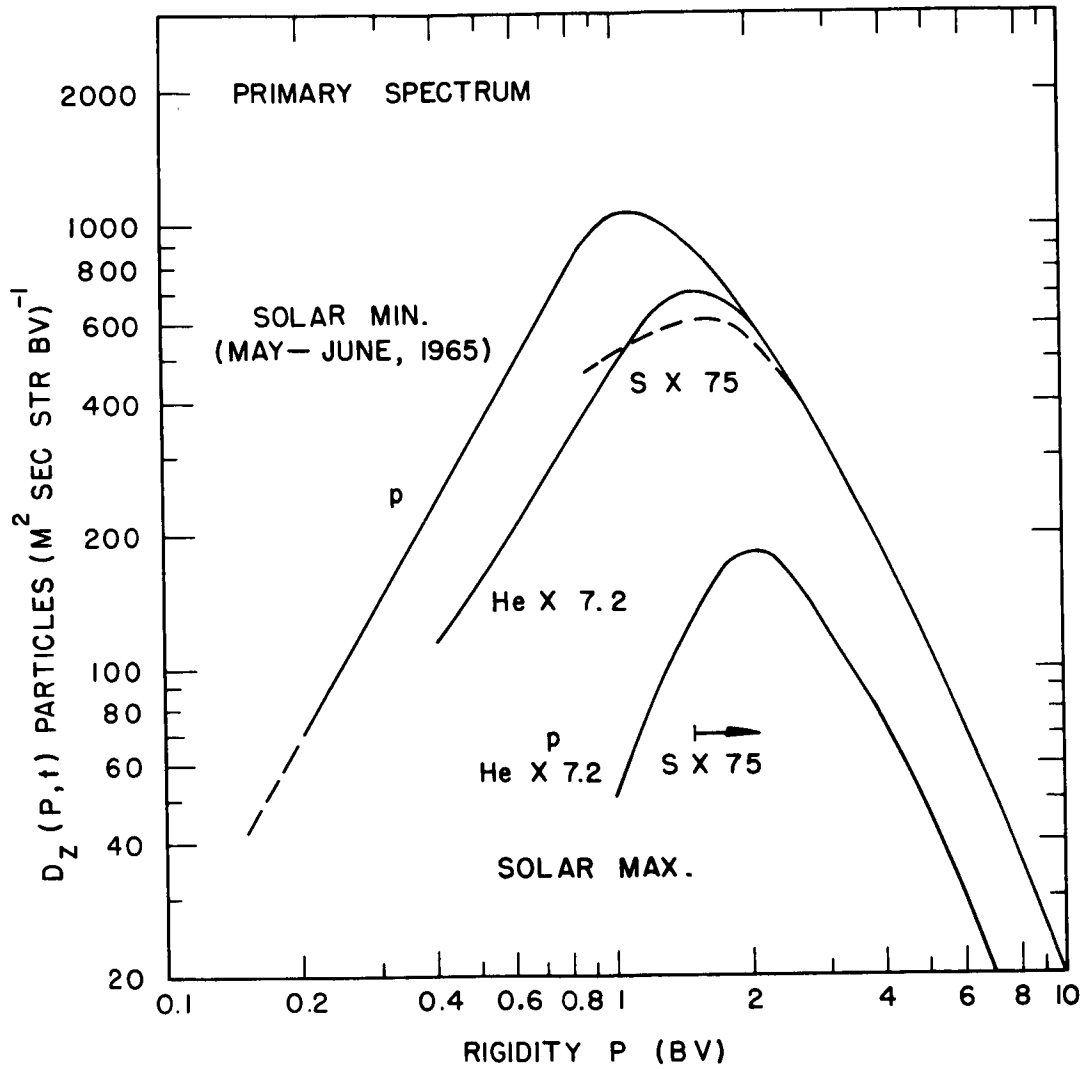
Figure 36

minimum and 3.6 and 3.8 BV at solar maximum.

(D)   RESPONSE OF CHAMBERS IN FREE SPACE

In the case of the ionization chambers in free space we
have to compute the differential response curve directly from
the primary cosmic ray spectrum. The present status of the
knowledge of the primary spectrum has been reviewed by
Webber (1962, 1967) and Freier and Waddington (1965). The
primary spectrum at the time of solar minimum is not known
accurately. In the current solar cycle the cosmic ray intensity
as measured by ionization chambers and neutron monitors reached
its maximum value in the middle of May, 1965 (see Figure 25).
Some measurements of the primary spectrum made at times close
to this period of maximum intensity are now available
(Comstock et al., 1966; Balasubrahmanyan et al., 1966). The
differential rigidity spectrum $D_Z(P,t)$ deduced from all the
available information is shown in Figure 36,(Professor Webber,
private communication). Here the intensity of the particles
in unit rigidity interval is plotted against the rigidity P.
The particles are divided into three groups, viz. protons,
He nuclei, and S nuclei (charge $Z \geq 6$). The last group consists
of the so-called medium and heavy nuclei. Since the spectra
for the individual nuclei are not well known, they have been
grouped together. The relative abundances of the individual
nuclei, as given by Webber (1967) are shown in Table 11 with
their respective charge Z and mass number A. For later

TABLE 11

NUCLEUS	CHARGE Z	MASS A	ABUNDANCE
C	6	12	1.0
N	7	14	0.46
O	8	16	0.61
F	9	19	0.09
Ne	10	20	0.18
Na	11	23	0.08
Mg	12	24	0.15
Al	13	27	0.03
Si	14	28	0.11
P	15	31	0.01
S-K	17.5	36.5	0.035
Ca	20	40	0.026
Ti	22	48	0.017
Cr	24	52	0.030
Fe	26	56	0.080
Ni	28	58	0.015

$$\overline{A} = \frac{\Sigma Aa}{a} = \frac{53.19}{2.92} = 18$$

$$\overline{z^2} = \frac{\Sigma z^2 a}{a} = \frac{295.5}{2.92} = 101$$

TABLE 12

PARTICLES	RIGIDITY P (BV)	PARTICLES M^{-2} SEC^{-1} STR^{-1}	
		SOLAR MIN	SOLAR MAX.
Protons	$\geq$ 4.5	648.0	468.0
He nuclei	$\geq$ 4.5	90.0	65.0
S nuclei	$\geq$ 4.5	8.5	5.6
Electrons	$\geq$ 0.0025	400.0	

reference the mean square charge $\overline{z^2}$ and the mean mass number $\overline{A}$ for the entire group of S nuclei are computed as shown in Table 11. It can be seen that $\overline{A}$ = 18 and $\overline{z^2}$ = 101.

In Figure 36 two groups of curves are shown, one for the solar minimum period and the other for the solar maximum period. For the solar minimum period, there are three distinct curves for protons, He nuclei, and S nuclei below about 2.5 BV rigidity. However, during the solar maximum period, the three curves coincide, the curve for S nuclei being valid only for rigidity P $\geq$ 1.5 BV. It should be noted that while plotting these curves the actual intensities of the He and S nuclei are multiplied by 7.2 and 75 respectively.

The absolute intensities represented by the primary spectra in Figure 36 are believed to be accurate within 5-10 percent. To the above species of nuclei one must add the electrons which have an integral flux of about 400 particles M^{-2} sec^{-1} $ster^{-1}$ above 2 MeV(Professor Webber - private communication). In order to compute the total ionization in the OGO chamber we also need to know the integral fluxes of the primary particles with rigidity P $\geq$ 4.5 BV. These are listed in Table 12.

The response of the OGO ion chamber to protons, heavy nuclei, and electrons has already been presented in Figures 12 and 15 as a function of the energy of these particles. For the present purpose we need the response to protons and heavier nuclei as a function of their rigidity. This is shown in Figure 37 which is based on Figure 12. The response curve for He nuclei given in Figure 37 is also applicable
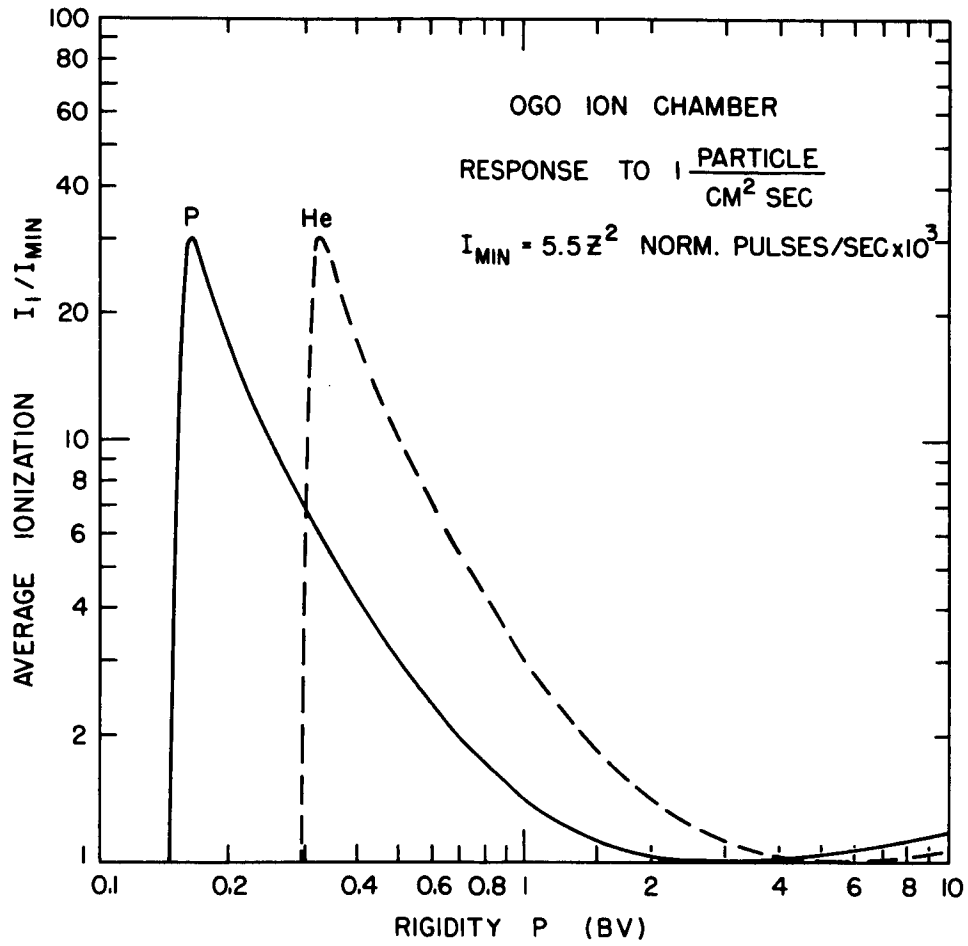
Figure 37

to S nuclei at rigidities $P \geq 0.7$ BV.

Let $I_1(Z,P)$ be the pulsing rate (norm. pulses $\sec^{-1} \times 10^3$) of the ion chamber due to an omnidirectional flux of 1 particle $cm^{-2} \sec^{-1}$ for particles of charge Ze and rigidity P BV. If $D_Z(P,t)$ particles $M^{-2} \sec^{-1} ster^{-1} BV^{-1}$ be the primary differential rigidity spectrum at time t for particles of charge Ze and rigidity P, the omnidirectional flux of these particles is $4\pi \times 10^{-4} D_Z(P,t)$ particles $cm^{-2} \sec^{-1} BV^{-1}$. Hence, the differential response of the chamber due to the primaries of this species is given by

$$\frac{\partial I_Z}{\partial P}(P,t) = 4\pi \times 10^{-4} I_1(Z,P) D_Z(P,t)$$

$$= 4\pi \times 10^{-4} \times 5.5 \ Z^2 \frac{I_1(Z,P)}{I_{Min}} D_Z(P,t)$$

$$\text{norm. pulses } \sec^{-1} BV^{-1} \times 10^3 \ . \qquad (5-4)$$

Now $D_Z(P,t)$ and I_1/I_{Min} are given in Figures 36 and 37 respectively. Therefore,

$\frac{\partial I_Z}{\partial P}$ can be immediately computed for protons, He nuclei, and S nuclei for various values of P. The results obtained are summarized in Table 13 for solar minimum as well as solar maximum conditions. If, for a particular time t, we add the contributions by the primaries with different charges corresponding to the same value of rigidity we get the total

TABLE 13

DIFFERENTIAL RESPONSE OF OGO ION CHAMBER
TO PRIMARY COSMIC RAYS

P (BV)	$\frac{\partial I}{\partial P}$ (NORM. PULSES SEC^{-1} BV^{-1} x 10^3)			
	SOLAR MINIMUM			
	P	He	S	TOTAL
0.15	1.19			1.19
0.2	8.32			8.32
0.3	6.87			6.87
0.4	6.99	7.41		14.40
0.6	7.96	5.58		13.54
0.8	9.52	5.23		14.75
0.9	10.04	5.24	15.29	30.57
1.0	10.45	5.28	13.84	29.57
1.2	9.06	5.43	12.01	26.50
1.4	7.54	5.15	10.51	23.20
1.6	6.30	4.62	9.47	20.39
1.8	5.34	3.93	8.47	17.74
2.0	4.57	3.78	7.29	15.64
2.2	3.87	2.73	6.09	12.69
2.4	3.34	2.29	5.14	10.77
2.6	2.83	1.88	4.39	9.10
2.8	2.48	1.61	3.83	7.92
3.0	2.18	1.38	3.30	6.86
4.0	1.24	0.73	1.74	3.71
5.0	0.78	0.43	1.02	2.23
6.0	0.53	0.24	0.68	1.45
7.0	0.37	0.20	0.47	1.04
8.0	0.27	0.14	0.34	0.75
9.0	0.20	0.10	0.25	0.55
10.0	0.16	0.08	0.19	0.43

TABLE 13   cont.

DIFFERENTIAL RESPONSE OF OGO ION CHAMBER
TO PRIMARY COSMIC RAYS

P (BV)	$\frac{\partial I}{\partial P}$ (NORM. PULSES SEC^{-1} BV^{-1} x 10^3)			
	SOLAR MAXIMUM			
	P	He	S	TOTAL
0.15				
0.2				
0.3				
0.4				
0.6				
0.8				
0.9				
1.0	0.48	0.57		1.05
1.2	0.69	0.73		1.42
1.4	0.89	0.85		1.74
1.6	1.07	0.94	2.24	4.25
1.8	1.24	1.01	2.40	4.65
2.0	1.30	0.74	2.34	4.38
2.2	1.26	0.91	2.16	4.33
2.4	1.15	0.79	1.88	3.82
2.6	1.03	0.69	1.64	3.36
2.8	0.93	0.60	1.44	2.97
3.0	0.83	0.53	1.26	2.62
4.0	0.50	0.30	0.71	1.51
5.0	0.32	0.18	0.42	0.92
6.0	0.21	0.11	0.27	0.59
7.0	0.15	0.08	0.19	0.42
8.0	0.11	0.06	0.14	0.31
9.0	0.09	0.04	0.10	0.23
10.0	0.06	0.03	0.06	0.15
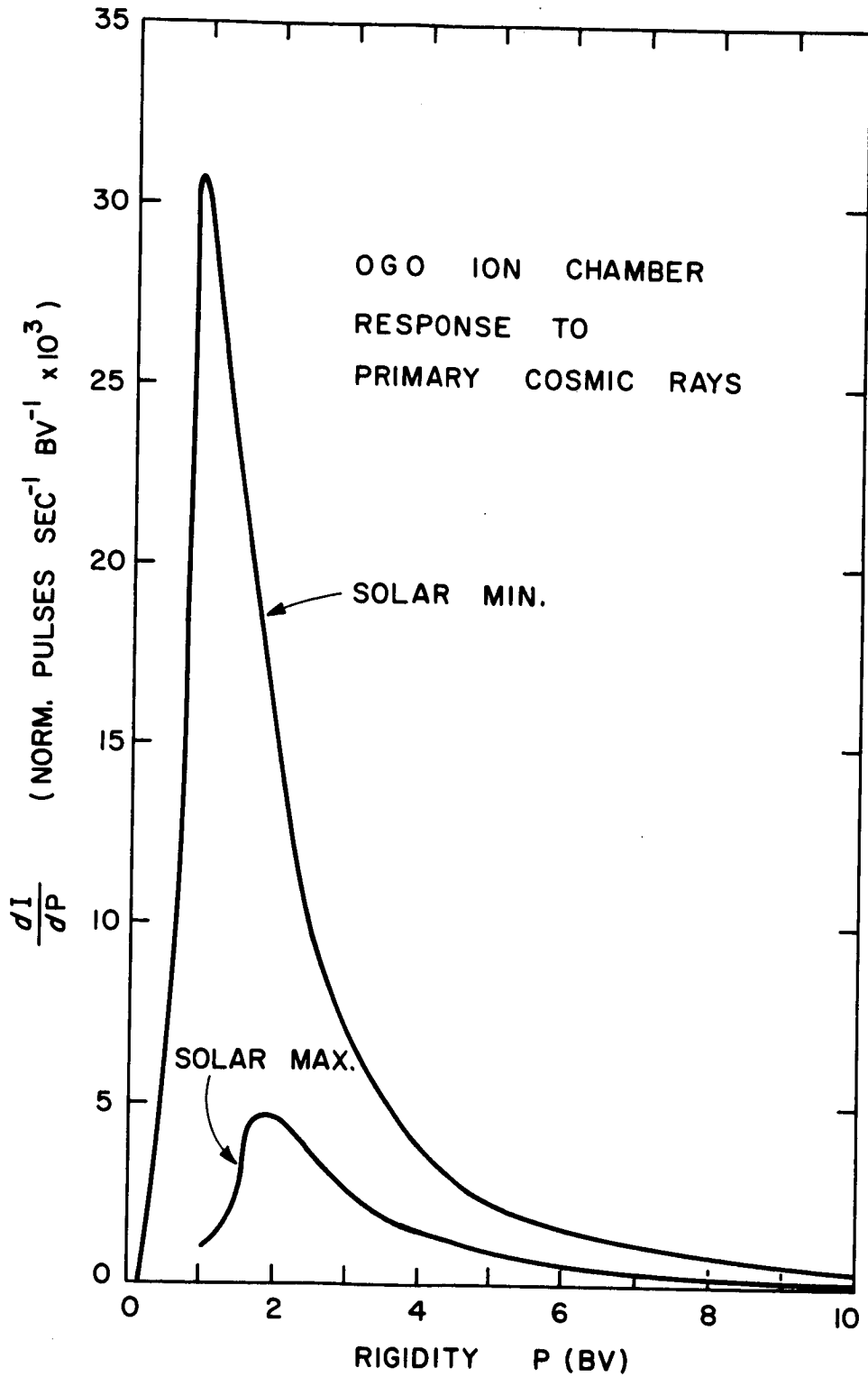
Figure 38

differential response

$$\frac{\partial I}{\partial P} (P,t) = 4\pi \times 10^{-4} \times 5.5 \sum_{Z} Z^2 \frac{I_1(Z,P)}{I_{Min}} D_Z (P,t)$$

$$\text{norm. pulses sec}^{-1} \text{ BV}^{-1} \times 10^3 \tag{5-5}$$

The values obtained are tabulated in Table 13 and are shown graphically by a smooth curve in Figure 38.

An idea of the total expected chamber rate at solar minimum and the contributions of protons, He nuclei, S nuclei, and electrons to this rate can be obtained from Table 14. The rates due to the various primary nuclei are computed by numerically integrating the differential response given in Table 13 between the rigidity interval 0.2 - 4.5 BV and then adding to this the rate due to the particles with $P \geq 4.5$ BV (given in Table 11) for which the ionization was taken as (see Figure 37)

$$1.05 \times 5.5 Z^2$$
$$= 5.78 Z^2 \text{ norm. pulses sec}^{-1} \times 10^3$$

From Table 14 and Figure 38 we note the following

1. The differential response of the OGO ion chamber to primary cosmic rays has a prominent maximum close to 1 BV at solar minimum and close to 2 BV at solar maximum.

2. At solar minimum, more than 80 percent of the observed chamber rate is due to primary particles with rigidity $P \leq 10$ BV.

TABLE 14

OGO ION CHAMBER RATE AT SOLAR MINIMUM

RIGIDITY P (BV)	NORM PULSES SEC^{-1} x 10^3			
	PROTONS	He NUCLEI	S NUCLEI	TOTAL
⟨ 1.5	10.4	5.5	7.3	23.2
1.5-4.5	9.0	5.6	12.3	26.9
4.5-10.0	2.3	1.2	2.9	6.4
⟩ 10	1.3	0.8	1.9	4.0
ALL NUCLEI	23.0	13.1	24.4	60.5
ELECTRONS P⟩2.5 MV				3.5
NUCLEAR INTERACTIONS				~10.0*
TOTAL COMPUTED OBSERVED				74.0 65.0

* See Section (G).

3. At solar minimum the contributions to the total chamber rate by protons, He nuclei, S nuclei, and electrons are about 31, 18, 33, and 5 percent respectively.

4. The observed chamber rate of 65 norm. pulses sec^{-1} x 10^3 at solar minimum (Figure 25) is about 12 percent lower than the computed rate of 74 norm. pulses sec^{-1} x 10^3. This discrepancy could be due to a number of known factors (e.g. uncertainties in the primary spectrum).

As in the case of the balloon ion chambers, we can now calculate the mean rigidity of response $\bar{P}$ for an ion chamber in free space by using the response curves $\frac{\partial I}{\partial P}$ (P,t) presented in Figure 38. As noted above, the contribution to the chamber rate from the particles with P > 10 BV is <19 percent. Therefore, we extend the integration only up to 10 BV rigidity and compute the mean rigidity of response using the following relation:

$$\bar{P}(t) = \frac{\int_{0.2}^{10} P \frac{\partial I}{\partial P} (P,t) \, dP}{\int_{0.2}^{10} \frac{\partial I}{\partial P} (P,t) \, dP} \tag{5-6}$$

The integrals have been evaluated numerically. The values obtained for $\bar{P}$ are 2.3 BV at solar minimum and 3.2 BV at solar maximum.

(E) DISCUSSION

The object of making the above calculations is to make an estimate of the mean rigidity of response of an ion chamber and to determine the extent to which it varies during a solar cycle. The accuracy of the calculations is limited by several factors. In the case of the ion chambers flown on balloons the differential response curve, which is deduced from the latitude surveys, is not known beyond about 5 BV rigidity. An extrapolation is therefore necessary in order to take into account the response at rigidities >5BV. In the case of the ion chambers in free space, the accuracy of the computations is limited by the uncertainties in the knowledge of the primary spectrum, contributions to the chamber rate from the nuclear interactions of the primary particles with matter in the vicinity of the chamber and in the chamber itself, and the fraction of the ionization in the ion chamber lost due to recombination especially in the case of heavily ionizing particles.

In view of the uncertainties mentioned above, the computations presented earlier, and the observations shown in Figure 34, we assign for the different ion chambers the following rigidity intervals in which most of their response is concentrated:

Location of the chamber	Rigidity interval (BV)
Free space	1.5 - 2.5
High latitudes (10 mb)	2.5 - 3.5
Minneapolis (10 mb)	3.0 - 4.0

These rigidity intervals are valid over the entire solar
cycle. Moreover, they apply also to individual primary charge
components because above about 1.5 BV the various primary nuclei
are known to undergo roughly similar long-term variation in all
rigidity intervals (Webber, 1962).

We have attempted to show here that although an integrating
type of detector, like an ion chamber, responds to primary
particles with a wide range of energy and charge, the gross
features of the measurements by such a detector can be interpreted
in terms of a mean rigidity of response as defined earlier.
The validity of such an interpretation depends primarily on
the sharpness of the differential response curve. The narrower
the curve, the better is the interpretation in terms of the
mean rigidity. In case of the studies of the long-term variation
from solar minimum to solar maximum conditions, another criterion
for the validity of the interpretation in terms of a mean
rigidity of response is the closeness of the value of the mean
rigidity of response at the solar maximum to that at the
solar minimum.

In case of ion chambers flown on balloons and on satellites,
all these three criterions are farily well satisfied, as can
be seen from Figures 35 and 38. The difference between the
mean rigidities of response at solar minimum and solar maximum
is about 1 BV, which is comparable to the rigidity intervals
in which the measurements of the differential rigidity spectrum

of the primary cosmic rays are made with charge discriminating particle detectors.

On this basis we would expect that the modulation of the balloon ion chamber at Minneapolis should be a fair representative of the long-term changes in the intensity of He nuclei between 3 and 4.6 BV. To check this, we consider the integral intensities of He nuclei above 3 BV and 4.6 BV as observed by various workers and summarized by Freier and Waddington (1965). Figure 39, taken from their paper, shows that the measurements $J(> 4.6 \text{ BV})$ are fairly consistent, and the solid regression line drawn by the authors seems to fit the data quite well. However, the measurements $J(> 3.0 \text{ BV})$ show considerable scatter. We therefore assume that the helium nuclei intensity $J(> 4.6 \text{ BV})$ is truly represented by the regression line, and, on the basis of the modulation observed with the Minneapolis ion chamber, we proceed to compute the expected helium nuclei intensity $J(> 3.0 \text{ BV})$.

Let the level of the cosmic ray intensity be indicated by the counting rate N of the Mount Washington neutron monitor. We take the reference level $N_0 = 1940$. Now, it has been demonstrated by Callender et al. (1965), Webber (1967), and Freier and Waddington (1965) that, at least on a long-term basis, the pulsing rate of an ion chamber or the intensity of primary He nuclei depends basically on the level of cosmic ray intensity as determined by the counting rate of a neutron monitor. Therefore, for long-term changes, we can use N
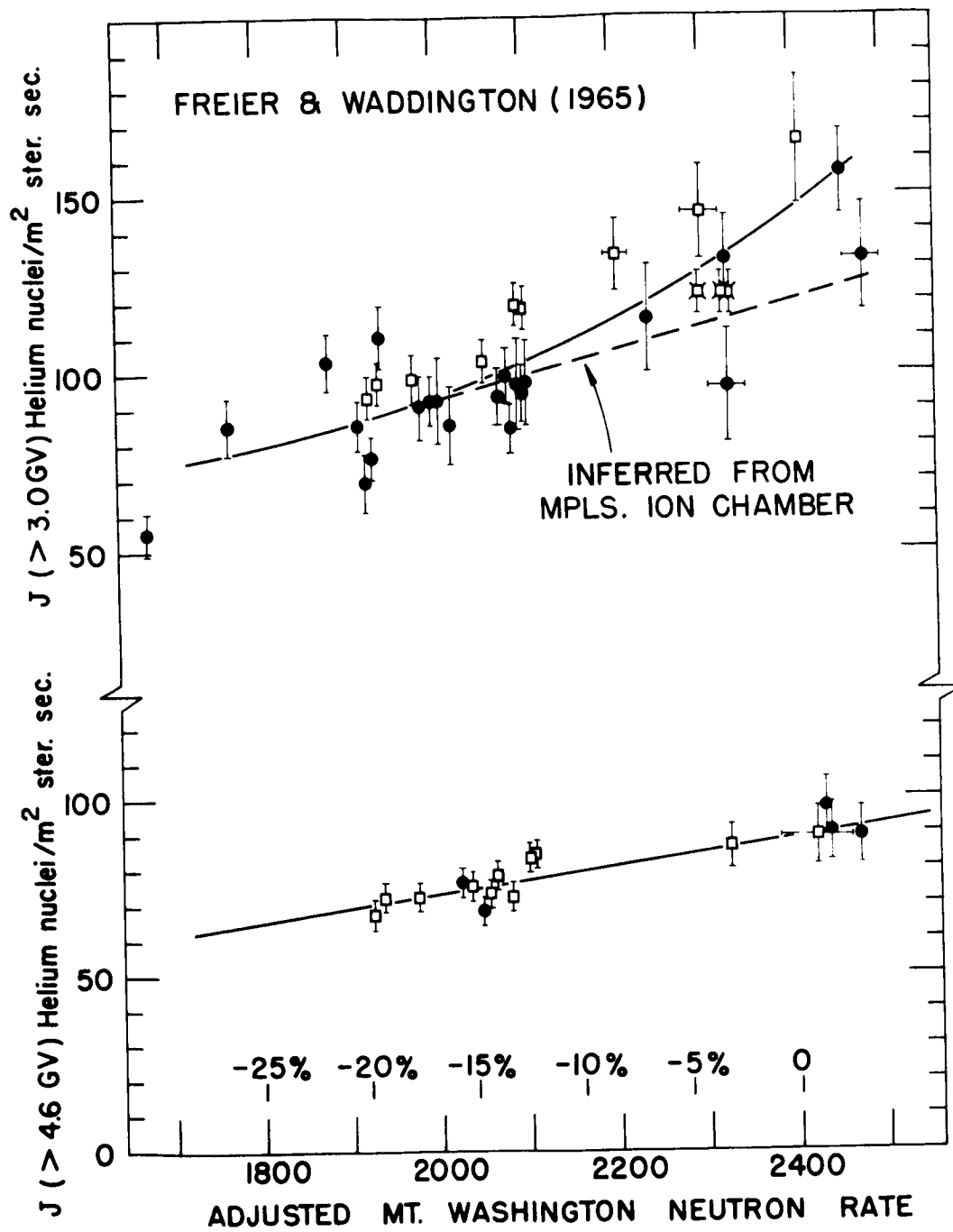
Figure 39

interchangeably with time t.

Let $I(N)$ be the pulsing rate of the Minneapolis ion chamber at 10 mb, and let $J(P > P_1, N)$ be the corresponding intensity of He nuclei with rigidity $P > P_1$ BV. Then, if we assume that the modulation of He nuclei with rigidity between 3 and 4.6 BV is the same as that of the Minneapolis ion chamber, we get

$$\frac{[J(P > 3.0,N_0) - J(P > 4.6,N_0)] - [J(P > 3.0,N) - J(P > 4.6,N)]}{J(P > 3.0,N_0) - J(P > 4.6,N_0)}$$

$$= \frac{I(N_0) - I(N)}{I(N_0)} \qquad (5-7)$$

or

$$J(P > 3.0,N) = [I(N)/I(N_0)] [J(P > 3.0,N_0) - J(P > 4.6,N_0)]$$

$$+ J(P > 4.6,N) \qquad (5-8)$$

The values of $I(N)$ and $J(P > 4.6,N)$ are known from Figures 31, 32, 33 and 39. If we take $J(P > 3.0,N_0)$ to be 89 He nuclei m^{-2} sec^{-1} $ster^{-1}$, as is consistent with Figure 39, we can calculate $J(P > 3.0,N)$ for various N by taking the corresponding values of the other quantities. The values of $J(P > 3.0,N)$ obtained in this way are shown by the dashed line in Figure 39. It can be seen that the calculated values are consistent with the observed values, indicating that the modulation observed with the Minneapolis ion chamber at 10 mb altitude is in fair

agreement with the modulation of the He nuclei in the rigidity range 3.0 - 4.6 BV.

It is important to note that the above analysis applies to quiescent cosmic ray intensity and its long-term variation. In case of short-term variations where the cosmic ray spectrum is considerably different from that shown in Figure 36, the mean rigidities of response deduced here are not applicable. In particular, the present analysis is not valid for solar cosmic rays because their energy spectrum is completely different from that of the galactic cosmic rays at any time during a solar cycle.

(F) RIGIDITY DEPENDENCE OF THE LONG-TERM VARIATION BETWEEN 1960 AND 1965

As an illustration of the use of the response characteristics of the various ion chambers deduced earlier, we proceed to determine the rigidity dependence of the long-term variation of the primary cosmic rays in the rigidity range 1.5 - 4.0 BV. This rigidity interval partially overlaps with the interval in which intensity measurements of He nuclei are usually made. We therefore expect that with the help of the ion chamber and He nuclei measurements reliable information can be obtained about the form of the modulation function in the rigidity range 1.5 - 4.0 BV where the changes in the primary spectrum are believed to be basically rigidity dependent.

The relevant observations have already been presented in Figure 34. Now we plot the total fractional change in the

PERIOD 1960–1965
(DEEP RIVER N.M. 1800–2150)

He NUCLEI ●
ION CHAMBER ■

$P^{-0.9}$
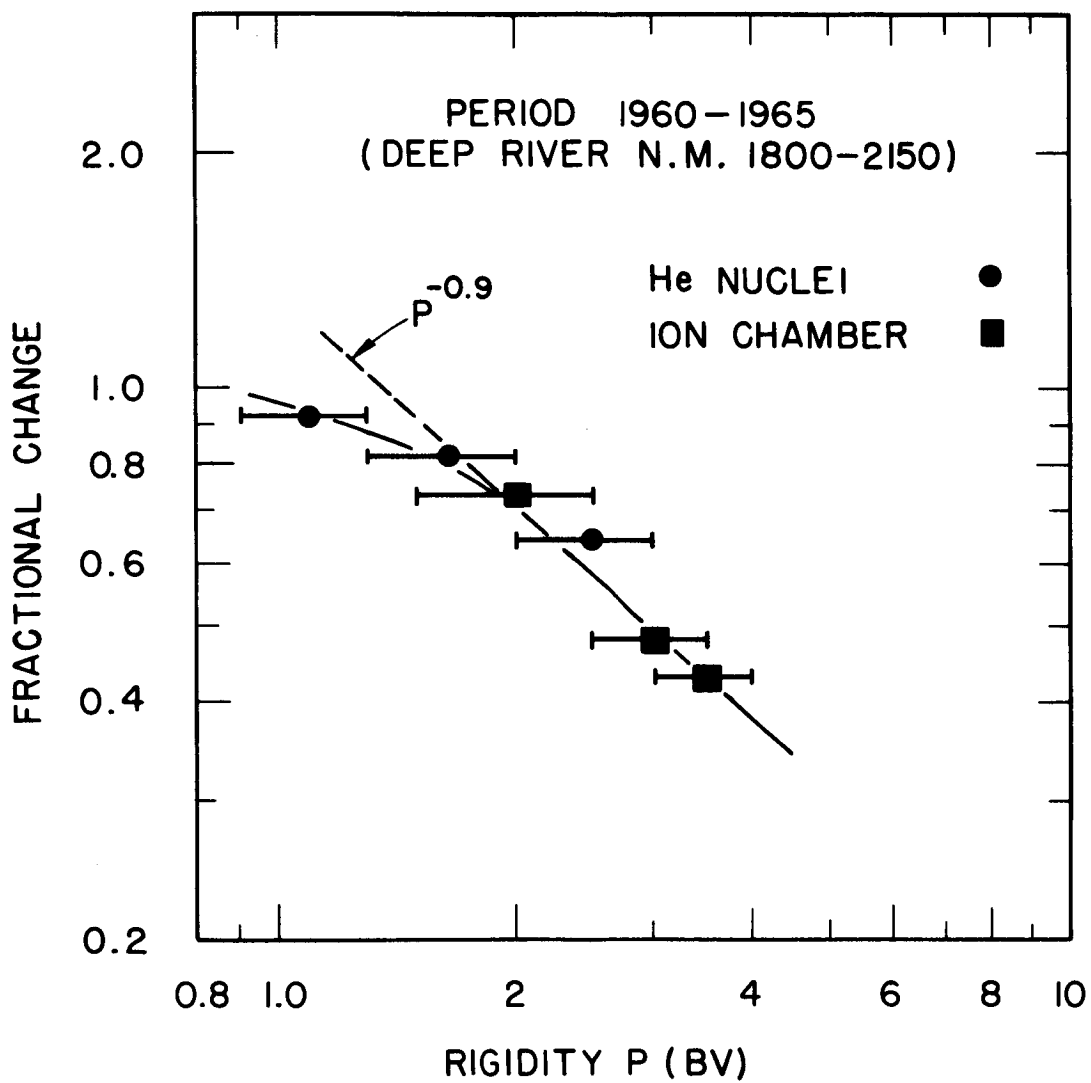
Figure 40

intensity of He nuclei and the ion chamber rates against the mean rigidity to which each of these measurements correspond. The results are shown in Figure 40. The horizontal bars shown in this figure correspond to the range of rigidity over which the measurement is valid. In case of He nuclei this range is the actual range of rigidities in which the measurements were made. In the case of the ionization chamber the bar represents the range of rigidity over which the mean rigidity of response varies during the solar cycle. From Figure 40 it can be seen that the observations above 1.5 BV are consistent with a modulation of the form

$$\frac{D(P,t) - D(P,t_0)}{D(P,t_0)} \simeq P^{-\beta} \tag{5-9}$$

where $D(P,t)$ is the primary differential rigidity spectrum at time t, P being the rigidity and t_0 the time corresponding to May 1965. The straight line in the figure corresponds to $\beta = 0.9$.

The nature of the rigidity dependence of the long-term variation deduced from Figure 40 is similar to that observed earlier by other workers for other periods of solar activity (see for example the summary by Webber, 1962). Here these results are presented primarily to illustrate the application of the response characteristics of the free space ion chamber deduced earlier. To determine the true form of the modulation function it is necessary to have observations over a rigidity

range considerably wider than the one available here. Several
workers have made measurements in various rigidity intervals at
times close to the last cosmic ray maximum, viz. May 1965.
All these measurements are not yet available. The points for
He nuclei shown in Figure 40 are based on measurements made
at times close to cosmic ray maximum in the previous solar cycle,
viz. 1954-55. Moreover, for studies of the mechanisms responsible
for the observed long-term variation during the solar minimum
period, the rigidities of interest are those below 1 BV, because
at these rigidities the modulation effects are larger and appear
to depend on the charge as well as the energy of the primary particle.
These ranges of rigidities are not covered by the present analysis.
Therefore no attempt will be made here to determine the exact form
of the modulation function or the mechanism which could give rise
to the observed modulation.
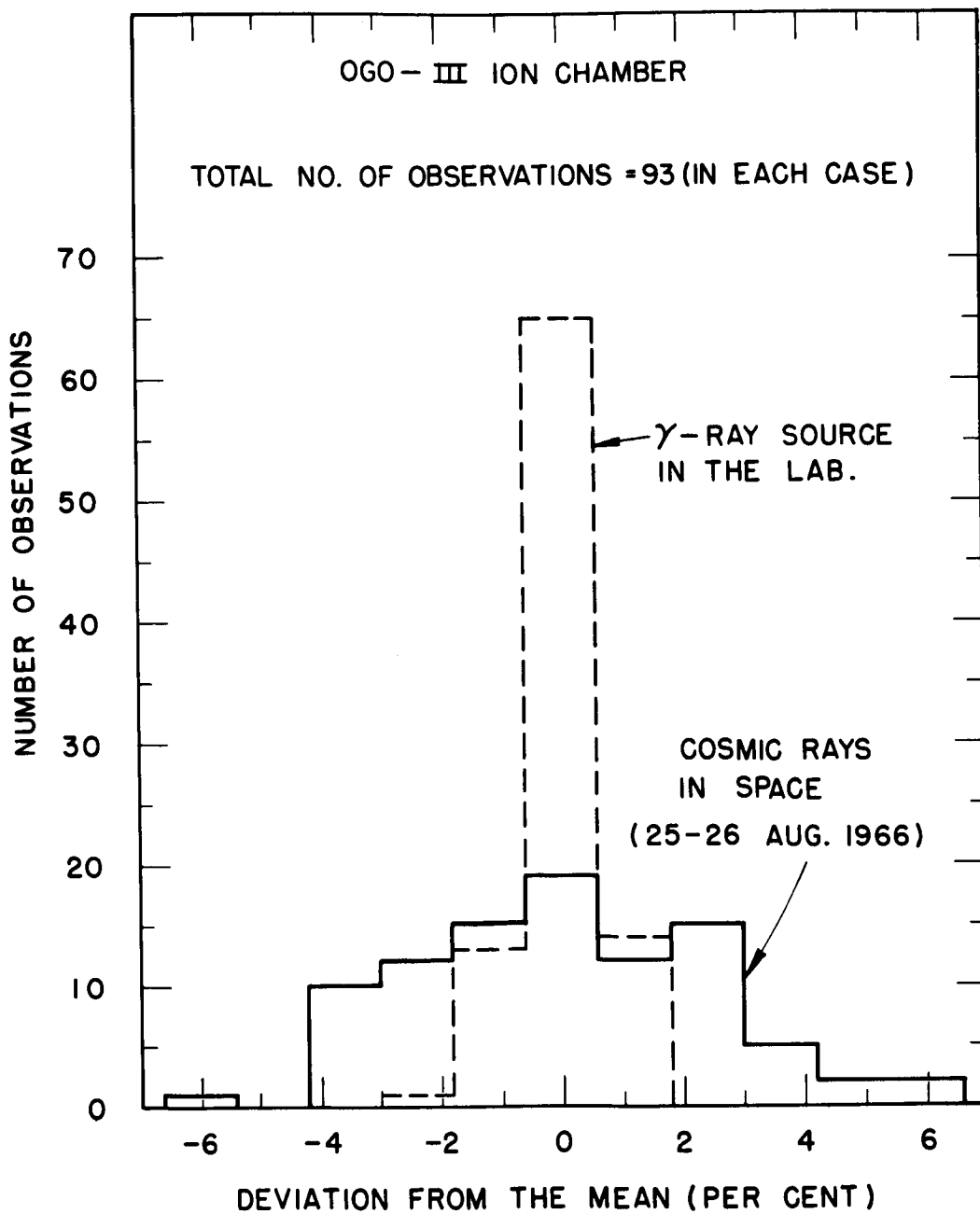
Figure 41

(G) FLUCTUATIONS

A characteristic feature of the cosmic ray measurements with an ion chamber on a balloon or in free space is the fluctuations of the chamber rate about an average value. It is important to know if there is any particular physical process (e.g. nuclear interactions or heavy nuclei stopping in the chamber) which is the principal cause of these fluctuations, because in that case the large sensitive volume of the chamber can be used with advantage to study that process.

Here we are concerned only with the ion chamber in free space. In Chapter IV it was noted that the OGO-I ion chamber rate in free space fluctuates about its average value by as much as 5%. In order to verify that these fluctuations are indeed a property of the ionization in free space, we compare the fluctuations that occurred during the calibrations in the laboratory with those observed in free space. During one calibration pulse (162 seconds) with the γ-ray source in the laboratory, about 10^5 photons interact in the chamber. Therefore the fluctuations are expected to be much smaller in the laboratory than in free space.

For the OGO-III ion chamber, the observed "clock time" during the laboratory calibration with a gamma-ray source has already been presented in Table 3. Dividing the normalization factor 4.806 by this time gives the pulsing rate of the chamber in units of normalized pulses sec^{-1}. A total of 93 such measurements are available. The mean of these 93 values is calculated and then the

percentage deviations of the individual values are computed.

The frequency of occurrence of these deviations is shown in

Figure 41, by the dotted histogram. It can be seen that 70

percent of all the values lie within ± 0.6 percent of the

mean value and 99 percent of all values lie within ± 1.9 percent

of the mean.

For comparison the results of a similar analysis on 93

consecutive measurements with the same (OGO-III) ion chamber

in free space are shown in Figure 41 with a solid line.

The data was obtained between 2000 hours on 25 August and

0020 hours on 26 August, 1966 when the satellite was at a

geocentric distance of 20 earth radii on the evening side of

the magnetosphere. The rates at this time are typical of

those due to cosmic rays in free space. From Figure 41 it can

be seen that the fluctuations due to cosmic rays are quite

different in nature from those observed with the gamma-ray

source in the laboratory. Unlike what is observed in the

laboratory, the 2-4 percent fluctuations in free space are

as common as those <2 percent. This clearly shows that

the fluctuations observed in free space are indeed a property

of the cosmic ray ionization.

The ion chamber rate in free space may fluctuate because
of the fluctuations in any one or more of the following:

1. Number of primary particles passing through the
   chamber in a given time.

2. Path length of a given type of particles inside the
   chamber.

3. Energy loss of a given type of particles inside the
   chamber (Landau fluctuations).

4. Number of nuclear interactions occurring in the
   chamber and its vicinity in a given time.

5. Energy deposited in the chamber as a result of a
   single nuclear interaction.

6. Heavy nuclei stopping inside the chamber gas.

Clearly the problem is very complicated especially since
primary nuclei with a wide range of charge and energy are
involved. No attempt will be made here to evaluate
accurately the effect of the various processes mentioned above.
In what follows we will briefly consider each of these
processes and make an order of magnitude estimate of the
fluctuations in the ion chamber that might occur as a result
of that process.

1. Fluctuations in the Particle Flux

Table 15 shows the integral intensities of electrons,
protons, He nuclei, and S nuclei in free space at the time
of solar minimum. These are deduced from the primary cosmic
ray spectrum presented earlier. For later reference, the

TABLE 15

COSMIC RAY INTENSITY AT SOLAR MINIMUM

	ELECTRONS	PROTONS	He NUCLEI	S NUCLEI	TOTAL
Integral Intensity (Particles M^{-2} sec^{-1} str^{-1})					
Min. ionizing	400	1194	90	6	1690
Total	400	2616	299	23	3338
Particles passing through the OGO chamber (Particles sec^{-1})					
Min. ionizing	126	375	28	2	531
Total	126	821	94	7	1048

minimum ionizing particles as well as the total number of
particles of each species are shown in Table 15. Also shown
are the total number of particles passing through the OGO
chamber in one second.

In free space the OGO-I ion chamber is found to have the
"clock" time equal to about 90 seconds. This is the time taken
by the ramp voltage to go from the first to the sixteenth
discriminator level. As determined earlier (Chapter III,
Section (D)), during this time a total energy E_o = 25.9 BeV
is deposited in the chamber by the cosmic ray particles.
The average rate at which energy is deposited in the chamber
is thus ≈ 288 MeV sec^{-1}. Due to statistical fluctuations in
the number of cosmic ray particles passing through the
chamber the actual energy deposited in the chamber in 90 seconds
will fluctuate about the mean value 25.9 BeV. Consequently,
the pulsing rate of the chamber will also fluctuate.

Let N_Z be the average number of particles of a given species
(charge Ze) passing through the chamber in 90 seconds. Then
the expected fluctuation in this number N_Z is $\simeq \sqrt{N_Z}$. If
these particles be minimum ionizing, the energy loss of each
particle in the chamber gas is 1.56 z^2 MeV g^{-1} cm^2. The average
path length of these particles inside the chamber gas is
2/3 x (diameter of the chamber), i.e. 2/3 x 0.1 g cm^{-2}.
Hence the average energy loss inside the chamber gas is

$$1.56 \ z^2 \ x \ 2/3 \ x \ 0.1 \ \approx \ 0.1 \ z^2 \ \text{MeV/particle.}$$

TABLE 16

FLUCTUATIONS DUE TO MINIMUM IONIZING PARTICLES

	ELECTRONS	PROTONS	He NUCLEI	S NUCLEI	TOTAL
Average no. of particles passing through the chamber in 90 sec.: N_Z (particles)	11340	33750	2520	180	47790
Expected fluctuation in N_Z: ΔN_Z particles	106	184	50	13	353
Energy deposited by ΔN_Z particles: ΔE_Z MeV	10.6	18.4	20.0	131.3	180.3
Expected fluctuation: $\dfrac{\Delta E_Z}{E_o} \times 100$ per cent	0.04	0.07	0.08	0.51	0.70

Therefore the fluctuation in the energy deposited by the particles N_Z in the chamber is

$$\Delta E_Z \approx 0.1 \; Z^2 \Delta N_Z \; \text{MeV}$$

The percentage fluctuation in the chamber rate is therefore

$$\frac{\Delta E_Z}{E_o} \times 100 \sim \frac{0.1 \; Z^2 \Delta N_Z}{25.9 \times 10^3} \times 100 = 3.86 \times 10^{-4} \; Z^2 \; \Delta N_Z \; \text{percent.}$$

$$(5-10)$$

The computed results obtained for minimum ionizing electrons, protons, He nuclei and S nuclei are shown in Table 16. It can be seen that the fluctuations caused by the minimum ionizing particles are ≈ 1 percent and are principally due to the fluctuation in the number of S nuclei passing through the chamber.

Here we have not considered low energy particles ($P \leq 2.5$ BV). Their contribution to the ion chamber rate is about the same as that due to the minimum ionizing particles. Since their ionization loss depends on their charge as well as energy, a simple treatment as above is not applicable. Fluctuations caused by low energy S nuclei will be considered later.

2. Path Length of a Given Particle.

For a given particle the path length inside the chamber depends on its arrival direction and can have any value between 0 cms. and the diameter of the chamber, viz. 17.8 cms.

This is particularly true about particles with energies high enough so that they can go completely across the chamber diameter. Most of the primary cosmic rays satisfy this requirement. For an infinite number of these particles arriving isotropically on the chamber, the mean path length inside the chamber is 2/3 x (diameter of the chamber), i.e. 11.9 cms. If N particles pass through the chamber in a certain time, the actual mean of their path lengths may differ from the "ideal" mean 11.9 cms. by the standard deviation of the latter, i.e. $\sqrt{11.9/N}$. Now the chamber rate is averaged over about 90 seconds and during this time about 9×10^4 particles pass through the chamber (see Table 16). Therefore the variation in the mean path length is

$$\simeq \sqrt{\frac{11.9}{9 \times 10^4}} = 0.011 \text{ cms.} \tag{5-11}$$

Thus the fluctuation in the average path length is $\simeq 0.1$ percent and hence the consequent fluctuation in the ion chamber rate will also be of the same order and may be neglected.

3. <u>Landau Fluctuations</u>

Consider a narrow beam of similar particles impinging on the chamber. Each of these particles, although similar in nature, may not deposit the same amount of energy inside the chamber. Because of Landau fluctuations in their energy loss, the energy deposited inside the chamber by the individual particles will be distributed about the most "probable value". The full width of this distribution function is $\simeq 20$ percent (Yuan and Wu, 1961b). Thus the energy deposited by the

Table 17

	Electrons	Protons	He	S	Total
$E_Z = 0.1\ Z^2\ N_Z$ (Bev)	1.1	3.4	1.0	1.8	7.3
ΔE_Z (MeV)	1.0	1.8	2.0	13.8	18.6
$\dfrac{\Delta E_Z}{E_O} \times 100$	0.00	0.01	0.01	0.05	0.07

individual particles fluctuates by ≈10 percent. If N_Z be the total number of particles of a given species passing through the chamber in 90 seconds, the expected fluctuation in the average energy deposited by these particles is ≈$10/\sqrt{N_Z}$ percent. That is, if E_Z be the average energy deposited by these particles, the fluctuation is

$$\Delta E_Z \sim \frac{0.1\ E_Z}{\sqrt{N_Z}} \tag{5-12}$$

Considering again only the minimum ionizing particles and using Table 16 we get the results shown in Table 17.

Thus the effect of Landau fluctuations due to relativistic primaries is ≈0.1 percent and may be neglected.

4. Number of Nuclear Interactions

The pulsing rate of the OGO ion chamber is partly due to the secondary particles produced in the nuclear interactions of the primary cosmic rays in the ion chamber experimental package and the OGO spacecraft. As stated earlier, the box containing the electronic circuits for the ion chamber experiment and the spacecraft subtend only 18 percent of the total solid angle at the center of the chamber. Therefore, in the following discussion only the chamber itself will be considered.

To estimate the number of nuclear interactions taking place in the aluminum wall and the argon gas in the chamber, we first calculate the cross-section for interaction σ and the interaction mean free path λ. Peters (1952) has given an empirical formula for σ, viz.

$$\sigma = \pi(r_1 + r_2 - 2\Delta r)^2 \quad cm^2 \qquad (5\text{-}13)$$

where the subscripts refer to the two colliding nuclei with

mass numbers A_1 and A_2,

$$r = 1.45 \times 10^{-13} A^{1/3} \quad cms.,$$

and $\qquad \Delta r = 0.85 \times 10^{-13} \quad cms.$

Once the cross-section σ is known, the mean free path of the

incident nucleus (subscript 1) in the target material (subscript 2)

is given by

$$\lambda = \frac{A_2}{N_o \sigma} \quad g \ cm^{-2} \qquad (5\text{-}14)$$

where $N_o = 6 \times 10^{23}$ mole^{-1}

is the Avogadro number.

Now if J particles $cm^{-2} \ sec^{-1}$ be the flux of the primary

particles of a particular species and λ the corresponding mean

free path for nuclear interaction in the target material whose

total mass is M grams, the rate at which nuclear interactions

occur is given by

$$N_i = \frac{JM}{\lambda} \quad \text{interactions/sec.} \qquad (5\text{-}15)$$

The results obtained for the OGO ion chamber are shown in Tables

18 and 19. It can be seen that about 11 interactions take place

in the chamber in one second. Out of these over 93 percent

TABLE 18

NUCLEAR INTERACTION CROSS-SECTIONS

NUCLEI	A	ALUMINUM (A_{al}=27)		ARGON (A_{ar}=40)		COPPER (A_{cop}=63)	
		σ (10^{-24} cm2)	λ (gcm^{-2})	σ (10^{-24} cm2)	λ (gcm^{-2})	σ (10^{-24} cm2)	λ (gcm^{-2})
p	1	0.53	84.9	0.70	95.2	0.96	109.4
He	4	0.77	58.4	0.97	68.7	1.28	82.0
S	18	1.31	34.4	1.56	42.7	1.94	54.1

TABLE 19

NUCLEAR INTERACTIONS IN THE CHAMBER

NUCLEI	OGO CHAMBER (1965)				COOR'S CHAMBER (1948)			
	C.R. FLUX J $\frac{Particles}{cm^2 sec.}$	INTERACTIONS/SEC (N_i)			C.R. FLUX J $\frac{Particles}{cm^2 sec.}$	INTERACTIONS/SEC (N_i)		
		Wall	Gas	Total		Wall	Gas	Total
p	3.28	8.4	0.61	9.01	1.08	6.9	0.18	7.1
He	0.38	1.4	0.10	1.50	0.15	1.3	0.03	1.3
S	0.028	0.2	0.01	0.21	0.01	0.1	0.00	0.1
TOTAL		10.0	0.72	10.72		8.3	0.2	8.5

OGO-I CHAMBER
Aluminum 217.4 g
Argon 17.7 g

COOR'S CHAMBER
Copper 1404 g
Argon 33 g

occur in the chamber wall. Moreover, 84 percent of the total interactions are due to protons, the contribution from the S nuclei being only about 2 percent.

The secondary particles produced in a nuclear interaction vary from event to event. It is therefore not possible to compute, in a simple way, the energy deposited in the chamber in each nuclear interaction. Therefore we will use the observations of the "ionization bursts" made by Coor (1951) with the help of a pulsing type ionization chamber flown on balloons in January and May, 1948. Unlike an integrating type ion chamber, which measures the average ionization during a time interval of the order of a minute, a pulsing type ion chamber records ionization pulses from individual particles or nuclear interactions. The energy deposited in the chamber during a particular event can be determined from the amplitude of the pulse.

Coor's chamber consisted of a thin spherical copper shell, 30.5 cm in diameter and 0.054 cm thick, filled with high purity argon to a pressure of 1.3 atmospheres. The chamber responded to events which deposited energy $\geq$ 5.1 MeV, the individual events being called "bursts". The variation of the burst rate with altitude in the atmosphere was very similar to that of the rate at which "stars" are produced in the photographic emulsions, indicating that both are produced by events essentially of the same type (Rossi, 1952b). Extrapolation of Coor's measurements to the top of the atmosphere gives 3200 ev $\sec^{-1}$ cm^{-3} of argon (STP) as the average energy deposited

in the chamber at the top of the atmosphere. To determine the
average energy per interaction we must compute the rate of
interactions in that chamber noting that the chamber was near
the earth (total solid angle $\approx 2\pi$) and that the cosmic ray
intensity in 1948 was close to the solar maximum value. The
results of such a computation are shown in Tables 18 and 19.
It can be seen that the total rate of interactions is 8.5 per
second, of which 98 percent interactions occur in the copper
wall. Also, as in the case of the OGO chamber, 81 percent
of all the interactions are due to primary protons, only about
1 percent being due to S nuclei.

The average energy deposited in Coor's chamber is
3200 ev $\sec^{-1}$ cm^{-3} of argon at STP which is equivalent to

$$\frac{3200}{1.7 \times 10^{-3}} = 1.9 \text{ MeV } \sec^{-1} g^{-1} \text{ of argon .}$$

Here we have taken the density of argon (STP) = 1.7×10^{-3} g cm^{-3}.
Therefore energy deposited per interaction is

$$\approx \frac{1.9}{8.5} = 0.22 \text{ MeV } g^{-1} \text{ of argon.} \tag{5-16}$$

If we assume that the same is true for the OGO ion chamber,
the rate at which energy is deposited in the OGO chamber as
a result of the nuclear interactions is

0.22 x Mass of argon x rate of interactions

= 0.22 x 17.7 x 10.7

= 41.7 MeV $\sec^{-1}$ $\tag{5-17}$

Hence in 90 seconds, the time over which the measurements are averaged, about 3.8 BeV energy is deposited in the OGO chamber as a result of about 960 interactions. Since the total energy deposited in the chamber during this time interval is about 25.9 BeV, the nuclear interactions give rise to about 15 percent of the total ion chamber rate.

In order to estimate the magnitude of fluctuations, we note that the statistical variation in the number of interactions is

$$\Delta N \approx \sqrt{960} = 31$$

Therefore the variation in energy deposited

$$\Delta E \approx 0.22 \times 17.7 \times \Delta N = 0.12 \text{ BeV} \qquad (5-18)$$

The fluctuations in the total ion chamber rate caused by the variation in the number of nuclear interactions is therefore

$$\approx \frac{0.12}{25.9} \times 100 = 0.5 \text{ percent.}$$

5. Energy Per Nuclear Interaction

In the above discussion we assumed that the energy deposited in the chamber due to each nuclear interaction is constant and was called the average energy per interaction. However, in practice the energy due to individual interactions is highly variable. Therefore, even if the number of interactions remains the same, the chamber rate will fluctuate because of the variation in the average energy per interaction. To estimate this effect, we note that the average energy per

interaction is the mean of the energies deposited in about
960 individual interactions. The variation in the average value
is therefore

$$\simeq \frac{\text{Average energy per interaction}}{\left(\text{Total number of interactions}\right)^{1/2}}$$

$$= \frac{0.22 \times 17.7}{\sqrt{960}} = 0.13 \text{ MeV} \tag{5-19}$$

The variation in the average energy is thus

$$\simeq \frac{0.13}{0.22 \times 17.7} \times 100 = 3.3 \text{ percent.} \tag{5-20}$$

The effect of this variation on the total chamber rate is thus

$$\simeq \frac{0.06 \times 960}{25.9 \times 10^3} \times 100 = 0.5 \text{ percent} \tag{5-21}$$

In this connection it is interesting to note that in order
to cause a one percent fluctuation in the total chamber rate,
a nuclear interaction must deposit about 260 MeV in the chamber.
The largest ionization bursts observed by Coor at an atmospheric
depth of 17 g cm^{-2} deposited about 100 MeV in his chamber,
and the frequency of occurrence of such bursts was about one
burst in 300 seconds. This indicates that single nuclear
interactions are not likely to cuase large (>> 1 percent)
fluctuations in the OGO ion chamber rate when it is averaged
over about 90 seconds. The expected fluctuation from single
events is $\simeq$1 percent.

6. Heavy Nuclei Stopping Inside the Chamber

Large fluctuations in the average ion chamber rate can be caused by single heavy nuclei stopping inside the chamber gas. To take an extreme case, consider an iron nucleus with kinetic energy equal to 59 MeV per nucleon incident normally on the chamber. Its range in aluminum is 0.32 g cm^{-2}. After passing through the chamber wall (0.22 g cm^{-2}) its residaul energy is 30 MeV/nucleon, the corresponding range being 0.1 g cm^{-2}. This nucleus will therefore be stopped in the chamber depositing a total energy of 1.68 BeV inside the chamber. This is 6.5 percent of the total energy 25.9 BeV deposited in the chamber in 90 seconds. The intensity of these nuclei is 10^{-3} particles M^{-2} sec^{-1} $ster^{-1}$ so that the number of particles passing through the chamber is

$$\simeq 4 \times 10^{-4} \times 10^{-3} \times 250 = 3.1 \times 10^{-4} \text{ particles/sec}$$

$$\simeq 1 \quad\quad \text{particle/hour}$$

(5-22)

Thus, although the fluctuation in the chamber rate due to low energy iron nuclei is large, it can occur only about once in an hour.

To take a moderate case, we consider an oxygen nucleus with kinetic energy 32 MeV/nucleon. It will also stop inside the chamber depositing 0.24 BeV which is $\simeq$ 1 percent of the total energy deposited in the chamber in 90 seconds. The intensity of these nuclei is about 6 x 10^{-3} particles M^{-2} sec^{-1} $ster^{-1}$ and so $\simeq$ 1.9 x 10^{-3} particles pass through the chamber

1960-1965

ION CHAMBER
IN FREE SPACE

ION CHAMBER
AT MPLS.
(BALLOON AT 10 MB)
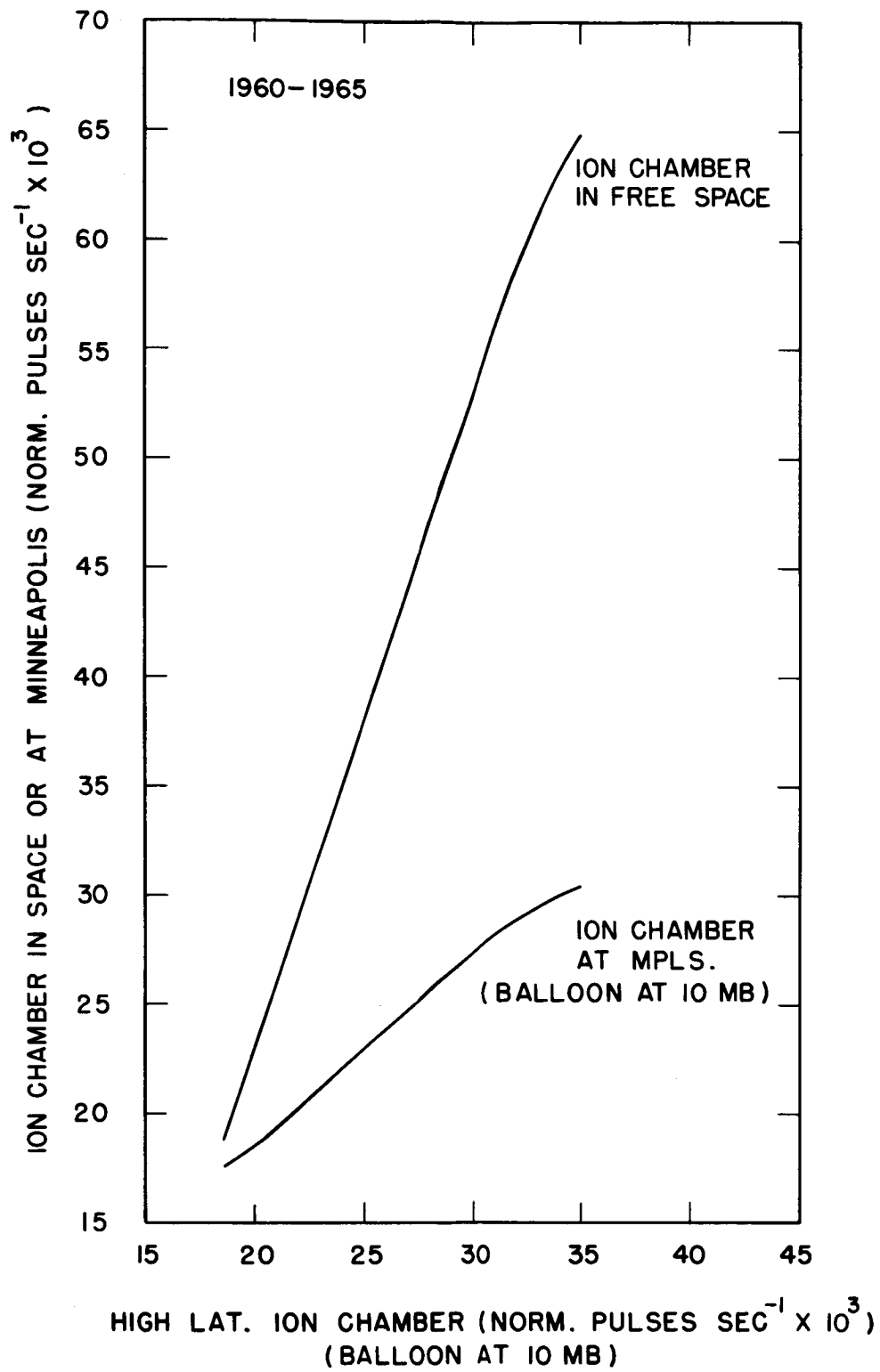
Figure 42

in one second or 1 particle in about 525 seconds. If we
consider all the M nuclei, which are the most abundant of all
the S nuclei, we find that about one particle passes through
the chamber in 300 seconds which is roughly three averaging
times. The probability of one M nucleus stopping in the
chamber during an averaging period of 90 seconds and causing
a fluctuation of ≃1 percent is thus ≃30 percent.

The above two examples show that S nuclei stopping inside
the chamber can cause fluctuations ≃1 percent in the 90 second
average rates, with an occasional fluctuation as large as
6.5 percent.

To summarize, fluctuations of ~1 percent can be caused
by the statistical fluctuations in (a) the number of
primaries passing through the chamber, (b) the number of nuclear
interactions, (c) the energy deposited in individual nuclear
interactions, and (d) S nuclei stopping inside the chamber.
These order of magnitude estimates indicate that the above
processes could be responsible for the observed fluctuations.

(H) RELATIONSHIP BETWEEN ION CHAMBERS IN FREE SPACE AND ON BALLOONS

The observed relationship of the ion chamber in free space
and at Minneapolis with the one at high latitude is shown in
Figure 42. This figure is based on the correlated rates in
the period 1960-1965 presented earlier in Table 10. It can
be seen that the relationship between these three ion chambers
is approximately linear.
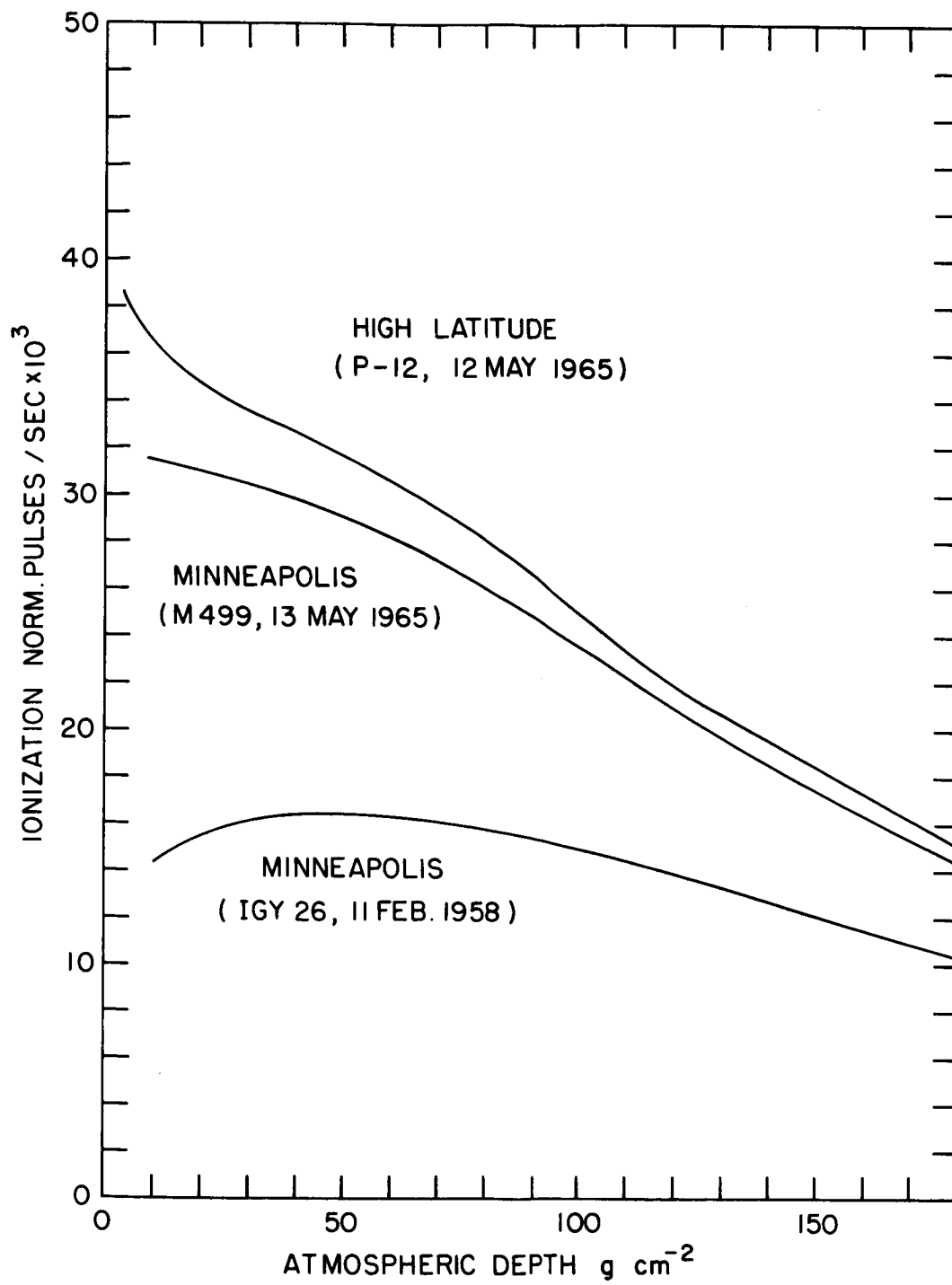
Figure 43
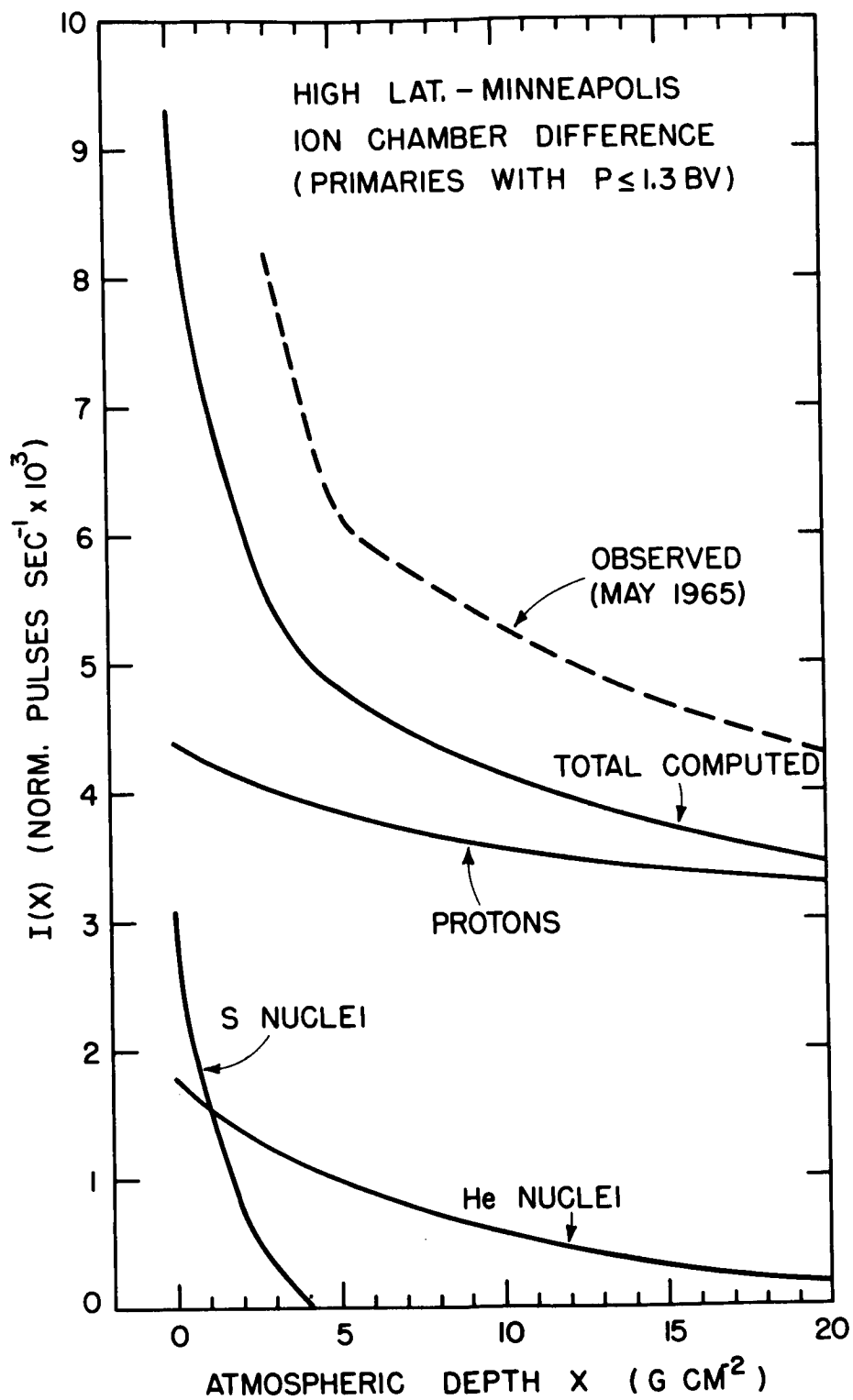
Figure 44

For a more direct relation between the balloon and free space ion chambers, we need to know the variation of the ion chamber rate with altitude above the earth's surface. The balloon measurements at solar minimum (May, 1965) and solar maximum (February, 1958) made by J. R. Winckler are shown in Figure 43. Here the chamber rate is plotted against the atmospheric depth. We note that at solar minimum, the rate vs. depth curve at high latitude tends to "turn-up" with decreasing depth. The probable cause of this turn-up was investigated by Kane et al. (1965b). They considered the difference between the high latitude and Minneapolis curves shown in Figure 43 and compared it with the computed ionization due to all primaries with rigidity $P \leq 1.3$ BV (the cutoff rigidity at Minneapolis). These computations have been revised recently and are presented in Figure 44. It can be seen that the computed and observed curves are very similar and that the turn-up at low depths is caused principally by the S nuclei.

A more complete picture of the ionization vs. altitude curve is shown in Figure 45. Here measurements made by J. R. Winckler on 27 June, 1960 and by D. J. Hofmann on 12 May, 1965 are plotted against the altitude above the earth's surface. Originally the chamber rate is available as a function of the atmospheric pressure in millibars. This pressure is converted into the equivalent altitude by using the relationship between these quantities in a standard

VARIATION OF ION CHAMBER
RATE WITH ALTITUDE

OGO-I
11-13 MAY, 1965

$$I(h) = \frac{1}{2} I(\infty) \left[1 + \frac{\{h(h+2)\}^{1/2}}{(h+1)} \right]$$

PIONEER $\underline{\text{V}}$
MARCH, 1960
(ARNOLDY et al, 1964)

HIGH LAT.
BALLOON

12 MAY, 1965
(HOFMANN, 1966)

27 JUNE, 1960
(WINCKLER)

ION CHAMBER RATE (NORM. PULSES SEC^{-1} x 10^3)

ALTITUDE ABOVE THE EARTH'S SURFACE h (EARTH RADII)
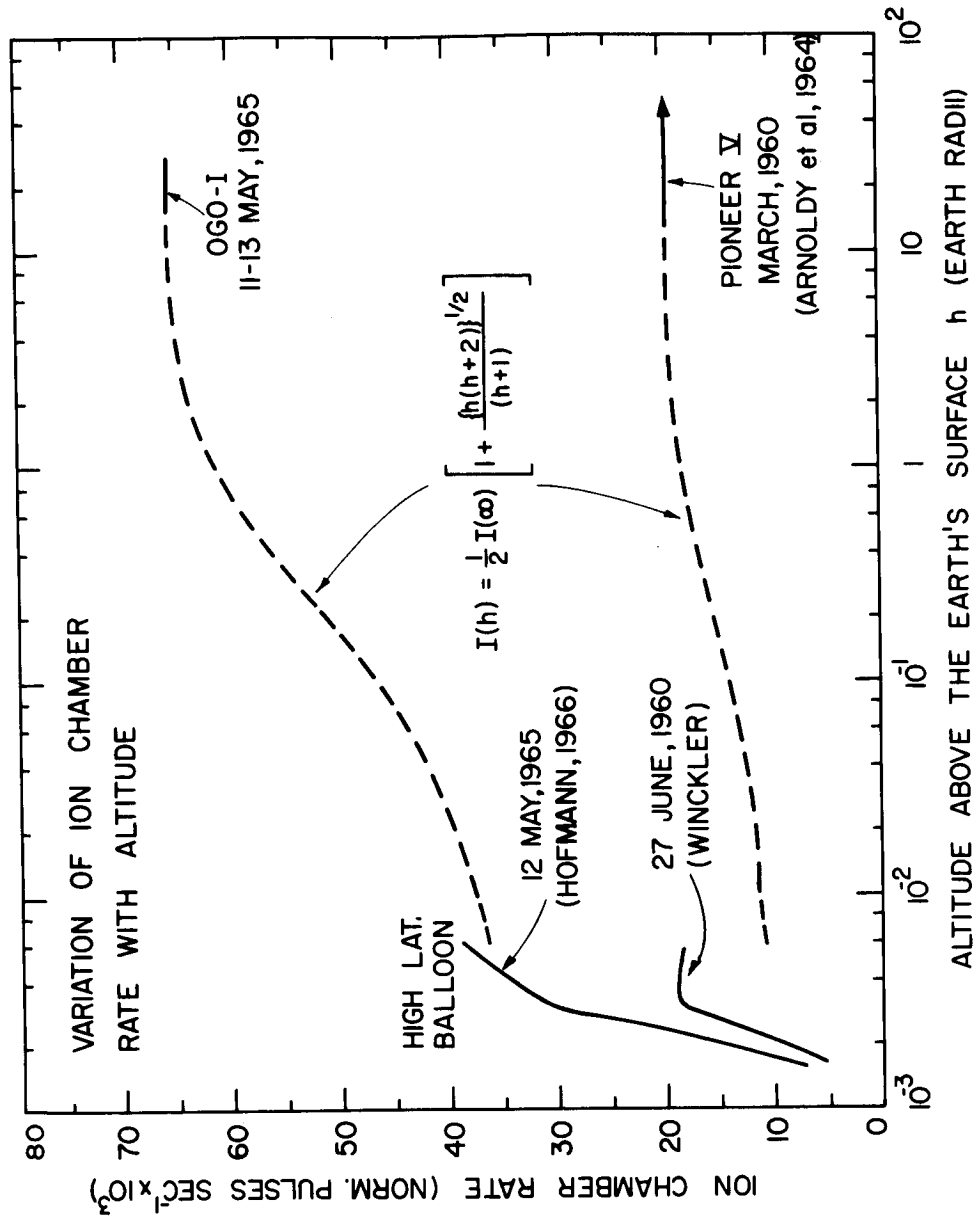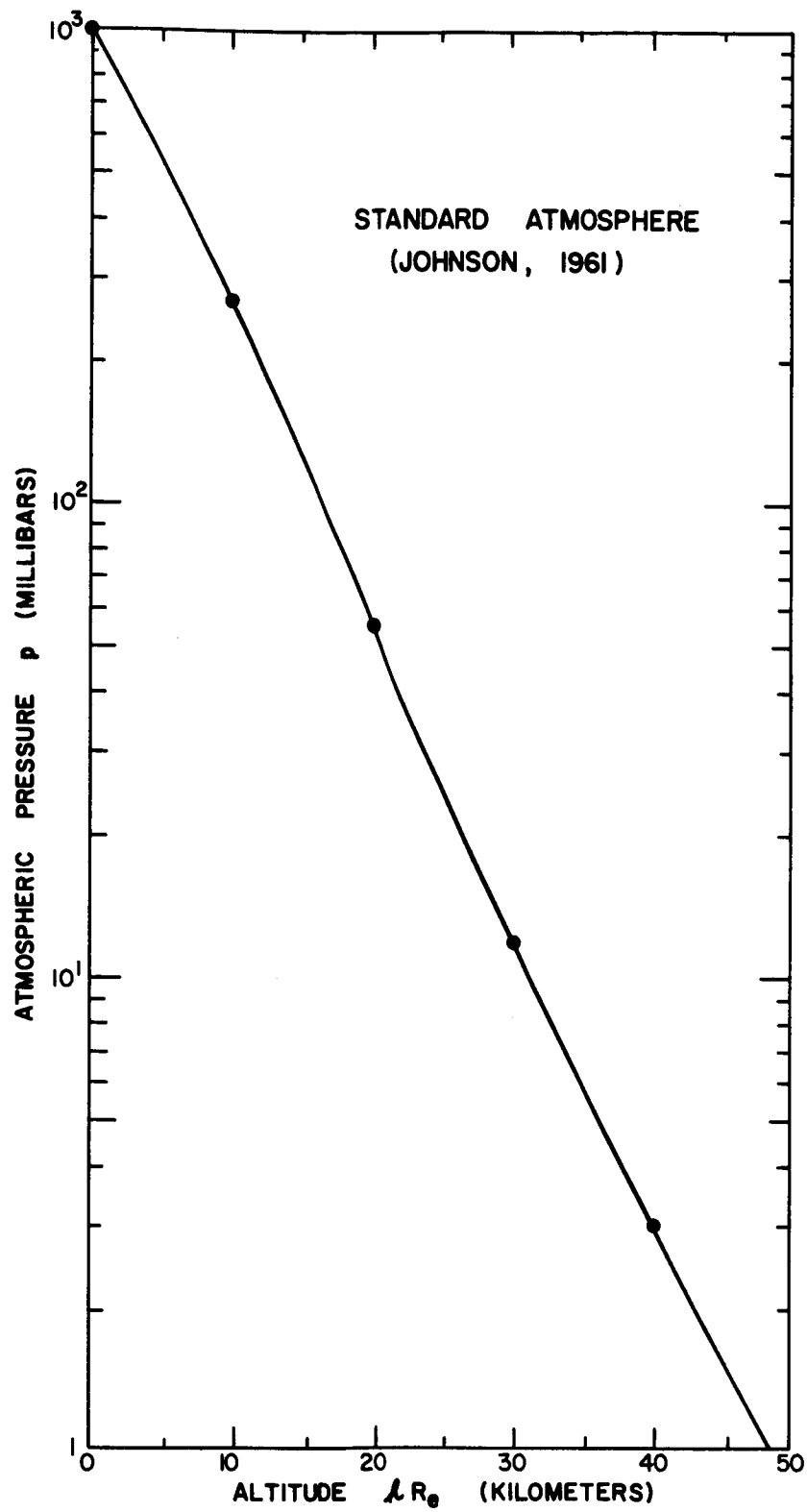
Figure 45

Figure 46

atmosphere given by Johnson (1961) and shown graphically in Figure 46.

In Figure 45 also shown are the ion chamber rates in free space as measured by the Pioneer V and OGO-I ion chambers during March, 1960 and 11-13 May, 1965 respectively. Although the high latitude balloon measurement during 1960 was made about three months after Pioneer V measurements, the counting rate of the Deep River neutron monitor on 27 June 1960 was 1827 counts/hour and the average rate for March, 1960 was 1830 counts/hour. Therefore these two measurements in 1960 may be considered simultaneous.

In order to study the variation of an ion chamber rate with altitude, we must consider the following effects at each point of observation:

1. Geomagnetic cutoff rigidity.

2. Absorption of the primary particles by the solid earth.

3. Atmospheric effects - energy loss of incident primary particles and the secondaries (albedo) produced in the atmosphere.

At high latitudes the geomagnetic cutoff rigidity is small compared to that due to chamber wall (≈ 0.2 BV for protons). The ionization due to the albedo particles is not well known. Therefore for simplicity we will consider only the absorption of the primary particles by the solid earth.

The geometry of the problem is shown in Figure 47. Let O be the center of the earth and C the location of the chamber.

Figure 47

172
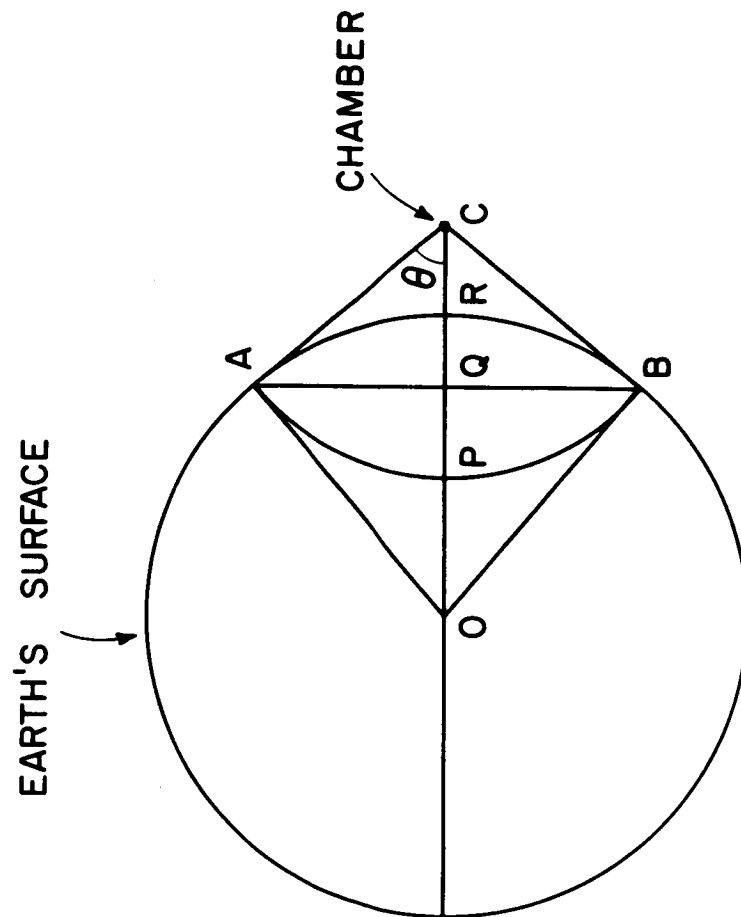
Let all distances be measured in units of the earth's mean radius (6371 km). Then

$$OA = OR = OB = 1 \qquad (5\text{-}23)$$

The solid angle subtended by the earth at the position of the chamber is the same as that subtended by the spherical segment APBQ at C. The curved surface of this segment is

$$S = 2\pi \times AC \times PQ$$

$$= 2\pi \times AC \times (PC - QC)$$

$$= 2\pi \times AC^2 \times (1 - \frac{QC}{AC}) \qquad (5\text{-}24)$$

Let $<ACR = \theta$. Then we have the following relations

$$\sin \theta = \frac{OA}{OC} = \frac{1}{1+h} \qquad (5\text{-}25)$$

$$\frac{QC}{AC} = \cos \theta = [1 - \frac{1}{(1+h)^2}]^{1/2}$$

$$= \frac{[h(h+2)]^{1/2}}{(h+1)} \qquad (5\text{-}26)$$

where $h = RC$ is the altitude of the chamber above the earth's surface. Therefore

$$S = 2\pi \times AC^2 \times \left[1 - \frac{\{h(h+2)\}^{1/2}}{(h+1)}\right] \qquad (5\text{-}27)$$

Hence the solid angle subtended at C is

$$\Omega_E = \frac{S}{AC^2} = 2\pi \left[1 - \frac{\{h(h+2)\}}{(h+1)}^{1/2} \right] \qquad (5\text{-}28)$$

This is also the solid angle subtended by the earth at the chamber. Let $I(\infty)$ be the ion chamber rate when the chamber is at a large distance ($h \gg 1$) from the earth so that the cosmic rays can arrive at the chamber from nearly all directions ($\Omega_E \simeq 0$). Then since the cosmic ray intensity is isotropic, the chamber rate at an altitude of h earth radii is given by

$$I(h) = I(\infty) \left(1 - \frac{\Omega_E}{4\pi}\right)$$

$$= \frac{1}{2} I(\infty) \left[1 + \frac{\{h(h+2)\}}{(h+1)}^{1/2} \right] \qquad (5\text{-}29)$$

Variation of I(h) with h is shown by dashed lines in Figure 45 for the solar minimum and solar maximum conditions. In each case the observed rate in free space ($h \geq 14$ earth radii) is taken as $I(\infty)$. It may be noted that at balloon altitudes the observed rate is always greater than the computed rate I(h). This indicates that the contribution from the secondaries produced in the atmosphere is important at these altitudes. In fact, at solar maximum the ionization due to secondaries is nearly equal to that due to primaries. As higher altitudes are reached, the chamber rate must smoothly join with the rate predicted by the dashed line.

VI. <u>CONCLUSIONS</u>

(A) SUMMARY AND CONCLUSIONS

1. In this thesis we described an integrating type ion chamber experiment flown aboard the OGO-I and III satellites. The construction of a resetting drift-type electrometer was discussed. The chamber-electrometer system was demonstrated to have a dynamic range of over six orders of magnitude and an accuracy and stability of $\sim$1 percent when operated in space over a period of nearly three years.

2. The response of the chamber to x-rays, electrons, protons and heavier nuclei was evaluated both experimentally and theoretically. The findings were as follows:

   (a) The minimum energy for penetration

   protons   12 MeV

   electrons $\sim$ 0.6 MeV

   (b) The chamber responds to non-penetrating (E < 0.6 MeV) electrons through the bremsstrahlung they produce in the chamber wall. At 40 KeV the response $\approx 10^{-7}$ x (response at energies >600 KeV).

   (c) In the 10-150 KeV region, the chamber response to x-rays is peaked at about 20 KeV. At energies $\leq$ 10 KeV, the response is $\leq 10^{-2}$ x (response at 20 KeV).

   (d) For an incident flux of 1 particle cm^{-2} sec^{-1} of 20 KeV x-rays, electrons with energy $\gtrsim$1 MeV, and minimum ionizing nuclei of charge Ze the respective pulsing rates

of the OGO ion chamber are 0.2, 7.0, and 5.5 z^2

norm. pulses sec^{-1} x 10^3.

3. The differential rigidity response of the chamber to the

"known" spectrum of the galactic cosmic rays was computed

and was found to have the following characteristics:

(a) The response is peaked at about 1 BV at solar minimum

and at 2 BV at solar maximum.

(b) Most of the response lies in the range 0.2 - 10.0 BV.

4. The OGO-I and III ion chamber measurements reported here

cover the period 10 September 1964 - 2 July 1966*, a period

following the minimum in solar activity. The cosmic ray

maximum, as determined from these measurements, occurred

during 11-15 May, 1965 when the ion chamber rate in free

space was 65.5 norm. pulses sec^{-1} x 10^3. For this time

the total chamber rate computed from the "known" cosmic

ray spectrum was found to be 74 norm. pulses sec^{-1} x 10^3,

the contributions from protons, He nuclei, S nuclei, electrons,

and nuclear interactions in the chamber being about 31, 18,

33, 5 and 13 percent respectively. A number of known factors

could be responsible for the 12% difference between the

observed and the total computed rates.

5. (a) The relationship between the ion chamber rates in free

space and Deep River neutron monitor during the period

1960-1965 was found to be linear -

$$\left(\frac{\Delta I}{I}\right)_{Space} \approx K \left(\frac{\Delta N}{N}\right)_{Deep\ River}$$

---

* The OGO ion chamber measurements are available at least up

to 15 July 1967.

where the constant $K \approx 4.5$. After May, 1965, the value

of K was < 4.5 indicating a hysteresis effect. That is,

as the solar activity decreased, the ion chamber rate

when plotted against the Deep River monitor rate moved

along a regression line until the cosmic ray maximum in

May 1965, but beyond the maximum the rates did not follow

the regression line but remained consistently above that

line.

(b) The relationship between the ion chamber rates in free

space, on high latitude balloons (10 mb) and on Minneapolis

balloon (10 mb) was very nearly linear during the period

1960 - 1964.

$$I \text{ (Space)} \approx 3 \text{ I(high lat.)} - 37 \quad \text{norm.pulses sec}^{-1} \text{x} 10^3$$

$$I \text{ (Mpls.)} \approx 0.86 \text{ I (high lat.)} + 1.6. \text{norm.pulses sec}^{-1} \text{x} 10^3$$

6. It was concluded that most of the response of an ion chamber

to galactic cosmic rays is concentrated in a rather narrow

rigidity interval, the precise interval depending upon the

location of the chamber. These rigidity intervals are

Free space	1.5 - 2.5 BV
High latitudes (10 mb)	2.5 - 3.5 BV
Minneapolis (10 mb)	3.0 - 4.0 BV

7. Using the available measurements with ion chambers and the

intensity of He nuclei, the rigidity dependence of the long-

term cosmic ray variation during the period 1960-1965 was

found to be consistent with the form $P^{-0.9}$ in the rigidity

interval 1.5 - 4.0 BV.

8. At high geomagnetic latitudes the variation of the ion
    chamber rate I(h) with the altitude h, taking into account
    the shadow effect of the solid earth but not the atmospheric
    effects, is given by

$$I(h) = \frac{1}{2} \, I(\infty) \, [\, 1 + \frac{\{h(h+2)\}^{1/2}}{(h+1)} \,]$$

where I(∞) is the chamber rate in free space. The relative
contribution of the secondaries produced in the atmosphere is
found to be much larger at solar maximum than at solar
minimum.

9. Fluctuations of $\sim 5\%$ magnitude were observed in the OGO ion
    chamber rate in free space averaged over about 90 seconds.
    It was concluded that these fluctuations are a characteristic
    feature of the cosmic ray ionization and can be explained
    in terms of the statistical fluctuations in (a) the number
    of primaries passing through the chamber, (b) the number of
    nuclear interactions in the chamber, (c) the energy deposited
    in individual nuclear interactions, and (d) heavy nuclei
    stopping inside the chamber. No single process was found
    to be the dominant factor responsible for the fluctuations
    in the chamber rate.

(B) FUTURE ANALYSIS

It is recognized that the ionization chamber is not ideally suited
for cosmic ray or other specific measurements because of its inability
to distinguish between different kinds of radiations and their energies.
However, the ionization chamber can be used to considerable advantage

for detecting different types of phenomena. For example, the OGO ionization chamber has yielded useful measurements in the radiation belts and also detected several solar x-ray bursts. These are being studied separately and are expected to contribute substantially to our knowledge of this phenomena. Even as a cosmic ray detector the chamber has proved to be a very stable monitor of galactic cosmic ray intensity. Due to its high sensitivity to low energy particles, the chamber in free space is able to detect solar particle events which might otherwise go un-noticed. These are being studied separately.

As regards the problem of fluctuations of the chamber rate in free space, only a preliminary analysis was presented in this thesis. In view of the possibility of being able to detect extremely rare very heavy nuclei in the primary cosmic rays a more extensive analysis is now being undertaken.

TABLE 3

CALIBRATION WITH RADIUM SOURCE

TIME ΔT (SEC) BETWEEN THE 1ST AND 16TH DISCRIMINATOR LEVELS

DATE	OGO-I				OGO-III			
	STOP WATCH		0.02 x CLOCK PULSES		STOP WATCH		0.02 x CLOCK PULSES	
	ACTUAL	MEAN	ACTUAL	MEAN	ACTUAL	MEAN	ACTUAL	MEAN
18 Oct. 1963	163.0	161.9						
	161.5							
	161.9							
	161.1							
19 Oct. 1963	161.0	161.2						
	161.5							
	161.0							
	161.2							
21 Oct. 1963	161.1	161.8			143.9	144.1		
	160.6				143.9			
	163.6				144.0			
	161.8				144.7			

TABLE 3 (continued)

DATE	OGO-I				OGO-III			
	STOP WATCH		0.02 x CLOCK PULSES		STOP WATCH		0.02 x CLOCK PULSES	
	ACTUAL	MEAN	ACTUAL	MEAN	ACTUAL	MEAN	ACTUAL	MEAN
22 Oct. 1963	162.8	161.9			144.5	145.2		
	161.0				144.5			
	164.1				145.9			
	160.6				146.0			
23 Oct. 1963	162.8	161.8						
	161.4							
	161.4							
	161.7							
25 Oct. 1963	163.5	162.3			144.8	145.7		
	161.0				144.1			
	161.2				147.0			
	163.5				146.7			
28 Oct. 1963	161.4	161.8			144.8	144.9		
	163.7				145.4			
	161.0				144.0			
	161.1				145.3			

TABLE 3 (continued)

DATE	OGO-I				OGO-III			
	STOP WATCH		0.02 x CLOCK PULSES		STOP WATCH		0.02 x CLOCK PULSES	
	ACTUAL	MEAN	ACTUAL	MEAN	ACTUAL	MEAN	ACTUAL	MEAN
30 Oct. 1963	161.0	160.6						
	159.6							
	160.0							
	161.8							
2 Nov. 1963	162.8	162.5	162.6	162.5				
	163.1		162.2					
	161.0		162.3					
	162.8		162.7					
15 Nov. 1963					142.0	143.6		
					145.6			
					143.4			
					142.4			
					144.4			

TABLE 3 (continued)

DATE	OGO-I				OGO-III			
	STOP WATCH		0.02 x CLOCK PULSES		STOP WATCH		0.02 x CLOCK PULSES	
	ACTUAL	MEAN	ACTUAL	MEAN	ACTUAL	MEAN	ACTUAL	MEAN
20 Nov. 1963					143.8	143.0		
					144.8			
					142.9			
					141.4			
					142.0			
18 Dec. 1963					147.0	145.9	144.0	144.0
					144.9		143.8	
					146.2		144.3	
					145.4		144.0	
21 Dec. 1963					147.0	145.3	144.4	144.6
					145.0		144.6	
					143.0		144.4	
					146.3		145.0	

182

TABLE 3 (continued)

DATE	OGO-I STOP WATCH ACTUAL	MEAN	OGO-I 0.02 x CLOCK PULSES ACTUAL	MEAN	OGO-III STOP WATCH ACTUAL	MEAN	OGO-III 0.02 x CLOCK PULSES ACTUAL	MEAN
28 Dec. 1963					144.0	144.9	142.9	143.1
					145.5		143.8	
					144.9		142.7	
					145.0		143.0	
31 Dec. 1963					147.1	145.9	144.4	144.4
					145.1		144.6	
					145.5		144.1	
					146.0		144.6	
3 Mar. 1964					147.4	147.2	144.7	144.9
					148.0		145.3	
					147.5		144.7	
					145.9		144.9	
4 Mar. 1964					146.3	147.6	144.3	144.8
					148.6		145.4	
					148.9		145.0	
					146.5		144.5	

TABLE 3 (continued)

DATE	OGO-I				OGO-III			
	STOP WATCH		0.02 x CLOCK PULSES		STOP WATCH		0.02 x CLOCK PULSES	
	ACTUAL	MEAN	ACTUAL	MEAN	ACTUAL	MEAN	ACTUAL	MEAN
10 Mar. 1964					145.8	146.8	144.8	144.8
					146.9		144.6	
					148.3		144.9	
					146.0		144.7	
19 Mar. 1964					146.8	145.9	144.2	144.6
					144.5		144.4	
					146.0		144.9	
					146.4		144.7	
30 Mar. 1964					146.5	147.0	145.6	145.1
					147.4		144.7	
					147.1		144.6	
							145.6	
8 Apr. 1964					147.4	146.2	144.7	144.1
					144.1		143.9	
					146.3		144.0	
					146.9		143.8	

TABLE 3 (continued)

DATE	OGO-I STOP WATCH ACTUAL	MEAN	OGO-I 0.02 x CLOCK PULSES ACTUAL	MEAN	OGO-III STOP WATCH ACTUAL	MEAN	OGO-III 0.02 x CLOCK PULSES ACTUAL	MEAN
11 Apr. 1964					147.7	147.7	145.4	145.7
					146.6		145.1	
					148.6		146.5	
					148.0		145.6	
2 May 1964					142.2	144.2	143.5	143.3
					143.4		143.2	
					147.0		143.7	
					144.5		142.9	
21 Dec. 1964					143.2	144.2	142.8	143.4
					142.9		143.3	
					144.7		144.1	
					146.0		143.8	
							142.9	

TABLE 3 (continued)

DATE	OGO-I STOP WATCH ACTUAL	MEAN	OGO-I 0.02 x CLOCK PULSES ACTUAL	MEAN	OGO-III STOP WATCH ACTUAL	MEAN	OGO-III 0.02 x CLOCK PULSES ACTUAL	MEAN
22 Dec. 1964					144.7	144.9	143.9	143.9
					145.9		144.1	
					146.0		144.0	
					143.2		143.5	
24 Dec. 1964					146.0	145.4	143.0	143.7
					145.0		144.0	
					145.0		144.0	
					145.6		143.8	
28 Dec. 1964					144.0	145.1	143.6	143.5
					145.2		143.1	
					146.8		143.4	
					144.5		144.0	
31 July 1965					148.6	147.9	145.6	145.4
					149.7		145.4	
					147.5		145.3	
					145.7		145.2	

TABLE 3 (continued)

DATE	OGO-I				OGO-III			
	STOP WATCH		0.02 x CLOCK PULSES		STOP WATCH		0.02 x CLOCK PULSES	
	ACTUAL	MEAN	ACTUAL	MEAN	ACTUAL	MEAN	ACTUAL	MEAN
1 Aug. 1965					147.2	147.4	145.4	145.2
					147.6		145.4	
					147.4		145.0	
							144.7	
					147.4		145.3	
2 Aug. 1965						147.3	145.2	145.4
					148.2		145.3	
					148.0		144.9	
					146.9		145.8	
					146.0		145.6	
19 Jan. 1966						146.4	144.5	145.0
					147.8		144.1	
					142.7			
					146.0		145.0	
					146.2		145.2	
					149.2		146.4	

TABLE 3 (continued)

DATE	OGO-I STOP WATCH ACTUAL	MEAN	0.02 x CLOCK PULSES ACTUAL	MEAN	OGO-III STOP WATCH ACTUAL	MEAN	0.02 x CLOCK PULSES ACTUAL	MEAN
22 Jan. 1966							145.1	144.7
							144.9	
							144.1	
							144.8	
25 Jan. 1966							148.5	145.3
							144.6	
							144.3	
							144.6	
							144.5	
AVERAGE		161.7				145.8	144.4	

TABLE 5

OGO-I ION CHAMBER-THERMAL VACUUM TEST

Environmental pressure 10^{-6} mm. of Hg.

Data run No.	Temp. (°C)	'Clock' time (sec)	Ramp time (sec)	Ramp (volts)		Discriminator levels (volts)				
				Min.	Max.	1	2	3	4	5
55	0	131.64	173	0.00	5.10	0.78	1.04	1.30	1.56	1.82
56	0	131.70	173	0.00	5.10	0.78	1.04	1.30	1.56	1.82
57	0	131.12	172	0.00	5.08	0.78	1.04	1.30	1.56	1.80
58	0	131.36	172	0.00	5.10	0.78	1.02	1.30	1.56	1.82
59	0	130.94		0.00	5.08	0.78	1.04	1.30	1.56	1.82
60	0	131.38	172	0.00	5.10	0.78	1.04	1.30	1.56	1.82
61	0	131.28	172	0.00	5.10	0.78	1.04	1.30	1.56	1.82
62	0	131.26	173	0.00	5.10	0.78	1.04	1.30	1.56	1.82
63	0	131.06	172	0.00	5.08	0.78	1.04	1.30	1.54	1.82
64	0	131.42	173	0.00	5.10	0.78	1.04	1.28	1.54	1.82
65	0	131.62	172	0.00	5.08	0.78	1.02	1.28	1.56	1.82
66	0	131.22	172	0.00	5.10	0.76	1.02	1.30	1.56	1.82
67	0	132.02	173	0.00	5.10	0.78	1.04	1.30	1.56	1.80
68	0	130.78	171	0.00	5.10	0.78	1.04	1.30	1.56	1.82
average	0	131.34	172	0.00	5.09	0.78	1.03	1.30	1.56	1.82

Table 5 cont.

Data run No.	Discriminator levels (volts)										
	6	7	8	9	10	11	12	13	14	15	16
55	2.08	2.32	2.60	2.84	3.08	3.54	3.60	3.86	4.12	4.38	4.66
56	2.06	2.34	2.60	2.84	3.10	3.34	3.62	3.86	4.12	4.38	4.64
57	2.06	2.32	2.60	2.84	3.08	3.36	3.62	3.86	4.12	4.38	4.64
58	2.08	2.34	2.60	2.84	3.10	3.36	3.62	3.88	4.12	4.38	4.64
59	2.08	2.34	2.60	2.84	3.10	3.36	3.62	3.88	4.12	4.40	4.64
60	2.08	2.34	2.60	2.82	3.08	3.36	3.60	3.88	4.12	4.38	4.64
61	2.08	2.34	2.58	2.84	3.10	3.36	3.60	3.88	4.12	4.38	4.64
62	2.08	2.32	2.60	2.84	3.08	3.36	3.60	3.86	4.12	4.38	4.62
63	2.08	2.32	2.60	2.84	3.08	3.34	3.60	3.86	4.12	4.38	4.64
64	2.08	2.34	2.60	2.84	3.10	3.36	3.64	3.88	4.12	4.38	4.64
65	2.06	2.34	2.60	2.84	3.08	3.36	3.60	3.86	4.12	4.38	4.64
66	2.08	2.34	2.60	2.82	3.10	3.34	3.60	3.88	4.12	4.38	4.64
67	2.06	2.34	2.60	2.84	3.10	3.36	3.60	3.88	4.12	4.38	4.64
68	2.08	2.34	2.60	2.84	3.10	3.34	3.60	3.86	4.12	4.38	4.64
average	2.07	2.33	2.60	2.84	3.09	3.37	3.61	3.87	4.12	4.38	4.64

OGO—I ION CHAMBER—THERMAL VACUUM TEST

Table 5 cont.

Environmental pressure 10^{-6} mm. of Hg.

Data run No.	Temp. (°C)	'Clock' time (sec)	Ramp time (sec)	Ramp (volts)		Discriminator levels (volts)					
				Min.	Max.	1	2	3	4	5	6
73	+40	132.20	177	0.04	5.10	0.74	1.00	1.26	1.54	1.80	2.06
74	+40	132.62	177	0.02	5.10	0.74	1.00	1.26	1.52	1.80	2.04
75	+40	132.74	177	0.04	5.10	0.72	1.00	1.26	1.52	1.80	2.04
76	+40	133.14	177	0.02	5.10	0.74	1.00	1.26	1.54	1.80	2.06
77	+40	132.44	177	0.04	5.10	0.74	1.00	1.26	1.52	1.80	2.06
78	+40	133.38	177	0.02	5.10	0.72	0.98	1.26	1.50	1.80	2.04
79	+40	132.94	177	0.02	5.10	0.72	0.98	1.26	1.52	1.80	2.04
80	+40	132.46	177	0.02	5.10	0.74	1.00	1.28	1.54	1.80	2.06
81	+40	133.14	178	0.04	5.10	0.74	1.00	1.28	1.52	1.80	2.06
82	+40	133.62	178	0.02	5.10	0.72	0.98	1.26	1.52	1.80	2.06
83	+40	132.92	178	0.02	5.10	0.72	1.00	1.28	1.52	1.80	2.06
84	+40	133.34	177	0.02	5.10	0.72	0.98	1.26	1.52	1.80	2.04
average	+40	132.91	177	0.03	5.10	0.73	0.99	1.26	1.52	1.80	2.05
Fractional difference between averages		0.012	0.028	1.00	0.002	0.064	0.039	0.031	0.026	0.011	0.010

Table 5 cont.

Data run No.	Discriminator levels (volts)									
	7	8	9	10	11	12	13	14	15	16
73	2.32	2.58	2.84	3.08	3.36	3.60	3.90	4.12	4.38	4.64
74	2.32	2.58	2.84	3.08	3.36	3.60	3.86	4.12	4.38	4.64
75	2.32	2.58	2.84	3.08	3.36	3.60	3.88	4.12	4.38	4.64
76	2.32	2.60	2.84	3.08	3.36	3.60	3.88	4.12	4.38	4.64
77	2.32	2.58	2.84	3.08	3.36	3.60	3.88	4.12	4.38	4.64
78	2.32	2.58	2.84	3.08	3.36	3.60	3.88	4.12	4.38	4.64
79	2.32	2.58	2.82	3.08	3.34	3.60	3.86	4.12	4.38	4.64
80	2.32	2.58	2.84	3.08	3.36	3.60	3.90	4.12	4.38	4.64
81	2.30	2.58	2.84	3.08	3.34	3.60	3.88	4.12	4.38	4.64
82	2.32	2.58	2.84	3.08	3.34	3.60	3.88	4.12	4.38	4.64
83	2.30	2.58	2.84	3.08	3.34	3.58	3.88	4.12	4.38	4.64
84	2.32	2.58	2.84	3.08	3.36	3.60	3.88	4.12	4.38	4.64
average	2.32	2.58	2.84	3.08	3.35	3.60	3.88	4.12	4.38	4.64
Fractional difference between averages	0.004	0.008	0.00	0.003	0.006	0.003	0.002	0.00	0.00	0.00

TABLE 9

DAILY MEAN COSMIC RAY INTENSITY

* Mariner IV ion chamber

YEAR, MONTH	DAY	FREE SPACE ION CHAMBER (NORM. PULSES SEC^{-1} x 10^3)		DEEP RIVER NEUTRON MONITOR (Hourly counts)
		OGO-I	OGO-III	
1964, Sept.	10	58.31		2078
	14	59.38		2097
	16	58.06		2090
	17	58.84		2085
	18	57.66		2086
	19	58.45		2093
	20	58.09		2093
	21	58.87		2086
	23	57.80		2086
	26	58.74		2095
	27	57.66		2096
	29	58.12		2092
	30	58.09		2096
Oct.	3	58.01		2104
	4	57.02		2098
	7	57.92		2090
	8	57.32		2090
	10	57.80		2103
	11	58.46		2102
	12	57.50		2096
	13	57.62		2097
	14	58.34		2096
	15	57.85		2095
	16	57.82		2095
	17	58.77		2097
	18	57.01		2093
	19	57.40		2100
	21	56.15		2096
	22	57.11		2099
	23	57.57		2104
	24	57.09		2102
	25	57.67		2103

Table 9 cont.

YEAR, MONTH	DAY	FREE SPACE ION CHAMBER (NORM. PULSES SEC^{-1} x 10^3)		DEEP RIVER NEUTRON MONITOR (Hourly counts)
		OGO-I	OGO-III	
Oct.	26	56.69		2096
	27	57.35		2096
	28	57.41		2096
	29	57.65		2103
	30	58.02		2105
	31	57.40		2103
1964,	1	57.72		2098
Nov.	3	58.61		2097
	4	58.61		2091
	5	58.76		2099
	6	58.27		2100
	7	58.72		2106
	8	58.27		2099
	9	57.45		2093
	11	57.19		2092
	12	57.89		2090
	13	58.51		2108
	14	58.19		2104
	15	58.70		2099
	16	57.03		2080
	17	56.80		2088
	19	57.22		2096
	20	57.66		2103
	21	58.49		2112
	22	58.25		2112
	24	58.02		2093
	25	57.86		2096
	27	58.22		2103
	28	57.96		2093
	29	59.00	56.83*	2100
	30	58.20		2108

Table 9 cont.

YEAR, MONTH	DAY	FREE SPACE ION CHAMBER (NORM. PULSES SEC^{-1} x 10^3)		DEEP RIVER NEUTRON MONITOR (Hourly counts)
		OGO-I	OGO-III	
1964, Dec.	1	58.14		2107
	2	58.78		2115
	3	58.44	57.44*	2118
	4		58.20*	2117
	5	59.51		2121
	6	59.70		2131
	7	59.45		2135
	8	59.37	58.75*	2132
	10	60.26		2121
	11	60.28	59.39*	2117
	12	60.47		2127
	13	61.10		2126
	14	60.61		2134
	15	60.04	59.93*	2137
	16	59.56		2120
	18	60.32		2126
	19		59.24*	2122
	27		60.21*	2124
	29	61.50		2115
	31		60.45*	2124
1965, Jan	4		60.14*	2125
	8		60.28*	2118
	12		59.39*	2123
	16		58.47*	2100
	20		59.39*	2117
	24		59.22*	2105
	25		59.69*	2114
	26		60.15*	2116
	27		59.86*	2123
	28		59.85*	2127
	30		60.36*	2125
	31		61.02*	2129

Table 9 cont.

| YEAR, MONTH | DAY | FREE SPACE ION CHAMBER (NORM. PULSES SEC^{-1} x 10^3) | | DEEP RIVER NEUTRON MONITOR |
		OGO-I	OGO-III	(Hourly counts)
1965, Feb.	1		61.01*	2127
	2		60.99*	2131
	3		61.35*	2141
	4		61.48*	2134
	5		60.61*	2124
	11		61.64*	2100
	12		60.81*	2108
	13		61.01*	2117
	14		61.00*	2113
	15		60.43*	2109
	16		60.64*	2106
	17		60.92*	2119
	18		61.37*	2132
	19		62.07*	2138
	20		62.03*	2134
	21		62.09*	2123
	22		60.68*	2135
	23		61.39*	2125
	24		60.97*	2112
	25		60.26*	2112
	26		60.39*	2120
	27		60.66*	2115
	28		60.76*	2116
1965, Mar.	1		61.10*	2117
	2		61.48*	2122
	3		62.06*	2104
	4		61.28*	2102
	5		59.80*	2110
	6		60.74*	2116
	7		61.17*	2120
	8		61.56*	2121
	9		61.86*	2124
	10		61.87*	2128
	11		61.98*	2132
	12		62.10*	2134
	13		62.62*	2128
	14		61.64*	2129

Table 9 cont.

YEAR,	DAY	FREE SPACE ION CHAMBER (NORM. PULSES SEC^{-1} x 10^3)		DEEP RIVER NEUTRON MONITOR (Hourly counts)
		OGO-I	OGO-III	
	15		61.54*	2133
1965, April	1	62.55		2138
	2	62.91		2140
	3	63.22		2141
	4	63.11		2139
	5	62.84		2136
	6	63.09		2137
	7	62.46		2138
	8	62.98		2141
	9	63.08		2143
	10	62.98		2146
	11	63.58		2146
	12	63.76		2152
	13	64.23		2159
	14	64.63		2150
	15	64.26		2156
	16	64.34		2163
	17	62.94		2161
	18	61.40		2135
	20	61.90		2126
	21	62.77		2130
	22	63.31		2135
	23	62.94		2139
	24	62.81		2143
	25	64.02		2148
	26	63.62		2154
	27	63.23		2150
	28	64.24		2157
	29	64.06		2159
	30	63.62		2151
1965, May	1	63.44		2150
	2	63.68		2146
	3	64.43		2151
	4	64.73		2153
	5	64.26		2158

Table 9 cont.

YEAR MONTH	DAY	FREE SPACE ION CHAMBER (NORM. PULSES SEC^{-1} x 10^3)		DEEP RIVER NEUTRON MONITOR (Hourly counts)
		OGO-I	OGO-III	
1965, May	6	64.03		2149
	7	63.44		2151
	9	63.81		2140
	10	64.04		2143
	11	65.80		2153
	12	65.40		2160
	13	65.72		2164
	14	65.79		2162
	15	65.69		2156
	16	65.07		2146
	17	64.52		2144
	18	64.34		2147
	19	64.62		2147
	20	63.86		2147
	21	63.68		2144
	22	64.09		2136
	23	63.66		2138
	24	63.66		2143
	25	63.78		2141
	26	64.49		2141
	27	63.73		2132
	28	63.41		2140
	29	63.31		2140
	31	63.81		2139
1965, June	1	63.72		2136
	2	63.43		2137
	3	63.71		2143
	4	63.12		2131
	5	63.07		2129
	9	63.67		2112
	10	63.51		2125
	18	60.75		2090
1965, Sept.	9	63.31		2107
	10	62.26		2110
	11	61.89		2114

Table 9 cont.

YEAR MONTH	DAY	FREE SPACE ION CHAMBER (NORM. PULSES SEC^{-1} x 10^3)		DEEP RIVER NEUTRON MONITOR (Hourly counts)
		OGO-I	OGO-III	
Sept.	14	60.12		2098
	16	61.40		2097
	17	61.90		2089
	19	61.88		2086
	20	61.98		2093
	21	62.58		2096
	22	63.28		2101
	23	63.02		2091
	24	62.32		2087
	25	62.09		2098
	26	62.04		2102
	27	61.27		2099
	28	61.12		2095
	29	61.65		2100
	30	61.94		2104
1965, Oct.	8	61.66		2083
	9	62.17		2092
	10	61.05		2101
	11	61.07		2102
	12	61.37		2113
	13	61.81		2118
	14	61.79		2115
	15	62.16		2115
	16	62.47		2119
	17	63.21		2122
	18	62.57		2110
	19	62.13		2102
	20	62.64		2116
	21	63.36		2118
	22	62.68		2117
	23	62.24		2118
	24	61.99		2122
	26	62.45		2124
	27	61.70		2125
	29	61.60		2118
	30	61.70		2118

Table 9 cont.

YEAR MONTH	DAY	FREE SPACE ION CHAMBER (NORMAL. PULSES SEC^{-1} x 10^3)		DEEP RIVER NEUTRON MONITOR (Hourly counts)
		OGO-I	OGO-III	
1965, Nov.	1	61.79		2130
	2	62.10		2124
	3	62.51		2122
	4	60.62		2107
	5	60.11		2105
	6	61.26		2111
	7	62.13		2118
	8	61.06		2124
	9	62.59		2128
	10	62.84		2128
	11	63.14		2128
	12	63.74		2130
	13	62.85		2125
	14	63.12		2133
	15	63.35		2126
	16	63.55		2125
	17	63.65		2136
	18	63.67		2135
	19	63.67		2128
	20	63.29		2123
	22	63.49		2132
	23	64.25		2136
	24	64.04		2134
	25	64.19		2132
	27	63.22		2125
	28	63.50		2132
	29	63.29		2131
	30	63.86		2132
1965, Dec.	1	62.70		2121
	2	62.52		2115
	3	62.84		2125
	4	63.11		2136
	5	62.47		2132
1966, Jan.	6	62.86		2123

Table 9 cont.

YEAR MONTH	DAY	FREE SPACE ION CHAMBER (NORMAL. PULSES SEC^{-1} x 10^3)		DEEP RIVER NEUTRON MONITOR (Hourly counts)
		OGO- I	OGO-III	
1966, Mar.	9	62.83		2120
	10	62.87		2118
	11	63.13		2120
	12	63.25		2125
	13	61.88		2098
	14	61.74		2108
	15	62.26		2115
	17	63.10		2123
	18	62.72		2120
	19	62.63		2118
	30	55.90		2034
	31	55.48		2040
1966, April	3	59.35		2066
	7	56.93		2067
	8	57.75		2083
	12	58.47		2090
	15	59.18		2090
1966, June	9		57.97	2063
	10		58.55	2076
	11		59.59	2083
	12		60.10	2080
	13		61.25	2084
	14		61.55	2086
	15		61.55	2094
	16		61.33	2093
	17		61.01	2093
	18		60.98	2089
	19		60.30	2082
	20		59.57	2068
	21		59.43	2074
	22		59.82	2073
	23		59.37	2071
	24		59.75	2061
	30		57.79	2043
1966, July	1		57.60	2043
	2		57.37	2038

the electronic shop and the machine shop of the Department of Physics and Astronomy. The author is particularly thankful to Mr. R. L. Howard for the electronic design and to Messrs. R. Thorness and J. Grund for the mechanical design of the experiment.

REFERENCES

Anderson, K. A., H. K. Harris and R. J. Paoli, Energetic electron fluxes in and beyond the earth's outer magentosphere, J. Geophys. Res., 70, 1039-1050, 1965.

Anderson, K. A. and J. R. Winckler, Solar x-ray burst on Sept. 28, 1961, J. Geophys. Res., 67, 4103-4117, 1962.

Arnoldy, R. L., R. A. Hoffman and J. R. Winckler, Observations of the Van Allen radiation regions during August and September 1959,

    Part 1 - J. Geophys. Res., 65, 1361-1376, 1960

    Part 4 - J. Geophys. Res., 67, 2595-2612, 1962a

    Part 5 - J. Geophys. Res., 67, 3673-3686, 1962b

Arnoldy, R. L., J. R. Winckler and R. A. Hoffman, Comparison of the total cosmic radiation in deep space and at the earth during the March-April 1960 events, J. Geophys. Res., 69, 1679-1690, 1964.

Balasubrahmanyan, V. K., D. E. Hagge, G. H. Ludwig, and F. B. McDonald, Galactic cosmic rays at solar minimum, 1965, preprint, NASA Goddard Space Flight Center, Greenbelt, Maryland, 1966.

Callender, R. H., University of Minnesota Masters thesis, December, 1964.

Callender, R. H., J. R. Manzano and J. R. Winckler, The response of high altitude ionization chambers during the 1954-1965 solar cycle, J. Geophys. Res., 70, 3189-3201, 1965.

Comstock, G. M., C. Y. Fan and J. A. Simpson, Abundances and
    energy spectra of galactic cosmic ray nuclei above 20 MeV
    per nucleon in the nuclear charge range $2 \leq Z \leq 26$,
    Astrophysical J., 146, 51-77, 1966.

Coor, T., Ionization chamber bursts at high altitudes, Phys.
    Rev., 82, 478-485, 1951.

Evans, R. D., The Atomic Nucleus, Chapter 23, McGraw-Hill
    Book Company, 1955.

Fan, C. Y., G. Gloeckler and J. A. Simpson, Phys. Rev. Letters,
    13, 149-153, 1964.

Forbush, S. E., On world-wide changes in cosmic ray intensity,
    Phys. Rev., 54, 975-988, 1938.

Forbush, S. E., World wide cosmic ray variations, 1937-1952,
    J. Geophys. Res., 59, 525-542, 1954.

Frank, L. A. and J. A. Van Allen, Measurements of energetic
    electrons in the vicinity of the sunward magnetospheric
    boundary with Explorer XIV, J. Geophys. Res., 69, 4923-
    1964.

Freier, P. S. and C. J. Waddington, The helium nuclei of the
    primary cosmic radiation studied over a solar cycle of
    activity (as interpreted by electric field model), Space
    Sc. Rev., 4, 313-372, 1965.

Hoffman, R. A., Standardization of ionization chambers,
    University of Minnesota Technical Report No. CR-27,
    March, 1960.

Hoffman, R. A., R. L. Arnoldy and J. R. Winckler, Observations of the Van Allen Radiation regions during August and September 1959,

> Part 3 - J. Geophys. Res., 67, 1-12, 1962a

> Part 6 - J. Geophys. Res., 67, 4543-4575, 1962b

Hofmann, D. J., A measurement of the spectrums of low energy primary cosmic ray hydrogen and helium nuclei at solar minimum, Univ. of Minnesota, Ph.D. thesis, November, 1965.

Johnson, F. S., Structure of the upper atmosphere, Satellite Environment Handbook, Ed. F. S. Johnson, Stanford University Press, Stanford, pp. 20-21, 1961.

Kane, S. R., J. R. Winckler and R. L. Arnoldy, Response of ion chambers in free space from 1960 to 1965, J. Geophys. Res., 70, 4107-4115, 1965a.

Kane, S. R., J. R. Winckler and R. L. Arnoldy, Studies of primary cosmic rays with ionization chambers, Proceedings of the Ninth International Conference on Cosmic Rays, Vol. 1, pp. 157-160, London, 1965b.

Kane, S. R., K. A. Pfitzer, and J. R. Winckler, The construction, calibration and operation of the University of Minnesota experiments aboard the OGO-I and OGO-III satellites, Technical Report CR-87, School of Physics and Astronomy, University of Minnesota, September 1966.

Ludwig, C. H., The Orbiting Geophysical Observatories, Space Sc. Rev., 2, 175-218, 1963.

May, T. C., A study of auroral x-rays at Minneapolis between 23 August 1959 and 1 August 1960, Technical Report CR-36, School of Physics, University of Minnesota, April, 1961.

Millikan, R. A., H. V. Neher and S. K. Haynes, Precision cosmic ray measurements up to within a percent or two of the top of the atmosphere, Phys. Rev., 50, 992-998, 1936.

Neher, H. V., An automatic ionization chamber, Rev. Scient. Instr., 24, 99=102, 1953.

Neher, H. V. and H. R. Anderson, Cosmic rays at balloon altitudes and the solar cycle, J. Geophys. Res., 67, 1309-1315, 1962.

Neher, H. V. and H. R. Anderson, Cosmic ray intensity at Thule, Greenland, during 1962 and 1963 and a comparison with data from Mariner II, J. Geophys. Res., 69, 807-814, 1964.

Neher, H. V. and H. R. Anderson, Results from the Mariner IV ion chamber experiment. Trans. Am. Geophys. Union, 46, 113-114, March 1965.

Peters, B., The nature of primary cosmic radiation, Progress in Cosmic Ray Physics, pp. 191-242, Ed. J. G. Wilson, North Holland Publ. Co., Amsterdam, 1952.

Peterson, L. E. and J. R. Winckler, Gamma ray burst from a solar flare, J. Geophys. Res., 64, 697-707, 1959.

Rossi, B., High Energy Particles, Prentice Hall, New York,

      p. 24,   1952a

      p. 441   1952b

Shamos, M. H. and R. A. Liboff, A new measurement of the intensity of cosmic-ray ionization at sea level, J. Geophys. Res. 71, 4651-4659, 1966.

Webber, W. R., Time variations of low rigidity cosmic rays during
the recent sunspot cycle, Prog. Cosmic Ray Phys., North
Holland Publ. Co., Amsterdam, 6, 75-243, 1962.

Webber, W. R., The spectrum and charge composition of the primary
cosmic radiation, Handbuch der Physik, 46(2), 164, 1967.

Winckler, J. R., Balloon study of high altitude radiations
during the international geophysical year, J. Geophys. Res.,
65, 1331, 1960.

Yuan, Luke C. L. and C. Wu, Methods of Experimental Physics,
Academic Press,

pp. 49-50, 1961a

pp. 17, 1961b